Tesis Doctoral

MODELADO DE FENÓMENOS DE HISTÉRESIS Y CONTACTOS EN TRANSISTORES ORGÁNICOS/POLIMÉRICOS.

Autor:

KARAM MOHAMMAD AWAWDEH

Director:

Juan Antonio Jiménez Tejada

Programa Oficial de Posgrado en Física
Dept. Electrónica y Tecnología de Computadores
Universidad de Granada

2013

Editor: Editorial de la Universidad de Granada
Autor: Karam Mohammad Awawdeh
D.L.: GR 2223-2013
ISBN: 978-84-9028-653-1

El doctorando KARAM AWAWDEH y el director de la tesis JUAN ANTONIO JIMÉNEZ TEJADA garantizamos, al firmar esta tesis doctoral, que el trabajo ha sido realizado por el doctorando bajo la dirección del director de la tesis, y hasta donde nuestro conocimiento alcanza, en la realización del trabajo, se han respetado los derechos de otros autores a ser citados, cuando se han utilizado sus resultados o publicaciones.

Granada, 25 de febrero de 2013

Director/es de la Tesis	Doctorando
Fdo.: Juan Antonio Jiménez Tejada	Fdo.: Karam Awawdeh

Dr. **Juan A. Jiménez Tejada**, Catedrático de Universidad del Departamento de Electrónica y Tecnología de Computadores de la Universidad de Granada.

CERTIFICA

Que el trabajo de investigación que se recoge en la presente Memoria, titulada " MODELADO DE FENÓMENOS DE HISTÉRESIS Y CONTACTOS EN TRANSISTORES ORGÁNICOS/ POLIMÉRICOS." presentada por D. **Karam Awawdeh** para optar al grado de Doctor, ha sido realizado en su totalidad bajo su dirección en el Departamento de Electrónica y Tecnología de Computadores de la Universidad de Granada.

Y para que así conste y tenga los efectos oportunos, firma este certificado en Granada, a 6 de Marzo de 2013.

Dr. J. A. Jiménez Tejada

MODELING CONTACT EFFECTS AND HYSTERESIS IN ORGANIC THIN FILM TRANSISTORS

By

KARAM MOHAMMAD AWAWDEH

A THESIS

SUBMITTED TO THE GRADUATE SCHOOL OF THE UNIVERSITY OF GRANADA IN PARTIAL FULFILMENT OF THE REQUIREMENTS FOR THE DEGREE OF DOCTOR OF PHILOSOPHY

UNIVERSITY OF GRANADA

DOCTORATE PROGRAM IN PHYSICS (2013)
DEPARTAMENTO DE
ELECTRÓNICA Y TECNOLOGÍA
DE COMPUTADORES
UNIVERSITY OF GRANADA
GRANADA, SPAIN

Title: MODELING CONTACT EFFECTS AND HYSTERESIS IN ORGANIC THIN FILM TRANSISTORS

Author: KARAM MOHAMMAD AWAWDEH

Supervisor: JUAN ANTONIO JIMÉNEZ TEJADA
CATEDRÁTICO DE UNIVERSIDAD,
DEPARTAMENTO DE ELECTRÓNICA Y
TECNOLOGÍA DE COMPUTADORES,
(UNIVERSITY OF GRANADA, SPAIN)

The research was carried out within the framework of a scholarship supported financially by the Erasmus Mundus External Cooperation Window and within the research Project No. TEC2010-16211 supported financially by the Ministerio de Educación y Ciencia and Fondo Europeo de Desarrollo Regional (FEDER).

Acknowledgements

I would like to express my profound gratitude to my research advisor, Dr. Juan Antonio Jiménez Tejada for his guidance and continuous support through all stages of this work and to Profs. J. Deen and A. Ray for their help in the development of this work. I would also like to extend my thanks to the University of Granada and especially to the Facultad de Ciencias and the staff at the Departamento de Electrónica y Tecnología de Computadores for their help and support during my doctorate work.

I would also like to thank my companions in Hebron university who encouraged me to study the PhD, especially, Prof. Awni Al-Khatib and Dr. Salman Al-Talahmeh.

It has been a pleasure to do the PhD research at the Departamento de Electrónica y Tecnología de Computadores en Granada (España)

Un agradecimiento especial va dirigido a mis compañeros de despacho y cafelitos: Celso, Trinidad, Pilar, José Luis, Abraham, Cristina y Enrique. Gracias a ellos por hacer más llevaderas las mañanas de trabajo en la facultad. Otros cuatro años más de doctorado y seguro que hubiéramos solucionado el mundo con nuestras discusiones de cafetería. Al profesor Rodríguez Bolívar me gustaría agradecerle también el haberme proporcionado la oportunidad de trabajar en un proyecto de innovación docente antes de comenzar mis estudios de doctorado. No quiero dejar de mencionar tampoco a los profesores Gómez Campos y López Villanueva por su apoyo durante mi estancia en Granada.

Finalmente, me gustaría agradecer a mi familia todo el apoyo recibido. A mis padres, Mohammad y Amna, quienes han contribuido con su propio sudor a que esto sea una realidad. Y a mi hermano Dr. Abdelbaset quien me ayudó durante en mi estancia en el extranjero. Y a mis hijos y a mi mujer quienes han esperado conmigo a lograr este objetivo. Y a mis hermanos y hermanas quienes se han preocupado por mí.

Thanks to all of you,

Karam

Abstract

The performance of modern organic semiconductor devices is limited by non-ideal effects which are not characterized by traditional models of transport. In this work, two major problems that affect the behaviour of organic/polymeric transistors are studied: contact effects and trapping de-trapping mechanisms. Moreover, if they are present simultaneously the analysis of the transistor is more complex.

A new compact model is developed for organic thin film transistors (OTFTs) by incorporating the effects of the contacts on the transistor's output characteristics. The model is based on physically realistic expressions that describe charge flow in the vicinity of the contacts and a previously developed drift model. The resulting new model maintains the compactness of the original drift-based model and is very suitable for circuit simulations. For proper modelling, accurate model parameters are important. Therefore, we also propose a modified method to extract the transistor's parameters, including ones related to the contact region.

The validity of the model is examined by applying it to experimental data obtained for OTFTs which used solution processed films of substituted zinc phthalocyanine derivatives as an active layer between the gold contacts as the source and the drain terminals. Both linear and non-linear responses in the low drain voltage regime of the output characteristics of the transistors are analysed. The new parameter extraction scheme provides a way to study the evolution with the gate voltage of the ratio of free to total charge density in the low conductivity region close to the contact.

At the same time, the validity of the parameter extraction scheme is examined by applying it to data obtained from a transistor which parameters are known. This transistor consists of an ideal transistor with added contact effects. All the parameters that define the complete structure are known.

The other problem that deteriorates the performance of the organic devices is the

trapping and de-trapping mechanism. It can cause instabilities that produce hysteresis in output or transfer characteristics of transistors. The combination of both contact effects and hysteresis make the interpretation of experimental data more difficult. A method to extract parameters in organic thin film transistors (OTFTs) showing contact effects and hysteresis is presented. The method is based on the previously mentioned compact model that reproduces the current voltage characteristics of OTFTs.

A suitable characterization technique for parameter extraction of mobility, threshold voltage and the variation of trapped charge during a hysteresis cycle is provided. The variation of the threshold voltage with trapped charges during voltage cycling and using existing transistor models results in different sets of parameters needed to reproduce the experimental data. However, not all of which have proper physical meanings. In order to find a unique physical solution, the current-voltage curves at the contacts and current voltage curves in the intrinsic transistor are extracted from the output characteristics measured at the transistor terminals, and analysed separately. The subsequent comparison of the evolution of the free charge density with the gate voltage, in both the contact region and the intrinsic channel, allows for finding this unique solution. The results of this method are compared with the results taken by other authors that employ more elaborate experimental techniques, such as the four-terminal method or transient experiments.

Finally, we compare different procedures to extract information about the trapping processes that occur in organic thin film transistors (OTFTs) during hysteresis mechanisms. The procedures are based on models that describe the transistor as the combination of an intrinsic transistor and the contact regions. The models are used to fit experimental output characteristics and to extract the current-voltage curves for the intrinsic transistor. We show the importance of eliminating the effect of the contacts completely, not only from fundamental parameters such as the mobility and the threshold voltage or the drain–terminal voltage but also from the gate–terminal voltage. This study aims to complement experimental procedures that also tend to eliminate contact effects. The previously developed compact model for the OTFT is presented as the best option to fulfil this objective.

Índice general

List of Acronyms

BS	Backward sweep
$c-FET$	Crystalline field-effect-transistor
FET	Field-effect-transistor
FS	Forward sweep
$HOMO$	Highest occupied molecular orbital
$IDLM$	Injection-drift limited model
$I-V$	Current-Voltage curve
$I_D - V_C$	Current-Voltage curve at the transistor contacts
$I_D - V_D$	Current-Voltage curve in the extrinsic transistor
$I_D - V_{DS}$	Current-Voltage curve in the intrinsic transistor
$I_D - V_G$	Current-Voltage curve in the extrinsic transistor
$I_D - V_{GS}$	Current-Voltage curve in the intrinsic transistor
$LUMO$	Lowest unoccupied molecular orbital
MIS	Metal-insulator-semiconductor
MOS	Metal-oxide-semiconductor
$OFET$	Organic field-effect transistor
OSC	Organic semiconductor
$OTFT$	Organic thin film transistor
$P3HT$	Poly 3-hexylthiophene
$PFET$	Polymer field effect transistors
$RFID$	Radio-frequency identification
$TDTs$	Tail-distributed traps
TFT	Thin film transistor
VRH	Variable range hopping

List of Symbols

$\Delta P, \overline{\Delta P}$	m^{-2}	Variation of the trapped particles per unit square and its average
η		Non-ideality factor of the diode
S	m^2	Cross-sectional area
γ		Enhancement mobility factor
I_D	A	Drain current
$I_{D_{saturation}}$	A	Drain current in the saturation region
L	m	Transistor's channel length
μ	m^2/Vs	Carrier mobility
μ_o	m^2/Vs	Carrier mobility at zero electric field
M	$\mathrm{A/V}^2$	Parameter describing non-linear $I-V$ curves at the contacts
$p(0)$	$\mathrm{Particle/cm}^3$	Free charge density at the metal-organic interface
t_i	μm	Thickness of the insulator
t_o	μm	Thickness of the organic semiconductor
ϕ_B	eV	Energy barrier at the metal-organic interface
R_C	Ω	Resistance at the contact
$\rho_{channel}$	$\mathrm{C/cm}^3$	Charge density in the channel
$\rho_{channel_{FS}}$	$\mathrm{C/cm}^3$	Charge density in the channel for forward sweep
$\rho_{contact_{BS}}$	$\mathrm{C/cm}^3$	Charge density in the channel for backward sweep
$\rho_{contact}$	$\mathrm{C/cm}^3$	Charge density in the contact
$\rho_{contact_{BS}}$	$\mathrm{C/cm}^3$	Charge density in the contact for backward sweep
$\rho_{contact_{FS}}$	$\mathrm{C/cm}^3$	Charge density in the contact for forward sweep
w	m	Transistor's channel width
x_P	nm	Characteristic length used in the $I-V$ model at the contacts
x_c	nm	Contact length

V_{AA}	V	Empirical parameter used in voltage dependent mobility models
V_C	V	Contact voltage
V_D	V	Drain-terminal voltage (Extrinsic transistor)
V_G	V	Gate-terminal voltage (Extrinsic transistor)
V_{DS}	V	Drain-to-source voltage drop in the intrinsic transistor
V_{GS}	V	Gate-to-source voltage drop in the intrinsic transistor
V_S	V	Contact voltage
V_T	V	Threshold voltage
$V_{T_{BS}}$	V	Threshold voltage in backward sweeps
$V_{T_{FS}}$	V	Threshold voltage in forward sweeps

1

Introduction and background

1.1. Structure of the Thesis

During the last decades there has been an enormous interest in the development of electronic devices based on polymers and organic films. Since the first fabrication of polymeric and organic materials, characterized by their long and short lengths of their molecules, respectively, many efforts have been devoted to realize inexpensive polymeric and organic thin film transistors [1]. The molecular semiconductor based on carbon chains has important advantages, such as the low cost processing and the possible use in flexible substrates [2]. They can also be fabricated at low temperature [3]. These advantages make the organic thin film transistors attractive to applications like electronic tags or drivers in active matrix displays. However, there are disadvantages too that must be solved. Many efforts are devoted to improve the performance of organic thin film transistors by increasing the charge carrier mobility [4]. Others are devoted to treat the effects associated to the contacts regions of the transistor. It has been reported that a substantial part of the externally applied drain source voltage, V_D, drops across the contact between the organic material and the source and drain metal electrodes, mainly between the source and the organic material [5]. Thus, in addition to the limited drift in the organic film, there is one more limit for the charge flow in $OTFTs$ owing to contact effects.

The contact regions can alter the output characteristics of the transistor making the traditional crystalline MOS model unable to interpret the performance of the transistor. In that sense, many efforts are also devoted to develop models aiming to reproduce output characteristics in the transistor, and to develop methods of parameter extraction [2][5][6][7][8]. The development of accurate and computationally efficient models is critical to reduce the cycle time between design, manufacturing and characterization. Furthermore, to guide the design process and to explicitly show relationships between material properties and device design and performance, physically-based compact TFT models for emerging thin-film technologies are indispensable [9]. In Chapter 2, we work with this idea. There, the main interrelated challenges of the thesis are presented (see Fig. 1.1):

a) A proper model for the output characteristics $I_D - V_D$ of a transistor,

b) A proper model for the current-voltage characteristic in the region close to the contact,

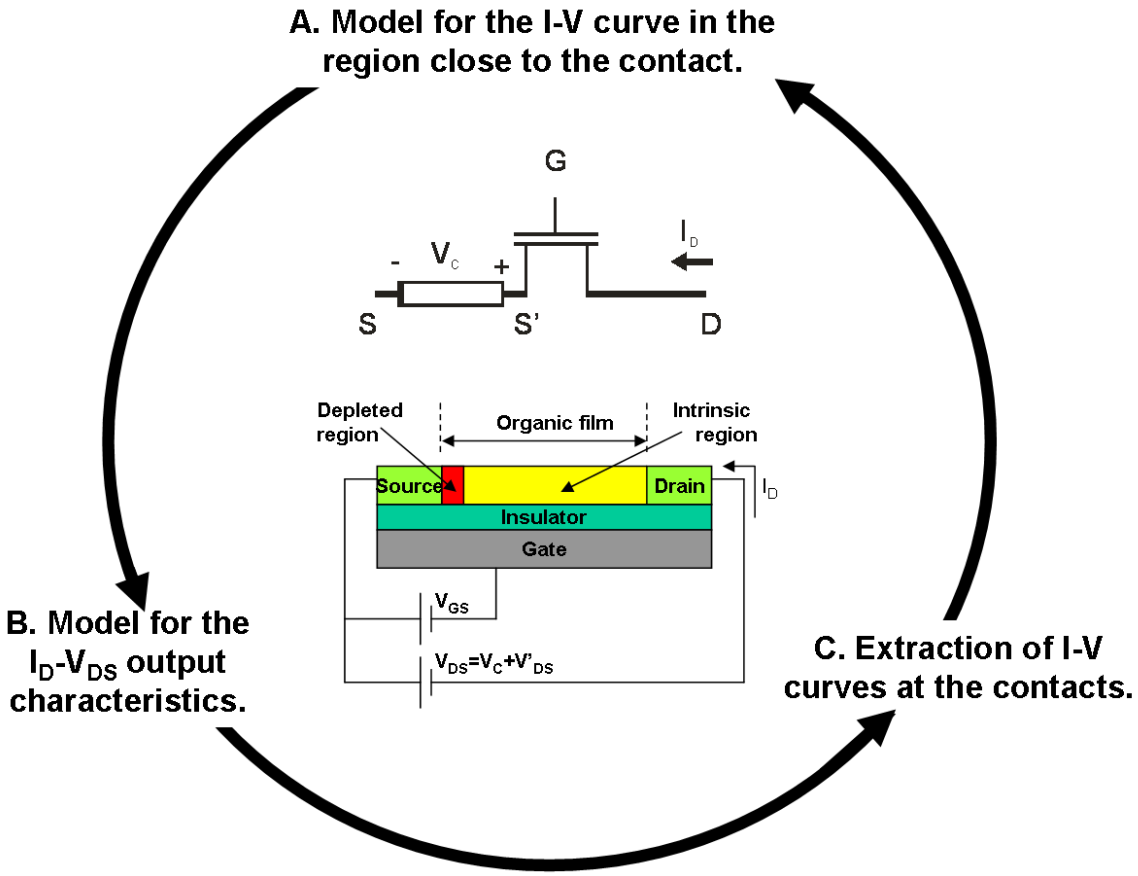

Figure 1.1: Scheme with the problems and challenges we can find when analysing organic transistors with contact effects: the proposal of a good model for the contacts, the integration of this model in transistor models, and finally the proposal of a technique that allows for the extraction of the different parameters that appear in the model.

$I_D - V_C$, and its incorporation in the output characteristics model, and

c) An extraction method of the $I_D - V_C$ curves at the contact and the rest of the model parameters out of the resulting combined model.

The objective is to improve the theoretical modelling of organic thin film transistors by the inclusion of the contact effects. The extraction procedure is initially applied to experimental data, taken by our collaborators in Brunel University, on Zinc Phthalocyanine based $OTFTs$.

In Chapter 3, the method is checked with output characteristics of a transistor with known parameters. One member of our team creates a set of output characteristics for a

transistor which parameters this member only knows. Another member of the team has to use the method developed in the previuos chapter to find the values of the parameters, and thus, validate the method.

In Chapters 4 and 5, we add a new problem in the characterization of organic transistors: the treatment of current voltage curves that show hysteresis phenomena and contact effects. The origins of the hysteresis phenomenon are the trapping and de-trapping mechanisms that take place in the $OTFTs$. They can cause instabilities that can produce changes in the carrier mobility and in the threshold voltage V_T of organic thin film transistors [10]. The study of the hysteresis is important as it can provide information about the trapped charge in the organic material. Subsequently, this information can be related to technological parameters with the objective of finding a better device design. Actually, one of the major problems that are pending the mass production of practical OTFTs is to obtain the stability during the successive operation or in alternating sweep directions. Hysteresis and V_T shift should be preferably minimized for many conventional applications except nonvolatile memory applications of OTFTs [11][12].

The combination of both hysteresis and contact effects makes the characterization task more difficult. There are some previous studies that characterize the hysteresis in organic transistors from transfer and output characteristic. In some cases, contact effects are not considered [13]. In other cases, contact effects are eliminated from the experimental data by using elaborate experimental procedures, like the four-terminal method, instead of the usual two-terminal one [14].

In Chapter 4, we propose a method to extract information of traps origin of the hysteresis mechanisms in current voltage curves obtained with the two-terminal procedure. The method solves the difficulty of processing $(I_D - V_D)$ curves where contact effects are present. We analyse experimental current voltage curves taken from the literature that show both contact effects and hysteresis [13][14]. Information is then extracted for the trapped charge in the organic material. The results are compared with other values reported in the literature. The accuracy of our method is checked by comparing our results with the ones obtained from the four-terminal method, which also considers the contact effects.

In Chapter 5, different ways to extract the variation of the trapped charge during voltage cycling are compared in order to find the one that provides the most accurate results. A graphical summary of Chapters 4 and 5 can be seen in Fig. 1.2.

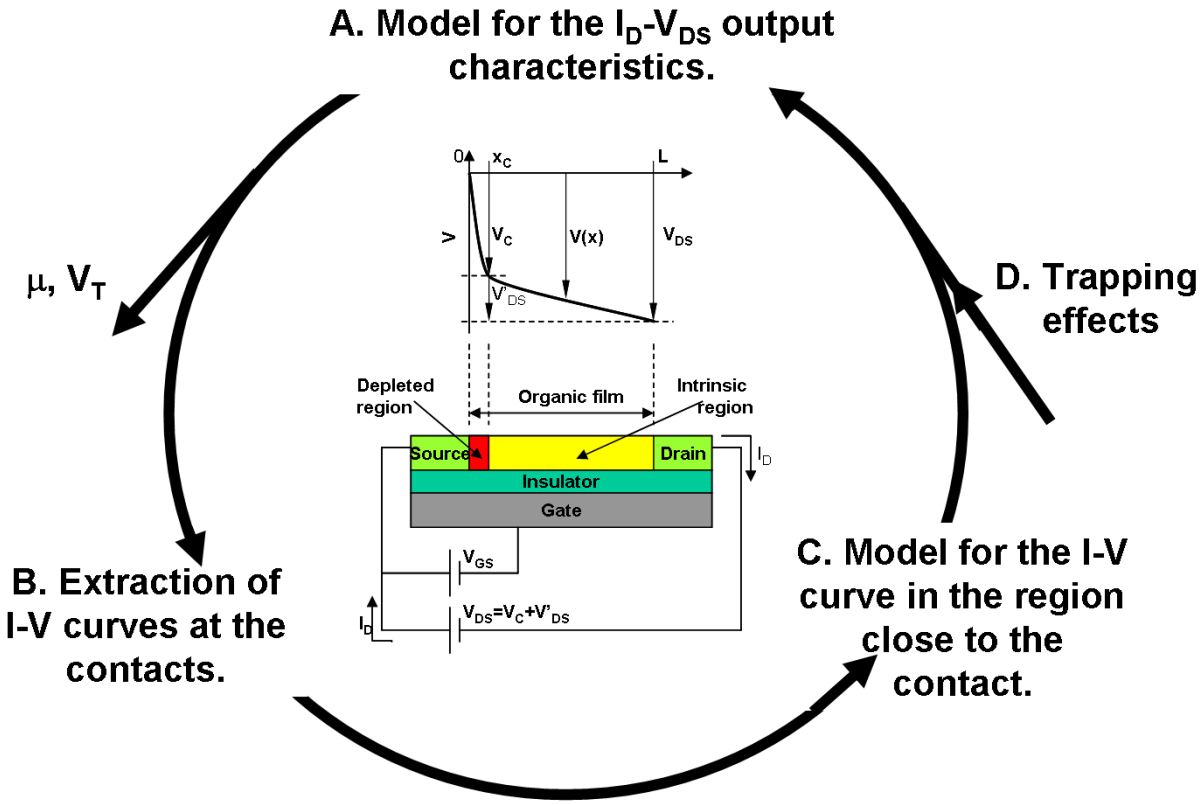

Figure 1.2: Scheme with the problems and challenges we can find when analysing organic transistors with contact effects and hysteresis: the trapping effects in the structure must be added to the problems detailed in the scheme of Fig. 1.1.

Prior to all this study, we enumerate the main objectives and the overall methodology followed in the work; although specific methods are detailed in each chapter. Some concepts related to different topics treated in this Thesis are also introduced in the rest of this chapter.

1.2. Objectives

1. To develop a compact model that describes the output characteristics of organic/polymeric transistors and includes the effect of the contacts. After the incorporation of the contact effects, the model must have parameters that can be characterized relatively easily, or even guessed, preventing unnecessary phenomenological fitting parameters.

2. To propose a characterization method that extracts the parameters of the model (mobility, threshold voltage and the new contact parameters) by comparing the experimental data with the theoretical results.

3. To apply the method to experimental data taken by us or by other authors.

4. To propose a test to verify the validity of the model.

5. To adapt the characterization method to experimental data that show both contact effects and hysteresis, overcoming the problem of working with a variable threshold voltage.

6. To characterize the presence of traps in the transistor by determining the variation of the trapped charge that occurs during voltage cycling.

7. To analyse different ways to determine the variation of the trapped charge and to compare the results.

8. To find a physical connection between the mechanisms that take place in the contact region and in the intrinsic channel of the transistor.

1.3. Methodology

The method to fulfil all these objectives is based on these main steps:

1. The study of the state-of-the-art of compact modelling of organic thin film transistors.

2. The proposal of simple mathematical models or modification of existing ones that describe the output characteristics of the transistor.

3. The development of a procedure to extract the parameters of the proposed model based on the analysis of experimental data. The experimental data can be taken by some of our collaborators or extracted from other authors' experiments.

4. The implementation in computing programs of such models and procedures.

The specific methods followed to treat the different topics of this Thesis are detailed in each chapter.

1.4. Basic concepts

1.4.1. Organic materials

Organic materials present in electronic devices can be classified into permanent conductors and insulators, semiconductors, and materials with added functionality, such as chemical recognition, piezoelectricity, and hysteresis.

Conductive polymers are preferred materials for leads and contacts in organic devices because of their suitability for printing. There are three main classes of conductive polymers used for printed electronics: polythiophenes (and related polypyrroles), polyanilines, and insulating polymers filled with conductive nanostructures.

The most prominent role for insulating polymers in organic devices involves the gate dielectric for organic field-effect transistors (OFETs). Many common polymers can be used, including poly(methyl methacrylate), poly(vinyl phenol) and other polystyrenes, polyvinyl alcohol, polyimides, silicone network polymers, and parylene.

Transistors, diodes, sensors, transducers, and memory elements can incorporate semiconductors consisting of organic molecular solids and/or semiconducting polymers (organic semiconductors, ($OSCs$)). Applications of these devices can be found in circuits of moderate complexity, such as display drivers, radio-frequency identification (RFID) tags, or pressure mapping elements.

The lowest unoccupied molecular orbital (LUMO) energy levels of most conjugated organic compounds lie outside the preferred ranges for electron transport. This is the reason why there are considerably fewer molecular structures that have been identified as preferentially electron-carrying (n-channel) transistor semiconductors in comparison with the hole-transporting (p-channel) semiconductors. The amount of holes in the semiconductor is determined by the highest occupied molecular orbital (HOMO) energy levels relative to contact work functions and environmental quenchers.

However, there is a particular need for n-channel (electron conducting) organic semiconductors with performance comparable to p-channel (hole conducting) materials, in order for organic electronics to realize the benefits of complementary circuit design. In complementary circuits, both positive and negative gate voltages are used to switch transistors, resulting in simpler circuits and lower power consumption than if only p-channel or n-channel devices are employed. In the last several years there has been increased at-

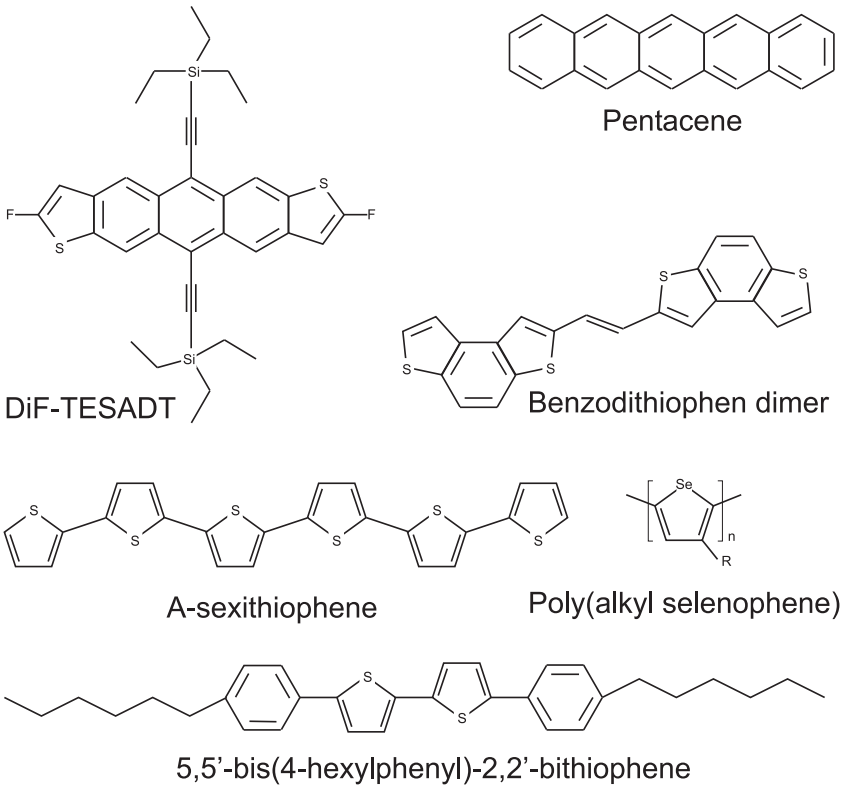

Figure 1.3: Some $p-channel$ semiconductors.

tention to n-channel TFT materials with corresponding improvements in the field effect mobility, the on-to-off current ratio, and the threshold voltage [15][16][17][18][19][20][21]. Still, the performance of the best n-channel materials is not quite as good as the best p-channel materials, such as pentacene,[22] which is the current benchmark organic semiconductor for OTFT applications. The main classes of hole-carrying molecular solid OSCs include fused rings (such as the mentioned pentacene or thienothiophene, benzodithiophene, dithienoanthracene, and tetracene), short oligomeric chains of rings (various combinations of thiophenes, phenylenes, thiazoles, and pyrroles), ethylene and ethynylene groups, and selenophenes. A few such structures are shown in Fig. 1.3.

1.4.2. Organic Field-Effect Transistors

An $OFET$ is an electronic device which structure turns around a capacitor-like structure. It is formed by a metallic gate, a dielectric, and semiconductor layers. Two metal

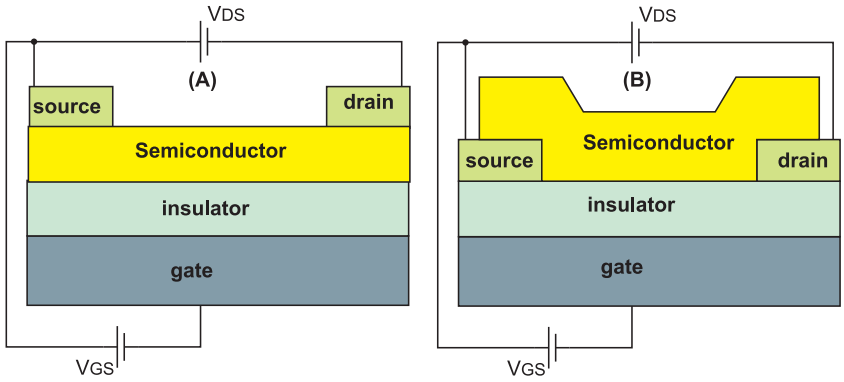

Figure 1.4: Typical structures for (*OFETs*): (a) Top contact configuration; and (b) bottom contact configuration.

contacts, the source and drain electrodes, are connected electrically to the semiconductor film, as shown schematically in Fig. 1.4. The position of these electrodes at the top of the structure or embedded between the semiconductor and the insulator define the top-contact and bottom-contact configurations, respectively. This structure was initially developed for amorphous silicon transistors [23][24]. The conductive gate electrode is also used as substrate, providing mechanical support to the structure. Insulating oxide or polymeric insulators coated on the gate, with or without surface treatment, act as dielectric layers. Without applied gate voltage V_{GS}, the intrinsic conductivity of most *OSCs* is low; when a voltage V_{DS} is applied between drain and source, very little current can flow through the thin semiconductor film, and the device is in the OFF-state. When a gate voltage V_{GS} is applied on the gate, the electric field existing across the capacitor structure attracts charges towards the dielectric-semiconductor interface. These accumulated charges are mostly mobile and give rise to a conducting channel between source and drain. These mobile charges can move in response to the applied V_{DS}. The transistor is working in the ON-state or accumulation mode.

There is a threshold voltage, V_T, above which the conducting channel is formed. The value of this threshold voltage depends on different internal mechanisms of the structure. Most *OSCs* are not intentionally doped so that charges are actually injected and extracted from source and drain electrodes. For most cases, there is a mismatch between the Fermi level of metal electrodes and the *HOMO* (*LUMO*) of the *p-channel* (*n-channel*) semiconductors, which induces charge injection barriers. A non zero V_{GS} is required to shift the molecular orbital energy levels of semiconductors up or down so

that the molecular orbitals become resonant with the Fermi level of metal electrodes and reduce the charge injection barriers. In addition, there are always trap states in the semiconductor film that are induced from impurities and defects (including grain boundaries), as well as molecules like H_2O and O_2 adsorbed from the environment. A non zero V_{GS} must be applied to fill these trap states before mobile charges can be transported along the conducting channel. The threshold voltage V_T was defined to account for all those effects.

The experimental current-voltage curves of the *OFET* are very similar to the MOSFET. This is the reason why the *OFETs* have extensively been described with the classical equations that describe the MOS transistor:

$$\begin{aligned} I_D &= \frac{w\mu_o C_i}{L}[(V_{GS}-V_T)V_{DS}-\frac{V_{DS}^2}{2}], V_{DS} < V_{GS}-V_T \\ I_D &= \frac{w\mu_o C_i}{2L}[(V_{GS}-V_T)^2], V_{DS} \geq V_{GS}-V_T \end{aligned} \tag{1.1}$$

where C_i is the gate insulator capacitance per unit area, V_T is the threshold voltage, μ_o is the carrier mobility and w and L are the channel width and length, respectively.

There are some aspects that need special consideration and make the *OTFTs* to separate from the ideal MOS model: The injection of charge from the contacts [25][26], the transport of charge in the organic semiconductor [3][8][27] and the instabilities created by the charge build-up in the structure [28][25][8]. They are summarized in Fig. 1.5. The charge injection from the source electrode limits the carrier number that can enter into the polymer material per unit time, while the effective mobility of charge hopping in the polymer determines the drift of the carriers toward the drain electrode [29]. The separation of electrical charge in a polymer material into mobile and trapped parts has already been proposed in [29], and the trapped charge is extensively used as an explanation of the hysteresis [30] in I_D–V_{GS} measurements and the non-stationary behaviour [8] of the threshold voltage V_T.

1.4.3. Carrier mobility

The transfer of charge is directly related to the charge mobility. Charge mobility μ defines the relation between the velocity acquired by the charge carriers under the effect of an electric field. The mobility is usually a function of the gate voltage. Although the char-

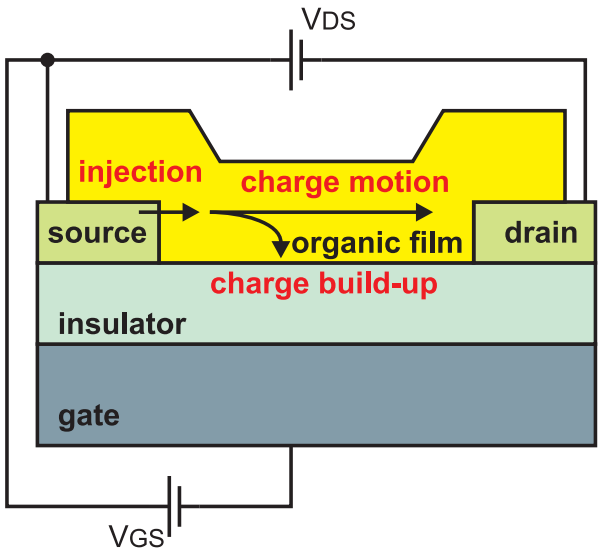

Figure 1.5: Mechanisms that make the OTFT separate from the ideal crystalline MOS model [29].

ge transport mechanism in *OSCs* is still under continued research, several models have been developed to interpret the gate voltage dependence of mobility [31][32][33][34][24]. In general, there are traps distributed in *OSCs*. When gate voltage is increased, more traps are filled by the injected charges, leaving fewer traps retarding the movement of charges. Hence, charges move faster at higher gate voltage, which is consistent with the fact that mobility usually increases with increased gate voltage for most *OFETs* reported.

1.4.4. Contact effects

In cases in which mobility does not seem to increase with increased gate voltage, contact resistance may have a relatively stronger effect on output currents at higher gate voltages, diminishing the apparent mobility. The contact regions of the organic transistor require a different study. Fig. 1.6 shows a scheme of a transistor where the low conductivity regions close to the drain and source regions are highlighted. There are experimental evidences that prove the existence of these regions. The first one is obvious because of the nature of the different material that constitute the contacts. We can find a second reason in surface micro-graphs of these regions. They show how the density of molecules in the organic material are not the same just at the metallurgical contact or

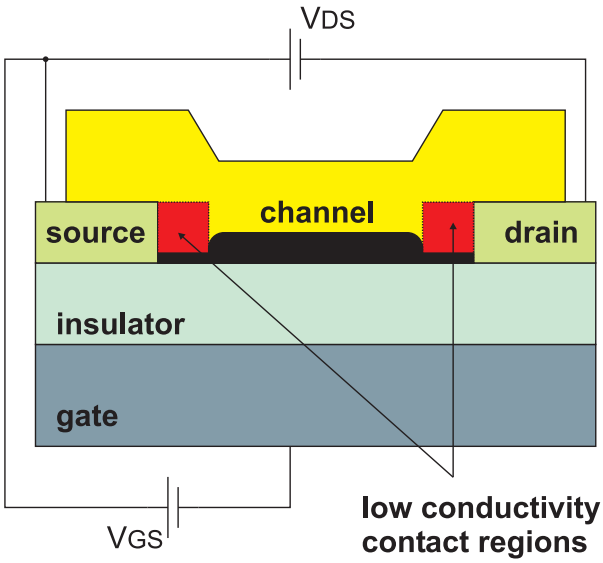

Figure 1.6: Organic transistor showing the low conductivity regions regions close to the contacts.

far from it [8]. A third reason is found in scanning potentiometer measurements. These measurements can monitor the voltage drop between source and drain. In many cases, they show a larger voltage drop between the source-contact (injecting contact) than in the drain contact (collecting contact) [35]. In this situation, we can neglect the voltage drop between drain and the intrinsic channel (Fig. 1.7).

We can find many works devoted to find the best contacts that favour the injection or extraction of charge from a metal contact to an organic semiconductor [36][37][38][39]. We can cite works where a thin layer is introduced between these two materials in order to modulate the energy barrier height at the contact [38]. Our concern in this work is to find a proper model for the contact region to be incorporated in the transistor model.

1.4.5. Hysteresis phenomena in OTFTs

Hysteresis in OTFTs is attributed to defects or traps in either the gate dielectric or the semiconductor material [10][40][41]. The study of current voltage curves with hysteresis can provide information about the defects and traps present in the organic transistor. The characterization of these traps can subsequently be used to achieve a better device design.

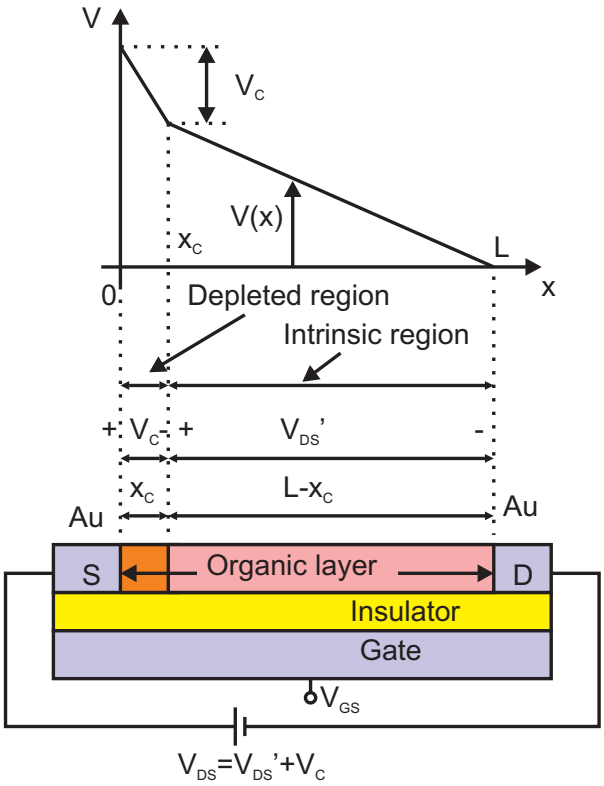

Figure 1.7: Schematics of a potential profile that can be observed along the channel of an OTFT showing a low conductivity region at the contacts. The contacts effects on the drain contact are neglected according to [35].

Hysteresis is shown as a cycle in transfer characteristics ($I_D - V_G$) or in output characteristics ($I_D - V_D$) where I_D depends on the sweep direction of V_G or V_D. These reversible electrical bi-stabilities are frequently observed in organic field effect transistors. Depending on the microscopic origin, the localization of the traps and defects, the hysteresis can result in a back sweep (BS) current (the sweep from on to off) that is either higher or lower than the forward sweep (FS) current (the sweep from off to on) [40].

Hysteresis can be divided into two classes: permanent and dynamic hysteresis [42]. Permanent hysteresis (no significant threshold voltage change over time) may be useful for applying to non-volatile memory devices (i.e., ferroelectric field effect transistors) but dynamic or volatile hysteresis causes a major problem against designing stable or reliable integrated circuits. There have been different explanations to discuss the origins of such dynamic hysteresis or instabilities. These explanations can be grouped into three general mechanisms, as shown in Fig. 1.8:

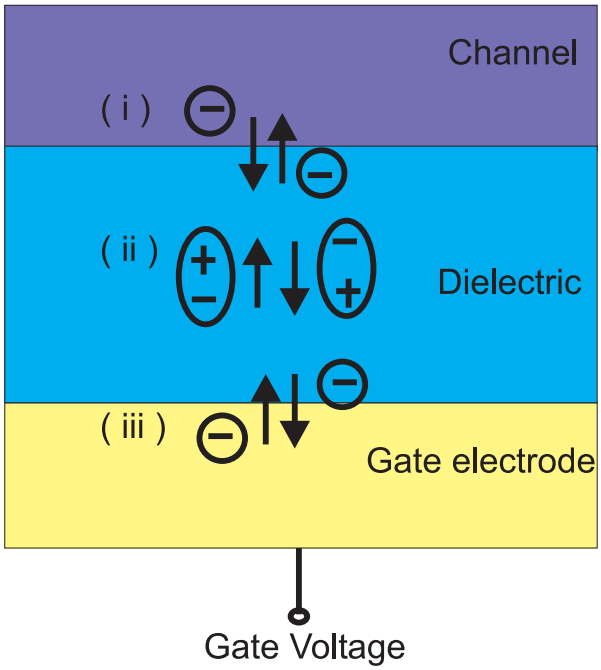

Figure 1.8: Illustration of hysteresis mechanisms: (i) channel/ dielectric interface-induced, (ii) slow polarization-induced, and (iii) gate charge injection-induced hystereses.

(i) channel/dielectric interface-induced effect,

(ii) residual dipole-induced effect (caused by slow polarization in the bulk organic dielectric), and

(iii) the effects of charges injected from gate electrode.

Mechanism (i) is often associated with the electrons trapped to hydroxyl groups (OH) at channel/dielectric interface [43][44][45]. Mechanism (ii) is related to dipole groups inside polymer dielectric materials, such as hydroxyl groups, which can be slowly reoriented by an applied electric field [42][44][46][47][45][48]. Mechanism (iii) attributes to the electrons which can be injected from gate electrode to a vulnerable dielectric and then trapped inside the dielectric [49][50]

Unfortunately, all the effects that make the transistor to separate from the ideal behaviour do not show alone, but combined among themselves. Fig. 1.9 shows an scheme of output characteristics with hysteresis and contact effects, and how our objective is to separate the contact effects from what occurs in the intrinsic channel of the transistor.

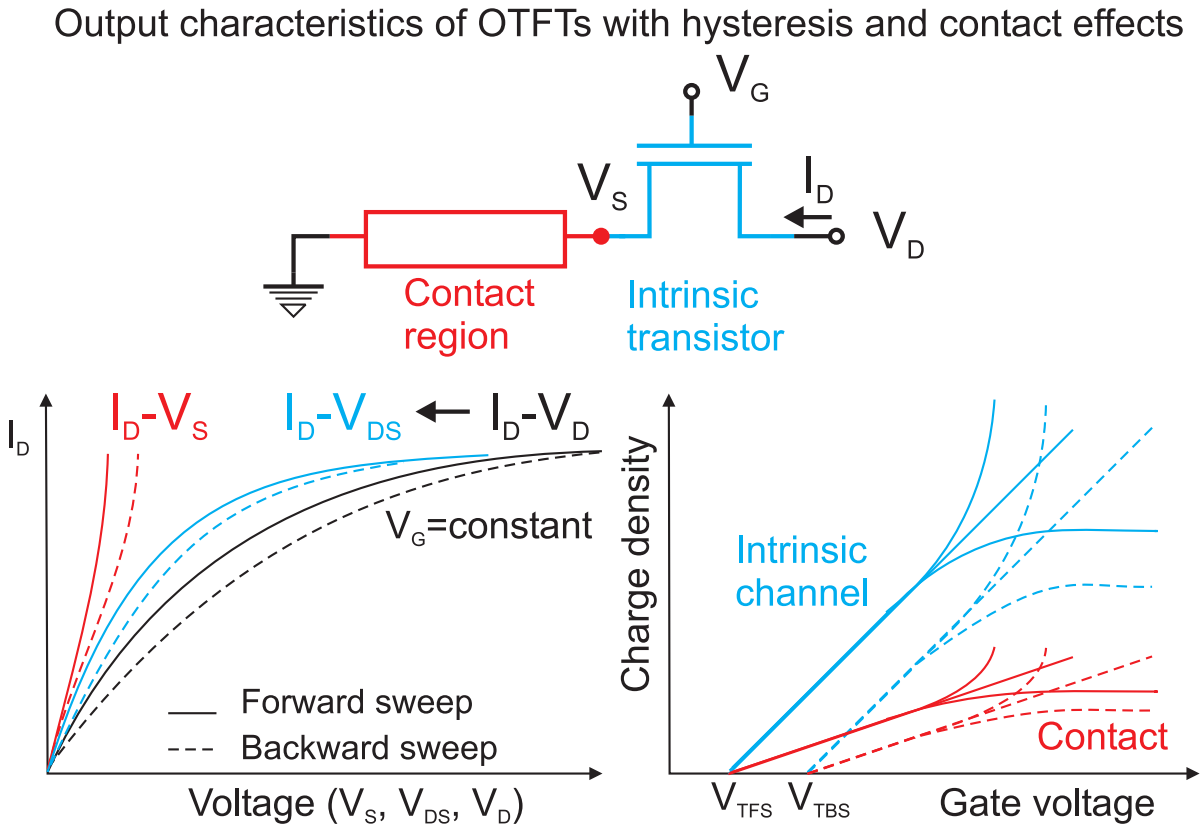

Figure 1.9: Graphical summary of the thesis. The figure at the top shows the model of a OTFT with a contact region. The figure at the bottom left shows current voltage curves of OTFTs with hysteresis and contact phenomena. The use of a compact model for the output characteristics of OTFTs allows for the separation of current voltage curves at the contact and in the intrinsic channel. The study of these separated curves allows for the determination of the charge density in the intrinsic channel and in the contact (bottom right). This finally leads to the determination of the variation of trapped charge during voltage cycling.

The figure at the top shows the model of a OTFT with a contact region. The figure at the bottom left shows current voltage curves of OTFTs with hysteresis and contact phenomena. The use of a compact model for the output characteristics of OTFTs allows for the separation of current voltage curves at the contact and in the intrinsic channel. The study of these separated curves allows for the determination of the charge density in the intrinsic channel and in the contact (bottom right). This finally leads to the determination of the variation of trapped charge during voltage cycling. The main objective of this thesis is to carry on a study where all these effects are present simultaneously.

2

Contact effects in compact models of organic thin film transistors

2.1. Introduction

The field of organic/polymeric thin film transistors has been attracting increased attention because they can be used as drive transistors in organic/polymeric light emitting diodes for large area displays, as sensors, and because of their very low-cost manufacturing. While they possess important advantages for low-cost, large-area electronics, displays and sensors, an important limitation is their degraded performance characteristics due to contact effects. In particular, part of drain (and also gate) voltage applied between the drain (or gate) and source terminals of a thin film transistor is lost due to a low conductivity region near the contacts, especially near the source contact region [35]. Many efforts have been devoted in the past to shed light on this phenomenon: to locate the region where the voltage drops near the contact, to relate its effects to physical variables in the transistor, and to introduce its effects in transistor models [37][51][52][53][54][55][56][57][58].

The development of accurate and computationally efficient models is critical to reduce the cycle time between design, manufacturing and characterization. Furthermore, to guide the design process and to explicitly show relationships between material properties and device design and performance, physically-based compact TFT models for emerging thin-film technologies are indispensable [9]. The main interrelated challenges that are studied in this chapter are the following: (a) a proper model for the output characteristics $I_D - V_{DS}$ of a transistor, (b) a proper model for the current-voltage characteristic in the region close to the contact, $I_D - V_C$, and its incorporation in the output characteristics model, and (c) an extraction method of the $I_D - V_C$ curves at the contact and the rest of the model parameters out of the resulting combined model.

In this chapter, we analyse tetrasubstituted zinc phthalocyanine ($ZnPc$) based organic thin film transistors in which contact effects are present. Based on experimental data measured on these transistors and from other authors' measurements, we critically evaluate some of the most important previous efforts in modelling $OTFTs$. The results of extracting the voltage drop at the contacts from these models are compared. Some of them are mainly useful when transistors with different channel lengths are available [59][60][61]. Others are strictly valid for linear current-voltage ($I_D - V_C$) responses in the contact [3]. Others, although valid to interpret nonlinear contact effect, offer an exclusive circuit vision of the problem [62].

We incorporate a model for the $I_D - V_C$ curves at the contact [4][63] in a recently proposed generic FET model [9]. We propose a method to extract the voltage drop at the contact ($I_D - V_C$ curves) for single length transistors showing both linear and non-linear responses in the low drain-voltage regime of their output characteristics. From the analysis of the voltage drop at the contacts with the gate voltage, a relation of the ratio of free charge density to the total charge density with the gate voltage is deduced.

2.2. Material. Zinc phthalocyanine-based transistors

In this chapter, we focus on experimental data of zinc phthalocyanine-based transistors. They were measured by our collaborators in Brunel University. Measurements taken by other authors in transistors with different organic materials are analysed as well. The active semiconducting materials in the OTFTs under test are as-deposited and annealed spun films of 2,9(10),16(17),23(24)-(13,17-dioxanonacosane-15-oxy)phthalocyaninato zinc(II) derivatives ($ZnPc$) (Fig. 2.1). The compound is liquid crystalline at a relatively low temperature of 11.5 ^{o}C. The synthesis and characterisation of this compound were reported in a previous publication [64]. The source and drain electrodes are Au (50 nm thick)/Ti (10 nm thick) films. The transistor configuration is bottom gated. The substrate is n-silicon (100) wafer. The gate dielectric is thermally grown SiO_2 with thickness t_{ox}=250 nm. Transistors of 10 μm channel length, L, 1 mm width, W, and 150 nm organic-film thickness, t_{ox}, have been analysed. The relative dielectric constant is assumed ϵ_r=3 in the semiconductor film [65]; similar values are also reported for other organic materials [4][31]. The electrode work function is considered around 5.14 eV, and the $HOMO$ and $LUMO$ levels for the organic film are 3.34 and 5.28 eV respectively [65].

2.3. DC models

Fig. 2.2(a) and (b) show experimental output characteristics measured in $Au-ZnPc$ bottom gated transistors at V_{GS} = 0, -10, -20, -30 and -40 V (symbols). Lines represent the fitting with the simple crystalline field-effect-transistor model ($c-FET$):

(2.1)

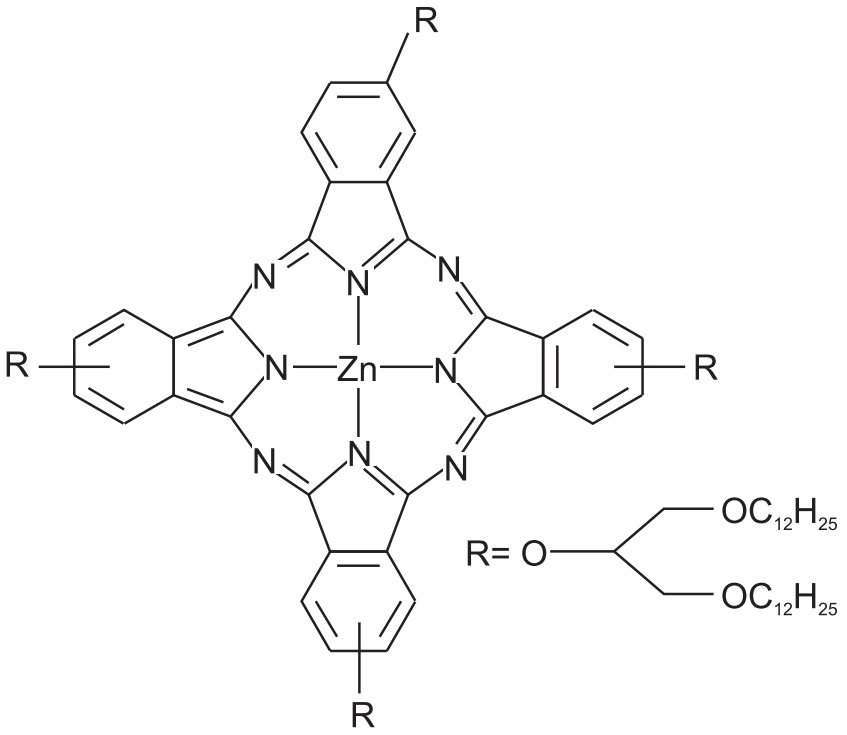

Figure 2.1: Active semiconducting material analysed in the work: 2,9(10),16(17),23(24)-(13,17-dioxanonacosane-15-oxy)phthalocyaninato zinc(II) derivatives [65].

$$
\begin{aligned}
I_D &= \frac{w\mu_o C_i}{L}(V_{GS}-V_T)V_D - (\frac{V_D^2}{2}); V_D \leq (V_{GS}-V_T) \\
I_D &= \frac{w\mu_o C_i}{2L}(V_{GS}-V_T)^2; V_D \geq (V_{GS}-V_T) \\
k &= \frac{w\mu_o C_i}{L} \\
C_i &= \frac{\varepsilon_i}{t_i}
\end{aligned}
$$

where $C_i = \varepsilon_i/t_i$ is the gate insulator capacitance per unit area, ε_i is the insulator dielectric constant, t_i is the insulator thickness, V_T is the threshold voltage, μ_o is the mobility at zero electric field and w and L is the width and length of the organic material in the transistor, respectively. The drain current is defined as positive when entering the drain terminal Fig. 2.3(a). The similarity of the output characteristics of $OTFTs$ with the $I_D - V_D$ curves in $c-FETs$ and amorphous thin-film transistors $a-TFTs$ has been observed and explained in the past [66][1]. The fitting of experimental and theoretical curves in the saturation region produces the following parameters: $k = 3.7 \times 10^{-13}\mathrm{A/V}^2$

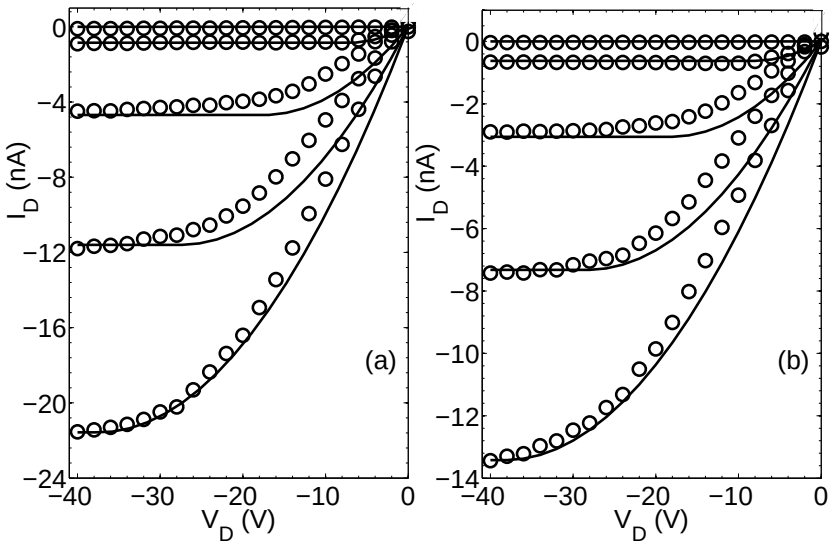

Figure 2.2: Output characteristics of Au-ZnPc bottom gate transistors at V_{GS} = 0, -10, -20, -30, and -40 V (from top to bottom). Symbols represent the experimental data. Lines represent the fitting with the simple c-FET model without contact effects. (a) Annealed $ZnPc$ k=3.7 $\times 10^{-13}$ A/V^2 and V_T= -2.52 V; (b) as-deposited $ZnPc$ k=1.8 $\times 10^{-13}$ A/V^2 and V_T = -1.73 V

and $V_T = -2.52$ V for Fig. 2.2(a) and $k = 1.8 \times 10^{-13}$A/V^2, and $V_T = -1.73$ V for Fig. 2.2(b). It is clear that the fitting is not good in the linear region of the curves. We can see that the experimental data are displaced several volts. A voltage drop at the contacts can explain this.

Apart from the contact effects, there are other significant differences between organic and $c - FETs$, although a similarity in the current - voltage and other characteristics in these transistors exists [1]. The extraction of the mobility from the linear region ($k = 2.3 \times 10^{-13}$ A/V^2 and $k = 1.4 \times 10^{-13}$ A/V^2 for Figs. 2.2(a) and (b), respectively) produces lower values than in the saturation region . Clearly, contact effects are reducing the apparent mobility extracted in the linear region. We can find in the literature different models that incorporate the voltage drop at the contacts, and associated methods to extract this voltage drop from the output characteristics of a transistor. This is not a trivial task because the contact effects interfere with other dependences in $OTFTs$ [1]. The total source-drain voltage, V_{DS}, can be assumed split into a channel component, $V_{DS'}$, and a voltage drop at the contact, $V_C = V_{S'S}$ Fig. 2.3(a). This model takes into account that part of the external drain-source voltage is lost at low conductivity regions

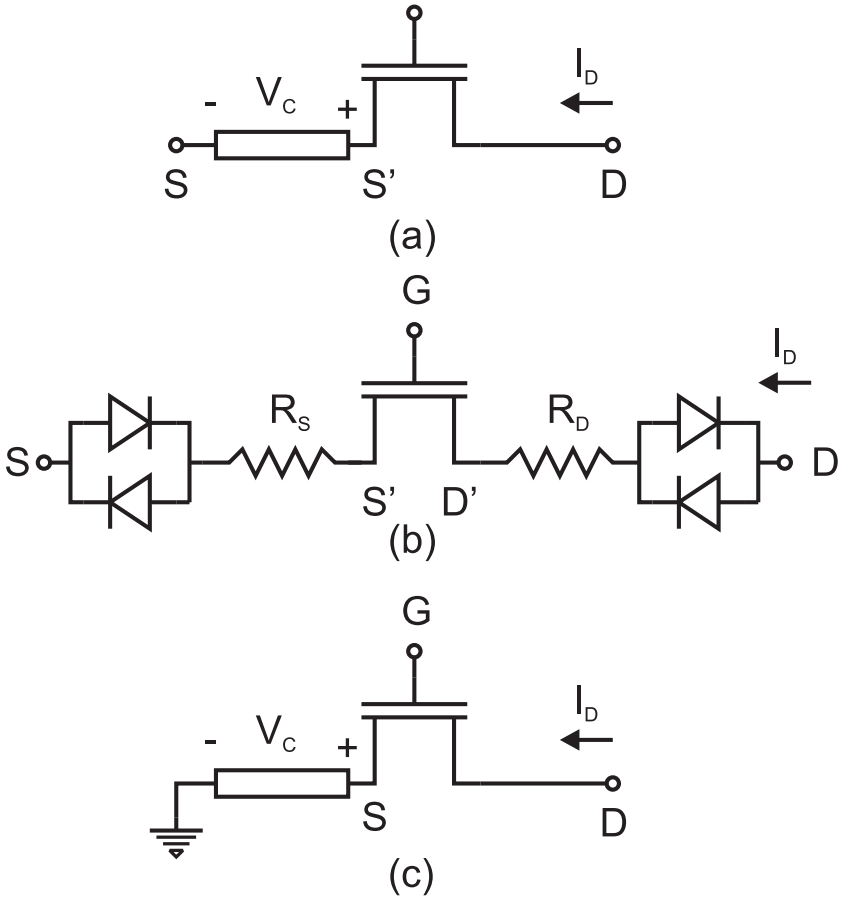

Figure 2.3: a) Equivalent circuit of a bottom contact TFT including a voltage drop at the source contact V_C. V_{DS} is the extrinsic drain voltage. b) Equivalent circuit of the bottom contact TFT including non-linear source and drain contact resistances [62]. c) Equivalent circuit of a bottom contact TFT including a voltage drop at the source contact V_C

near the contacts.

However, this voltage drop V_C is located in the injecting contact (source). No voltage drop is considered at the extracting contact (drain). The reason is that the voltage lost at the extracting contact is much less important than the voltage lost at the injecting one, as supported by scanning potentiometry [35] and is therefore ignored. By using the gradual channel approximation in the intrinsic channel and after integration of the potential along the channel, the current of $OTFTs$ is obtained as [59][39]:

$$I_D = -\frac{kL}{L - x_C}((V_{GS} - V_T)(V_{DS} - V_C) - (\frac{{V_{DS}}^2}{2} - \frac{{V_C}^2}{2})) \tag{2.2}$$

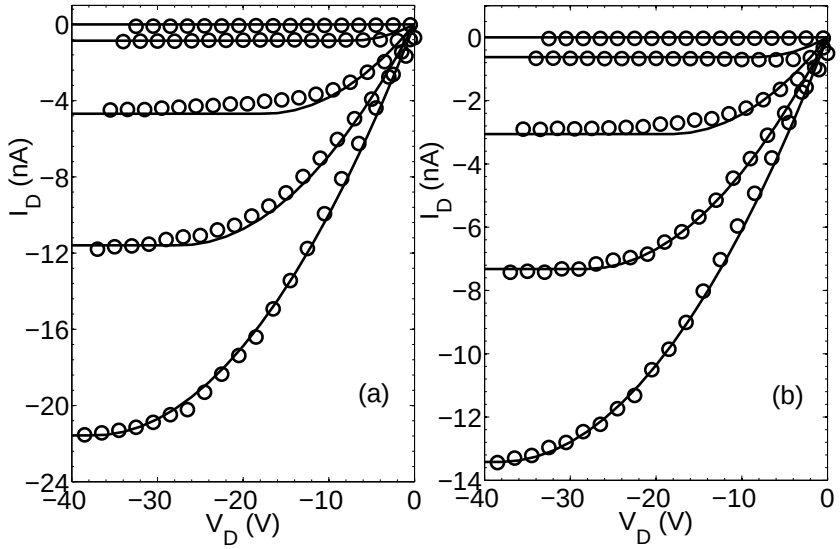

Figure 2.4: Output characteristics of an Au-ZnPc bottom gate transistor at V_{GS} = 0, -10, -20, -30, and -40 V (from top to bottom). Symbols represent the experimental which are displaced around $n \times 1.5$ V where n= 5, 4, 3, 2, 1 for V_{GS} = 0, -10, -20, -30, and -40 V, respectively. Lines represent the fitting with the simple c-FET model without contact effects. (a) annealed samples, k=3.7 $\times 10^{-13}$ A/V^2 and V_T= -2.52 V; (b) as-deposited samples, k=1.8 $\times 10^{-13}$ A/V^2 and V_T = -1.73 V

$$V_{DS} = V_{DS'} + V_C, \alpha \equiv \frac{V_C}{V_{DS}}$$

where x_C is the width of the low conductivity region at the contact. This model is especially useful in identically processed transistors with different channel lengths (but the same channel width) [59][60][61]. This characterization technique, however, has two limitations. One is that a series of devices with different channel lengths, but otherwise identical, has to be available. Another is the channel transport properties in different devices might not be exactly the same. In such cases, alternative characterization techniques with variable gate biasing can be found in the literature [31][67][36]. Some of these techniques assume α as gate voltage dependant $\alpha = \alpha(V_{GS})$ but independent on V_{DS} [67][36]. That means that V_C is proportional to V_{DS}. For low values of V_{DS} the $(I_D - V_{DS})$ relation in (2.2) reduces to a linear one.

$$I_D = -k(V_{GS} - V_T)(V_{DS}) - (1 - \alpha(V_{GS})) \tag{2.3}$$

Other techniques model the contact effect by a series contact resistance, R_S [31]. The voltage drop across this series resistance modifies the $(I_D - V_{DS})$ relation. At low drain voltages this relation reduces to:

$$\begin{aligned} I_D &= -k(V_{GS} - V_T)(V_{DS} - I_D R_S) \\ &= -\frac{k(V_{GS} - V_T)V_{DS}}{1 - KR_S(V_{GS} - V_T)} \end{aligned} \tag{2.4}$$

Non-linear $I_D - V_{DS}$ relations such as the ones seen for low V_{DS} voltages in Fig. 2.2(a) and (b) are thus no reproducible by such linear expressions in (2.3) and (2.4). Other approaches should be used instead [62]. Necliudov et al. proposed a model in which a gate voltage mobility is:

$$\mu = \mu_{oo}((V_G - V_T)/V_{AA})^{\gamma}; \gamma > 0 \tag{2.5}$$

and highly non-linear drain and source contact series resistances are taken into account. In order to simulate non-linear $I_D - V_{DS}$ output characteristics for organic bottom contact $TFTs$, they proposed an equivalent bottom contact TFT circuit that consists of the TFT with linear source and drain access resistances R_D and R_S , respectively, and a pair of anti-parallel leaky Schottky diodes connected to each access resistor in series, see Fig. 2.3(b). Two diodes in parallel are needed to obtain a symmetric current-voltage characteristic. The diode non-ideal factor, η, which is responsible for the steepness of the current voltage characteristic, and the access resistances are the fitting parameters. There, $V_{DS} = V_{D'S'} + R_S I_D + R_D I_D + 2V_{diode}$. The idea of a gate voltage dependent mobility ($\mu \propto (V_G - V_T)^{\gamma}, \gamma > 0$) is based in theories such as the charge drift in the presence of tail-distributed traps ($TDTs$) [68] or variable range hopping (VRH) [69][70].

Another approach where this gate voltage dependent mobility was incorporated can be seen in [9]. In that work, authors propose a generic analytical model for the current voltage characteristics of organic thin film transistors $OTFTs$ [9] Fig. 2.3(c).

$$\begin{aligned} I_D \frac{L}{w} &= \frac{\mu_o C_i}{\gamma + 2}[(V_G - V_T - V_S)^{\gamma+2} - (V_G - V_T - V_D)^{\gamma+2}] \\ k_o &= \frac{\mu_o C_i w}{L} \end{aligned} \tag{2.6}$$

where V_G and V_T are the gate bias voltage and the threshold voltage, respectively. The result is equivalent to the well known and widely used generic FET model with a constant mobility. It is derived considering a voltage drop between the external source terminal and the internal source ($V_S \equiv V_C$) and the mobility μ is written according to the aforementioned common theoretical result [68], and [69] or [71],

$$\mu = \mu_o(V_G - V_T - V_x)^\gamma$$

where V_x is the potential in the semiconducting film of the TFT.

Assuming the values of k_o, γ and V_T are known, a value for V_C can be found from an experimental drain current. Thus complete $I_D - V_C$ curves can be extracted from experimental output characteristics $I_D = I_D(V_G, V_D)$. The extraction of the $I_D - V_C$ curves requires the previous determination of k_o, γ and V_T. The authors that proposed this generic drift model also proposed an extraction method to determine these parameters. It consists of a several step process [72] developed on identically processed transistors with different channel lengths (but the same channel width). It is similar to the model with a constant mobility in (2.2). By choosing the correct value for k_o, it makes all the $I_D - V_C$ curves extracted from the different transistors to coincide. Thus, the usefulness of this extraction method is reduced to situations where several devices with different channel lengths, but otherwise identical, are available. In any case, prior to the determination of k_o, proper parameter extraction techniques are required to determine V_T and γ in (2.6)[73]. As mentioned in the introduction, the voltage drop at the contact region seriously affects the extraction of these and other parameters. Unless there is a method that eliminates these effects, an iterative procedure should be more convenient. Moreover, it would be very useful to find a simple and physically based model for the $I_D - V_C$ relation at the contact in order to introduce this model in a previous generic FET model. It should employ as few parameters as possible, in order to maintain the compactness of the receiver generic FET model. In this chapter, we have chosen (2.6) to incorporate the contact effects in, as it allows for an easy implementation and modification. Other details of the versatility of this model can be found in [1]. Our purpose is that the resulting model, after the incorporation of the contact effects, has parameters that can be characterized relatively easily, or even guessed, preventing unnecessary phenomenological fitting parameters. This is done in the following sections.

2.4. Contact model

For the contact region a functional model of the carrier injection $V_C = V_C(I_D)$, developed in [4][36] is initially used:

$$V_C = V_{injection}(I_D) + V_{redox}(I_D) + V_{drift}(I_D) \tag{2.7}$$

The model takes into account different physical chemical mechanisms that take place at the contact: carrier injection through the barrier, $V_{injection}$, ion formation at the interface (redox reactions), V_{redox} , and charge drift in the low conductivity region of the organic material at the contact, V_{drift}. The expressions for the different components in (2.7) are detailed in [63]. For low values of the energy-barrier height (cases expected in well designed transistors), (2.7) is reduced to $V_C \approx V_{drift}(I_D)$. It is shown in [36] that the voltage drop associated with the charge drift depends on the free charge density at the interface, $p(0)$:

$$\begin{aligned} V_{drift} &= \frac{2}{3}\left(\frac{2J}{\varepsilon\mu\theta}\right)^{\frac{1}{2}}\left([x_C + x_p]^{\frac{3}{2}} - [x_p]^{\frac{3}{2}}\right) \\ x_p &\equiv \frac{J\theta\varepsilon}{2e^2\mu[\theta p(0)]^2} \end{aligned} \tag{2.8}$$

where $J = I_D/S$ is the current density, ϵ is the permittivity of the organic material, μ is the mobility of the carriers, q is the ratio of free to total charge density, x_C is the length of the contact region in the organic material, and the characteristic length x_P is defined as the point from the contact interface towards the organic film, at which the charge density $p(x_p)$ decays to $p(0)/\sqrt{2}$. (*Note*: Please, be aware that the notation x_p and x_C have the same meaning similar to those defined in [36]. In Ref. [4], L and x_C were used instead of x_C and x_p, respectively). Eq (2.8) shows two asymptotical trends [36]. If the characteristic length x_p is a few times larger than the contact length x_C, Eq. (2.8) tends to Ohm's law:

$$I_D \approx qSp(0)\mu\theta V_C/x_C \equiv V_C/R_C \tag{2.9}$$

A non-linear relation between the current and voltage in the drift term occurs when the characteristic length x_p is much smaller than the contact length x_C and Eq. (2.8) reduces

to the Mott–Gurney law [74][26]:

$$I_D \approx (9/8)\varepsilon\mu\theta S V_C^2/x_C^3 \equiv M \times V_C^2 \tag{2.10}$$

These linear and quadratic behaviours are present in experimental data. An example of this can be seen in poly (3-hexylthiophene) $OTFTs$ with different source and drain electrodes, Cr and Au, (Fig. 2 in [75]). The existence of different metallic electrodes produces different contact voltage curves, showing these linear or non linear responses. Transitions from linear to quadratic regimes can be seen not only by changing the electrodes but also with the same electrode and varying the injection regime. This transition can be seen in Fig. 3 in [76], where current voltage curves for hole injection into $P3HT$ through Au are represented. The inclusion of the $I_D - V_C$ relations (2.9) or (2.10) in the generic model (2.6) adds a new parameter to the model. Drawing current curves $I_D = I_D(V_D, V_G)$ knowing the set of parameters (V_T, k_o, M or R) is an easy task. However, extracting these parameters from experimental output characteristics is a major problem. There are well established parameter extraction techniques for $FETs$ that can be used to extract the parameters in (2.6). An appropriate technique is proposed in [73], by the so called H_{VG} function, which extracts the values of γ and threshold voltage V_T from the linear operation regime of the $OTFT$. The H_{VG} function is the ratio of the integral of the drain current over the gate bias divided by the drain current. The corresponding equation for the H_{VG} function derived from the TFT generic model (2.6) is:

$$\begin{aligned} H_{VG}(V_G) &= \frac{\int_{<V_T}^{V_G} I_D dV_G}{I_D(V_G)} \\ H_{VG}(V_G) &= \frac{1}{\gamma+3}\frac{(V_G - V_T - V_S)^{(\gamma+3)} - (V_G - V_T - V_D)^{(\gamma+3)}}{(V_G - V_T - V_S)^{(\gamma+2)} - (V_G - V_T - V_D)^{(\gamma+2)}} \end{aligned} \tag{2.11}$$

$$\begin{aligned} H_{VG}(V_G) &\approx \frac{(V_G - V_T)}{(\gamma+2)}[1 - R_2(\frac{V_D}{V_G - V_T})], V_D \ll (V_G - V_T) \\ H_{VG}(V_G) &= \frac{(V_G - V_T - V_S)}{(\gamma+3)}, V_D > (V_G - V_T) \end{aligned} \tag{2.12}$$

where $R_2(V_D/(V_G - V_T))$ is the remainder term, that represents the error in approximating $H_{VG}(V_G)$ by the above first order power series. In these equations, as stated in [73], H_{VG}

becomes a linear function of gate overdrive $(V_G - V_T)$ by setting $V_S = 0$, while k_o is cancelled, which is the advantage of the method. However, Eq(2.12) explicitly neglects the effect of the contacts, as V_S is assumed null. That means that the values of V_T and γ may not be correct. To check this fact a hypothetical p-type transistor with the following parameters is considered: $V_T = 4.5$ V, $\gamma = 1$, $V_S = V_C = I_D R$, R varying in the range $(10^2 - 10^8 \Omega)$ and k_o in the range $(10^{-6} - 10^{-12}$ A/V$^2)$. The H_{VG} function, as defined in Eq(2.12), is built, and parameters V_T and γ are determined in the saturation region as recommended in [72].

Fig. 2.5 shows the results of this method. There are ranges of R in which the extracted values for V_T and γ differ significantly from the original ones. A direct and easy-to-implement method like this one, in the absence of contact effects, is clearly altered under the presence of contact effects. Contact effects can really be a bottleneck in the extraction of the main parameter of the transistor. Despite these difficulties, we propose an extraction method in which the advantages of these methods are considered. In the next section, we propose a procedure to extract from experimental $I_D - V_D$ curves, not only the values of V_T and γ, but also the contact voltage V_S, characterized by parameters M or R (Eqs. (2.10, 2.9) and, respectively), and the value of k_o.

2.5. Parameter extraction method

Upgrading a model by the introduction of new physical effects means the incorporation of additional fitting parameters that may not be possible to adjust consistently, or interfere with previous parameters of the model. The interference among parameters can be eliminated by a good initial estimation of some of them. In the case of contact effects, we provide a procedure that initially estimates the parameters associated to the contacts by slightly modifying the ideal $c - MOS$ model. Although the ideal $c - MOS$ model cannot accurately reproduce the complete output characteristics of an $OTFT$, it does provide a good initial estimation of the transistor parameters to be subsequently determined in (2.6), in particular those associated to the contacts. In this section, we define the steps followed to determine the complete set of parameters in (2.6), including the parameter associated to the contact region.

1. Estimation of V_T and k from the ideal $c - MOS$ model in saturation (2.1).

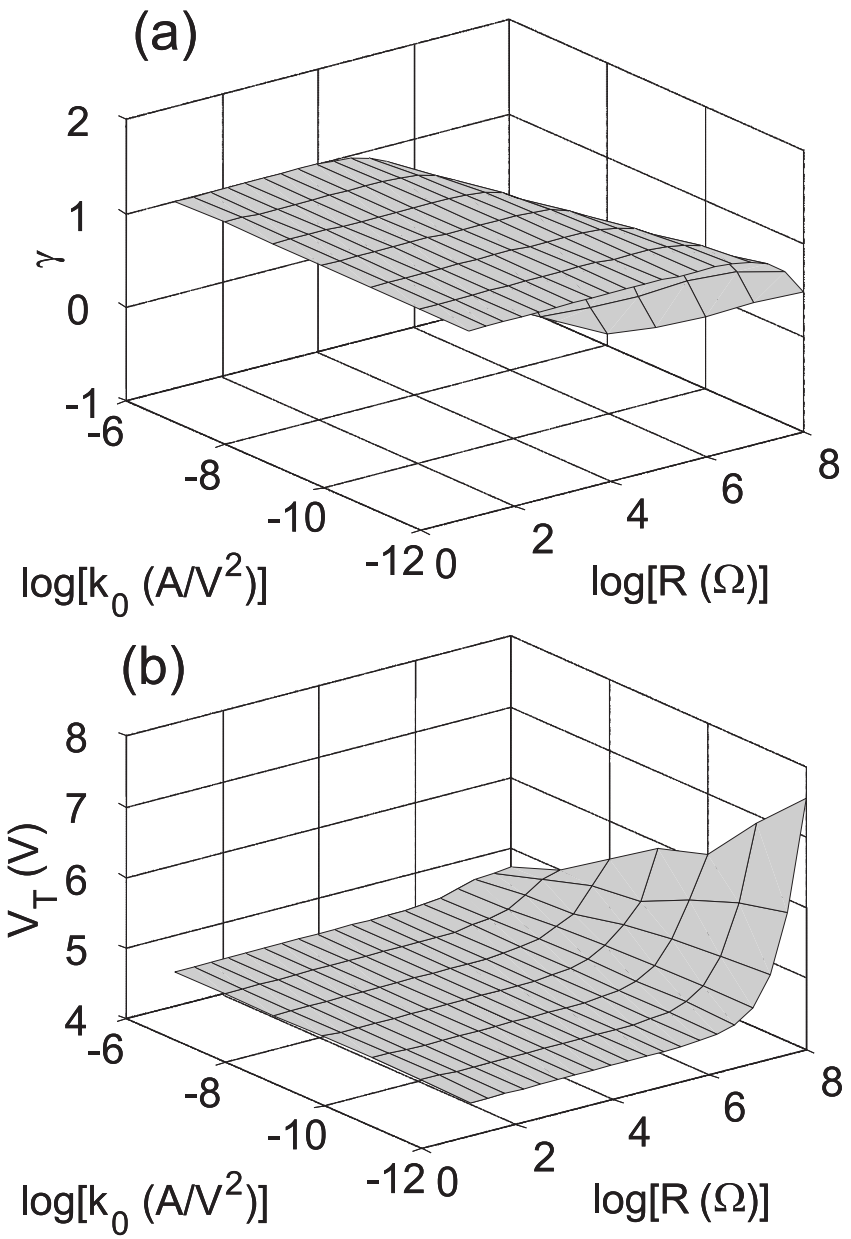

Figure 2.5: a) Extracted μ , and b) extracted V_T from the generic drift model (2.6) using the H_{VG} method [73][72] for a transistor with initial parameters $V_T = 4.5$ V , $\gamma = 1$ and contact effects showing a linear behaviour $V_S = V_C = I_D R_C$. The extracting γ and V_T represented for transistors with different k_o and R. Neglecting the voltage drop at the contact in the H_{VG} function makes the extracted values to differ from the original ones.

2. Estimation of the electric field degradation of mobility by analysing the saturation region of the transistor. Eq. (2.5) is introduced in (2.1) and parameters defining the gate voltage dependent mobility are determined from the saturation region.

3. Estimation of contact parameters (curves $I_D - V_C$: $I_D = M(V_{GS})V_C^2$ or $I_D = V_C/R(V_{GS})$. The drain source voltage is modified in (2.1) by the inclusion of the voltage drop at the source contact. The model is represented in Fig. 2.3(a). For the TFT the usual analytic expression for the MOS transistor can be used:

$$I_D = -k((V_{GS'} - V_T')V_{DS'} - V_{DS'}/2) \tag{2.13}$$

where $V_{DS} = V_{DS'} + V_C$ and V_T' is an internal threshold voltage defined for the intrinsic transistor in Fig. 2.3(a). V_T' can be evaluated as $V_T' = V_T - \overline{V_C(I_{D_{sat}})}$, where V_T is the threshold voltage extracted from the saturation region of the experimental data and $\overline{V_C(I_{D_{sat}})}$ is the average value of the contact voltage evaluated in saturation, $I_D = I_{D_{sat}}$, and different gate voltages. V_T' is not known, as the contact voltage is not known at this step. In a first estimation, the modification of the gate voltage by the contact effects is neglected. It can be checked that this simplified model can reproduce the data in the linear region, where the contact effects are clearly dominant, by assuming $(V_{GS'} - V_T') \sim (V_{GS} - V_T)$ in Eqs. (2.13), (2.7) and (2.9)(or (2.10)). The effect of the contact voltage on the gate voltage is compensated by a modification of the threshold voltage for the intrinsic TFT. The idea of the internal threshold voltage is formally introduced and physically derived in (2.2) (or in (2.6) if the gate voltage dependent mobility is considered). In this work, (2.13) is preferred for an initial estimation of the parameter M (or R). It avoids the mutual interference between the contact parameter M (or R) and the rest. It avoids the need of introducing an intrinsic threshold voltage, V_T', in the $OTFT$ model by the existence of contact effects.

4. Estimation of an average value for the contact voltage V_S in the saturation region. Once the M (or R) parameter is extracted from the experimental data ($M = M(V_{GS})$ or $R = R(V_{GS})$), the average value of the contact voltages evaluated at $I_D = I_{Dsat}$ for different gate voltages can be determined, $V_S = \overline{V_C(I_{D_{sat}})}$.

5. Determination of V_T and γ from the H_{VG} function. The H_{VG} function can be

evaluated introducing this average value for V_S in the saturation region:

$$H_{VG}(V_G) = (V_G - V_T - V_S)/(\gamma + 3) \tag{2.14}$$

Once the effects of the contacts are introduced in this function, V_T and γ can be determined more accurately. The problems associated to the contact effects make the linear region no valid for the determination of such parameters. The saturation region has previously been suggested as the most appropriate region to carry on this characterisation [72].

6. *a*) Final determination of k_o and $M(V_{GS})$ (or $R(V_{GS})$). At this step, values for all the variables appearing in the drift generic model (2.6) have been derived. V_T and γ have been determined by considering the contact voltage and using a technique that eliminates the dependence with k_o (see 2.11). Thus, k_o and M (or R) are the only parameters that require a final adjustment. In this case, Eq. (2.6) is used to find these values by comparing this equation with the experimental data. The parameter k_o mainly affects the saturation region and M (or R) affects the linear region. Thus, these parameters are modified in order to fit the current voltage curves in these respective regions. Slight modifications of these two parameters found this way may be necessary to reproduce the complete set of experimental $I_D(V_D, V_G)$ curves.

   b) Direct extraction of the $I_D - V_C$ curves from (2.6). The objective of this step is twofold: (i) as a test to check the values of the parameters obtained in step 6*a* or (ii) as an alternative step for 6*a* when non reasonable values for γ are obtained in step 5.

      (i) An inspection of Eq. (2.6) shows that with the values of the parameters k_o, V_T, γ and M (or R) and the experimental $I_D(V_D, V_G)$ curves, one can derive $I_D - V_C$ curves at different V_G. These $I_D - V_C$ curves must match the ones obtained in step 6*a* (controlled by Eqs (2.9) and (2.10)). Step 6*b* alone can be used to determine a unique $I_D - V_C$ curve for several devices with different channel lengths, but otherwise identical [59][60][61], as mentioned in the previous section. All the extracted curves must converge into one. However, step 6*b* alone cannot be employed for the case

of a set of single lengths transistors, as convergence is not guaranteed. Steps 1-5 provide such a procedure towards a convergence, towards the physical trend given by Eqs. (2.9) and (2.10). In any case, the extraction of different $I_D - V_C$ curves for different values of k_o, and its comparison with the value of k_o and the curves extracted in step 6*a* are suggested.

(ii) The other situation where this step is necessary is when abnormal values of γ or V_T are obtained in previous steps, despite introducing an estimated value for the contact voltage V_S. A negative value of γ clearly indicates that the characterization needs further processing (see Fig. 2.5(a)). In these situations, convergence in Step 6*a* is not achieved. An iterative procedure is suggested in this step 6*b*. The initial values used for γ, V_T and k_o in this procedure depend on the value of γ estimated in previous steps. The value of the threshold voltage is assumed initially correct. In case the value of γ extracted from step 2 is positive, this should be assumed as an initial estimation. On the contrary, the initial value for γ is assumed zero. For the selected value of γ, k_o is varied until a physical result for the $I_D - V_C$ curves is obtained. If it does not exist the value of γ is increased and k_o is again modified. The values of γ and k_o are alternatively modified until the $I_D - V_C$ curves behave like (2.9) or (2.10). An arbitrary set of values for V_T, γ and k_o, different from the actual solution, produces current voltage curves at the contact with no physical meaning (such as a change of the sign of the contact voltage or strange trends in the $I_D - V_C$ curves). In case, the extracted $I_D - V_D$ curves provide a value of $V_S = \overline{V_C(I_{D_{sat}})}$ different from the one initially estimated in step 5, a new iteration is necessary. A new value for the threshold voltage would be determined in step 5 and step 6*b* would be repeated.

2.6. Application to experimental results

To check the validity of the extraction method for the contact voltage drop and the rest of the basic parameters appearing in the TFT generic model (2.6), we analyse data showing both linear and non-linear effects. We analyse measured $I_D - V_D$ curves in $ZnPc$-based organic thin film transistors and data taken from other authors' experiments.

2.6.1. Non-linear contact current-voltage curves

Experimental data on ZnPc based transistors.

In first place, we analyse the experimental data depicted in symbols in Fig. 2.2(a)and (b). They show a clear non-linear behaviour at low drain voltages pointing out the existence of contact effects. Considering the values of the $HOMO$ and $LUMO$ levels for the organic film and the electrode work function given above, the energy barrier of the $Au - ZnPc$ contact can be considered small enough to prevent current to flow through it. The current is thus dominated by the drift term. Due to the high non-linearity of the $I_D - V_D$ curves, the current-voltage relation at the contact is modelled by (2.10). The extraction procedure detailed in the previous section can be followed in Fig. 2.6.

We initially consider that the values of the mobility (assumed gate voltage dependent) and threshold voltage are extracted by fitting the experimental data in the saturation region with the ideal $c - MOS$ model: $V_T = -2.52$ V, $\gamma = -0.0224$, $V_{AA} = 24.4$ V and $\mu_{oo} = 1.8 \times 10^{-6}$ cm^2/Vs for the transistor of Fig. 2.2(a) and $V_T = -1.7$ V, $\gamma = -0.03$, $V_{AA} = 24.4$ V and $\mu_{oo} = 4.4 \times 10^{-6}$ cm^2/Vs for the trnasistor of Fig. 2.2(b). The result of these fitting (steps 1 and 2) can be seen in Fig. 2.2(a) and (b). If the contact effects are introduced in the ideal MOS model (step 3) a good agreement between the experimental data (symbols) and the combined expression resulting from (2.10) and (2.13) (solid lines) is seen in: Fig. 2.6. The values of M introduced in (2.10) to achieve such an agreement are M =(1.2, 1.5, 1.66, 5.0, 1.5)$\times 10^{-10}$ A/V^2 for V_{GS} =0, 10, 20, 30 and 40 V, respectively, for the transistor of Fig. 2.6(a), and M =(1.0, 1.2, 1.2, 4.0, 9.5)$\times 10^{-10}$ A/V^2 for V_{GS} =0, 10, 20, 30 and 40 V, respectively, for the transistor of Fig. 2.6(b). The contact $I_D - V_C$ curves resulting from these parameters are depicted in dashed lines on the right region of Fig. 2.6(a) and (b). Once we know these curves, the contact voltage can be evaluated in the saturation region for each gate voltage. These points are marked with the tips of the dashed arrows in Fig. 2.6(a) and (b). An average value $V_S(average) \approx -3$ V and -4 V for Fig. 2.6(a) and Fig. 2.6(b), respectively, are obtained from these points (step 4).

The fifth step corresponds to the determination of V_T and γ from the H_{VG} function, once a value for the contact voltage in the saturation region has been estimated. The analysis of the H_{VG} function provides the following values: ($\gamma = 1.026$ and $V_T = 10.51$ V) and ($\gamma = 0.8$ and $V_T = 13$ V) for the transistors in Fig. 2.7(a) and (b), respectively. Very different values for the threshold voltage are obtained in comparison to the ones

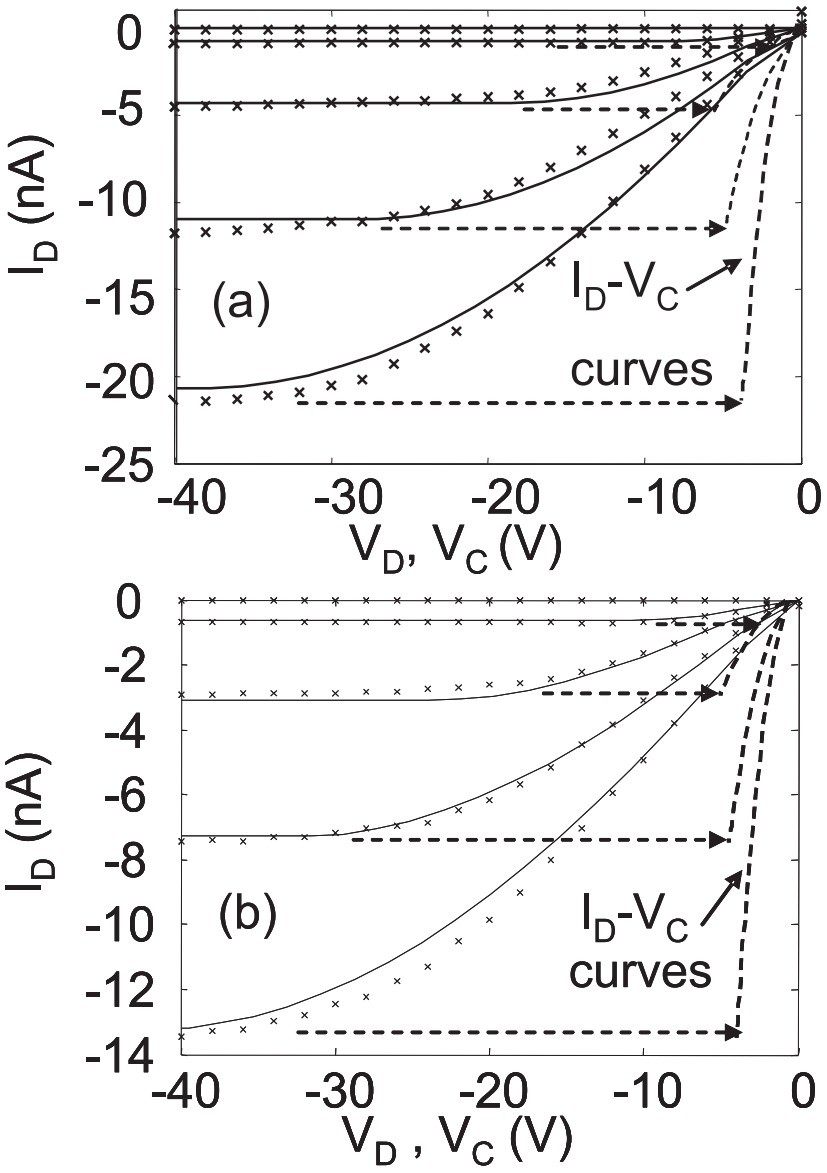

Figure 2.6: Comparison of output characteristics of two $Au - ZnPc$ bottom gated transistors measured at $V_{GS} = 0$, -10, -20, -30 and -40 V (from top to bottom in symbols) with the theoretical results obtained at our fitting procedure. Fitting with the ideal MOS model corrected with the contact effects (Eq. (2.13)). The values of the mobility and threshold voltage are extracted from the saturation region. The mobility is considered gate voltage dependent, following expression (2.5); (a) $V_T = -2.52$ V, $\gamma = -0.0224$, $V_{AA} = 24.4$ V and $\mu_{oo} = 1.8 \times 10^{-6}$ cm^2/Vs; (b) $V_T = -1.7$ V, $\gamma = -0.03$, $V_{AA} = 24.4$ V and $\mu_{oo} = 4.4 \times 10^{-6}$ cm^2/Vs. The current-voltage curves at the contact are modelled with the parameter $M(V_{GS})$. The parameter M is extracted by fitting the experimental data in the linear region; (a) M =(1.2, 1.5, 1.66, 5.0, 1.5)$\times 10^{-10}$ A/V^2; (b) M =(1.0, 1.2, 1.2, 4.0, 9.5)$\times 10^{-10}$ A/V^2 for $V_{GS} = 0$, -10, -20, -30 and -40 V, respectively). The dashed curves on the right of each figure represent the current-voltage curves at the contact evaluated with the previous M parameter. The tips of the dashed arrows point out the value of the contact voltage evaluated in the saturation region for each gate voltage. An average value of $V_{S_{average}} \approx -3$ V and -4 V are obtained for (a) and (b), respectively

.

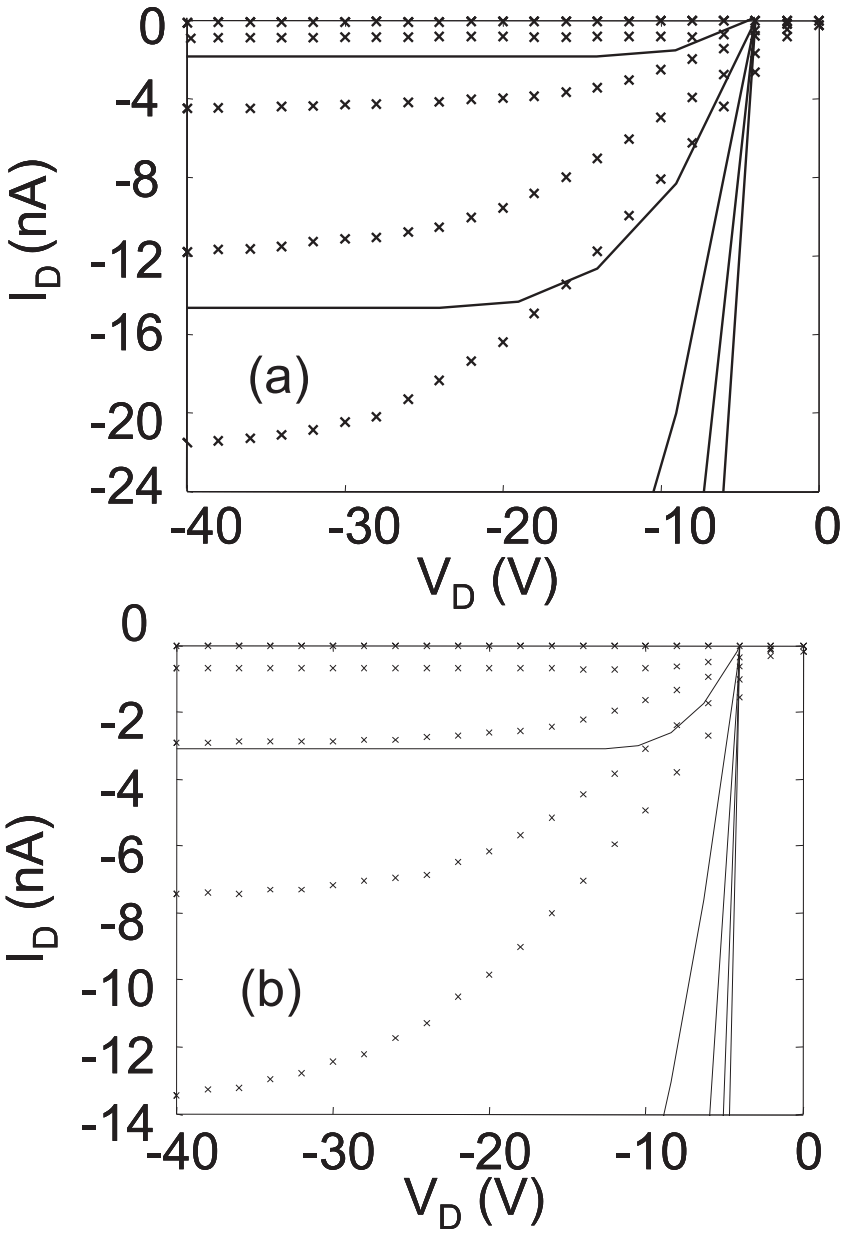

Figure 2.7: Comparison of output characteristics of an $Au - ZnPc$ bottom gated transistor measured at V_{GS} = 0, -10, -20, -30 and -40 V (from top to bottom in symbols) with the theoretical results obtained at our fitting procedure. Fitting with the generic drift model (2.6). This equation is evaluated with the following parameters. Parameters V_T and γ are determined with the H_{VG} function (2.12) including the contact effects $V_S = V_{S_{average}}$ ($\gamma = 1.026$, $V_T = 10.51$ V, $\gamma = 0.8$, $V_T = 13$ V for a and b, respectively); the value of μ_o is the one calculated from the saturation region with the ideal MOS model ($\mu_o = 1.8 \times 10^{-6}$ and 4.4×10^{-6} cm^2/Vs for a and b, respectively); and $V_S = 0$. The last two parameters make the theoretical result to disagree with the experimental curves.

extracted in step 1. Figs. 2.7(a) and (b) illustrate the comparison of the experimental data with the generic drift model (2.6) using the values of these last two parameters, the value of μ_o determined from the saturation region with the ideal $c-MOS$ model ($\mu_o = 1.8 \times 10^{-6}$ for Fig. 2.7(a)) and (4.4×10^{-6} cm^2/Vs for Fig. 2.7 (b)), and $V_S = 0$. It is apparent that the mixture of values of parameters extracted from different models and ignoring the contact effects produce such a disagreement.

A change of the value of the mobility to 1.8×10^{-7} cm^2/Vs and 1.7×10^{-7} cm^2/Vs for Figs. 2.8(a) and (b), respectively is necessary in order to fit the experiments in the saturation region (Fig. 2.8(a) and (b)). In these figures, V_S is maintained null in order to highlight this fact. Finally, the contact effects, by means of the parameter M in (2.10), are introduced in the generic drift model (2.13). The combined model fits the experimental data for the following set of values: M =(0.2, 0.8, 1.42, 3.32, 4.02)$\times 10^{-10}$ A/V^2 in Fig. 2.9(a), and M =(0.3, 10, 0.7, 1.2, 5.0, 9.5)$\times 10^{-10}$ A/V^2 in Fig. 2.9(b) for V_{GS} =0, -10, -20, -30 and -40 V, respectively. A unique value for M should be expected for a compact model. However, the compactness of this parameter is justified below by its relation with the charge density in the intrinsic channel.

The analysis of the values of the different parameters extracted in the six steps shows that the variations in V_T and γ (from the initial estimations to the final results) are very significant, while the parameter M is practically unaffected by when using either the ideal $c-MOS$ model or the generic drift model, both in combination with our contact model. On the one hand, the generic drift model is physically well based. However, the inclusion of new parameters in it makes their extraction more difficult. On the other hand, the use of simple models like the one propose in (2.13), although based on approximations, are really helpful in finding a proper initial estimation of the contact $I_D - V_C$ curves. This is necessary to proceed with the determination of the exact values of the parameters appearing in (2.6).

The current-voltage curves at the contact can be directly extracted from (2.6) once the parameters μ_o, γ and V_T are known [72]. These curves, for the as-deposited ZnPc transistor of Fig. 2.2(b), can be seen with symbols in Fig. 2.10. The values of these parameters correspond to the ones extracted with our procedure in the previous paragraphs. The inset of Fig. 2.10 shows the comparison of the experimental data with (2.6) including these current voltage curves. The agreement is clearly better than the one shown in Fig. 2.9(b). However, the current voltages curves extracted with our procedure (shown

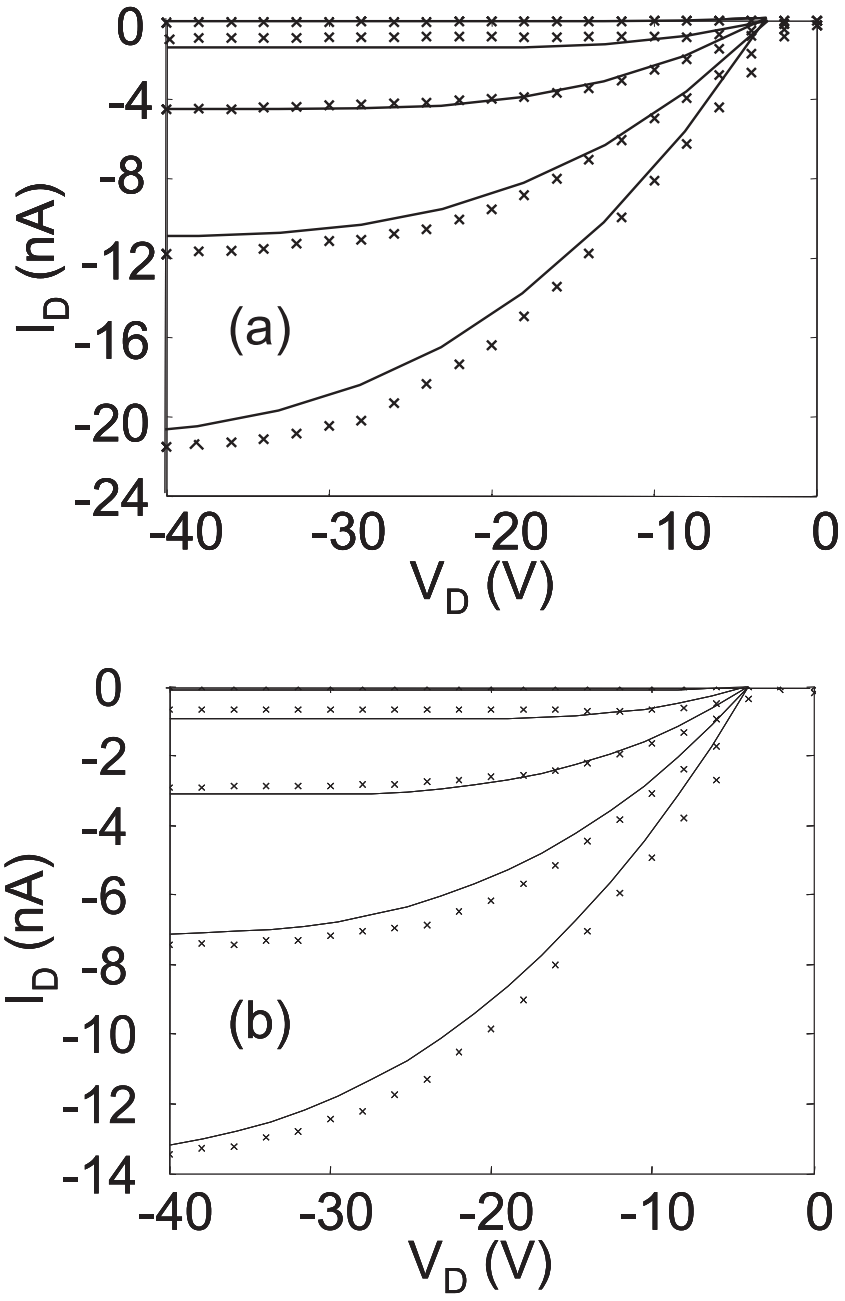

Figure 2.8: Comparison of output characteristics of an $Au - ZnPc$ bottom gated transistor measured at V_{GS} = 0, -10, -20, -30 and -40 V (from top to bottom in symbols) with the theoretical results obtained at different steps of our fitting procedure. Fitting with the generic drift model (2.6) changing the parameter μ_o to 1.78×10^{-7} cm^2/Vs and 1.7×10^{-7} cm^2/Vs for a and b, respectively; V_S is maintained null.

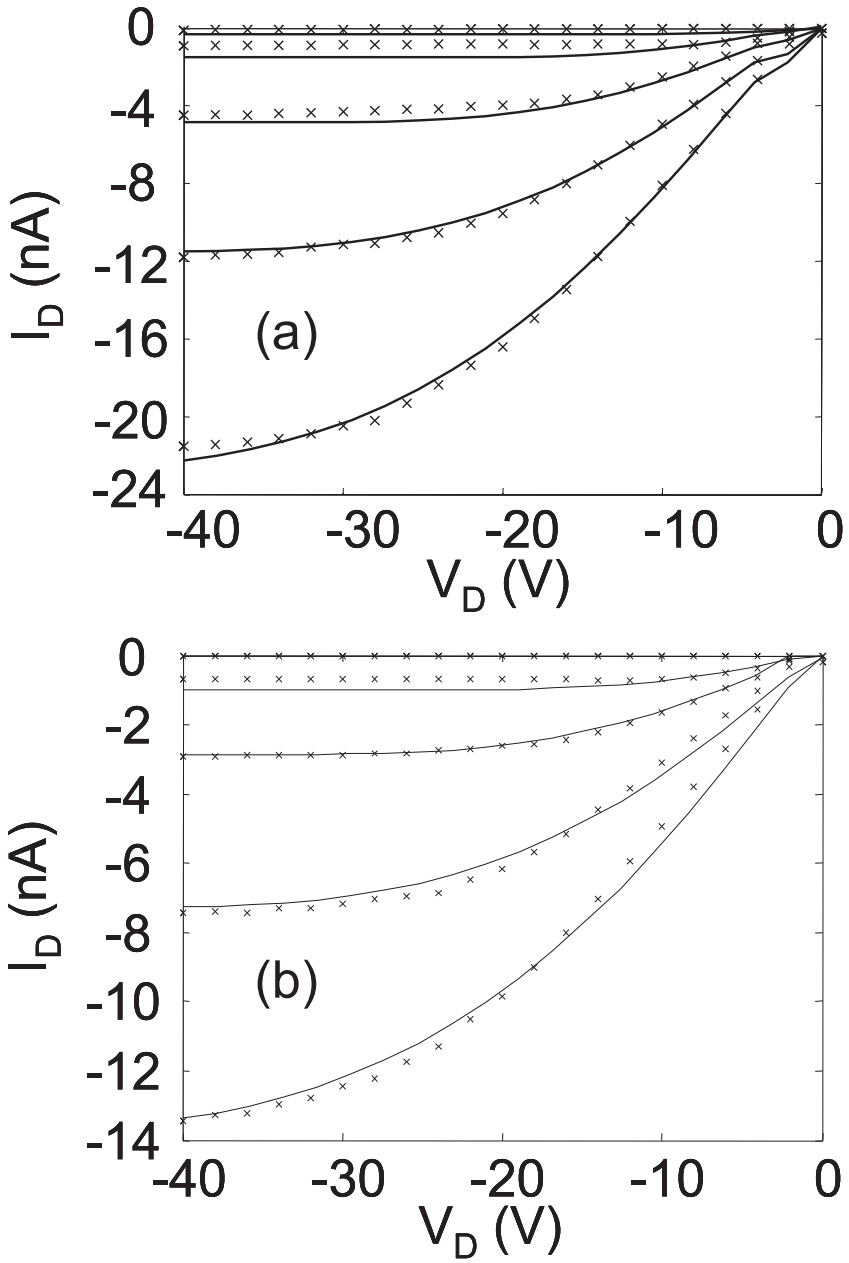

Figure 2.9: Comparison of output characteristics of an $Au - ZnPc$ bottom gated transistor measured at V_{GS} = 0, -10, -20, -30 and -40 V (from top to bottom in symbols) with the theoretical results obtained at different steps of our fitting procedure. Fitting with the generic drift model (2.6) introducing the contact effects. μ_o does not change. The extracted M parameter are: a)M=(0.5, 0.8, 1.4, 2.52, 4.029)$\times 10^{-10}$ A/V^2 and b) M=(0.3, 0.7, 1.2, 5.0, 9.5)$\times 10^{-10}$ A/V^2 for V_{GS} = 0, -10, -20, -30 and -40 V, respectively. Despite the large modification of the values of V_T and μ_o along the different steps of this procedure, the values of the parameter M associated to the contact voltage suffer almost no variation. That means that the use of single models, like the one propose in (2.13), helps finding a proper estimation of the contact $I_D - V_D$ curves.

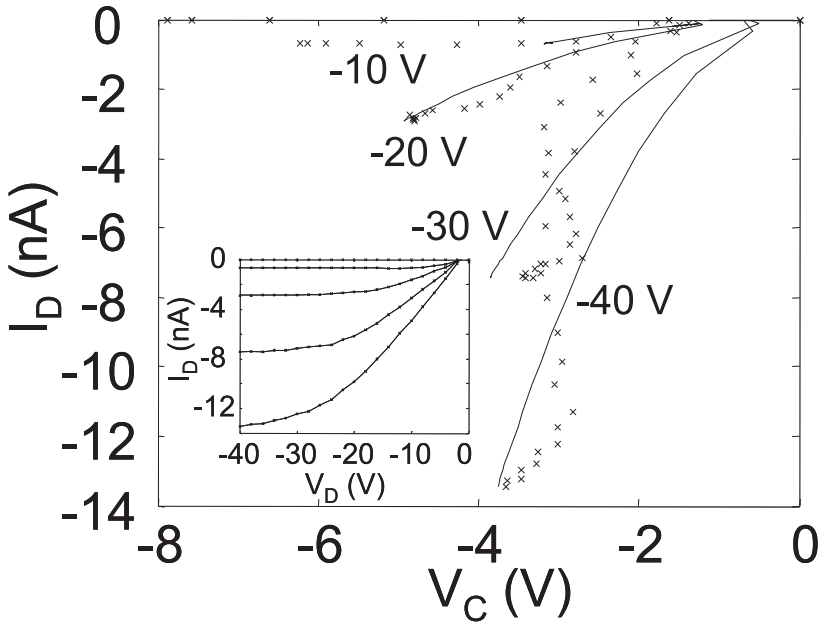

Figure 2.10: Current voltage curves at the contact extracted from the experimental output characteristics of the as-deposited ZnPc transistor of Fig. 2.2(b) at different gate voltages with our procedure (solid lines) and directly from the generic drift model (2.6) (symbols). The parameters employed in the calculation correspond to the final ones obtained in 2.6. Inset: Comparison of output characteristics of an $Au - ZnPc$ bottom gated transistor measured at V_{GS} =0, -10, -20, -30 and -40 V (from top to bottom in symbols) with the theoretical results from (2.6) using the $I_D - V_C$ curves shown in symbols in the main Figure.

as solid lines in Fig. 2.10) provide a physical trend and a way to interpret the ones shown as symbols.

Analysis of other experimental data.

Experimental data measured in an Au-pentacene $BC - TFT$ by other authors [62] are also reproduced by our model. Fig. 2.11 shows a comparison of the experimental data (symbols) with the generic drift model (2.6) in which the contact current-voltage relation (2.10) has been incorporated (solid lines). The transistor has the following characteristics: the SiO_2 gate-dielectric thickness is $t_{ox} = 290$nm, the gate length is $L = 20$ μm and the gate width $w = 220$ μm.

The model parameters have been extracted using the procedure detailed in the previous section. This is a case where the value of γ extracted in step 5 shows an abnormal

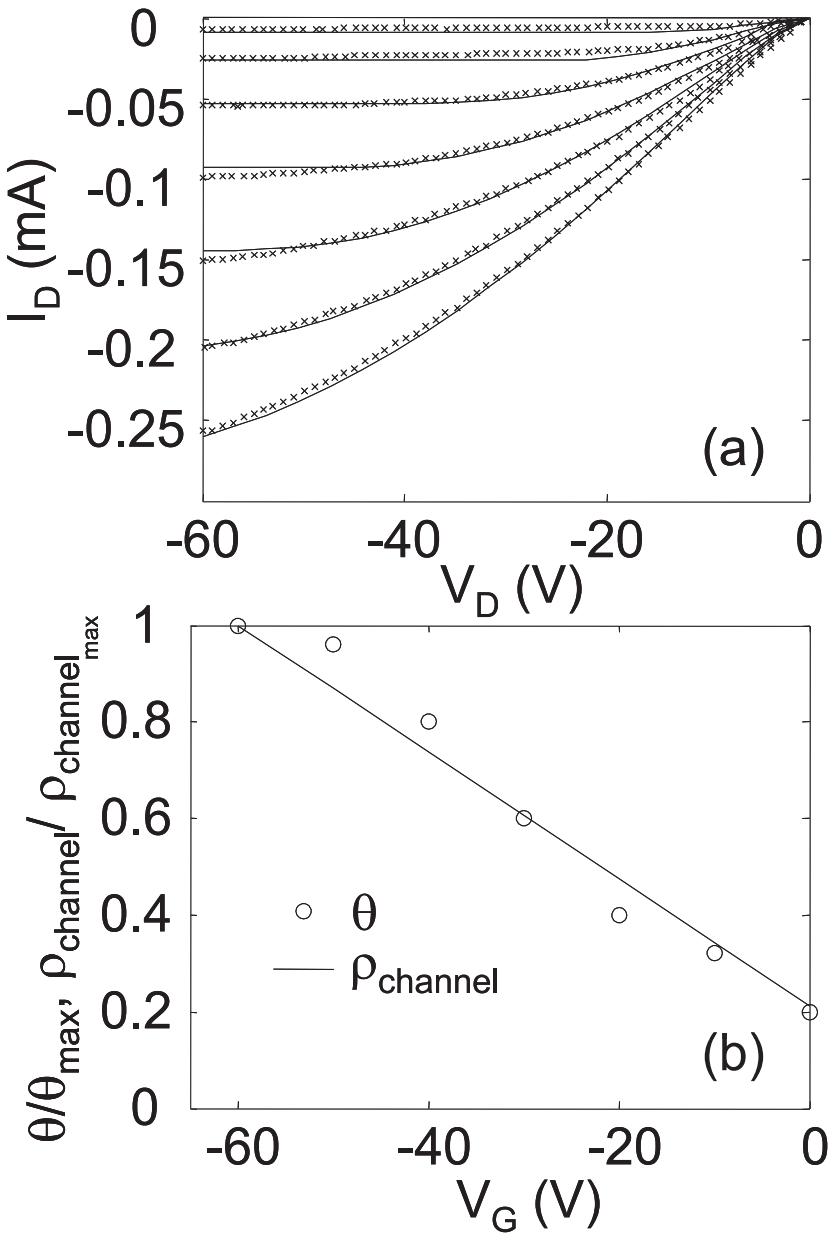

Figure 2.11: a) Comparison of output characteristics of an Au-Pentacene bottom gated transistor at V_{GS} =0, -10, -20, -30, -40, -50 and -60 V from top to bottom (symbols) with the generic drift model (2.6) including non-linear contact effects (2.10) (solid lines). The dimensions of the transistor are $t_{ox} = 290 \times 10^{-7}$ cm, $w = 220 \times 10^{-4}$ cm, $L = 20 \times 10^{-4}$ cm. The parameters used in the model, determined according to the method detailed in this work, are $k = 7.78 \times 10^{-8}$ A/V^2, $\mu_o = 0.19$ cm^2/Vs, $V_T = 17.3$ V, $\gamma = 0.118$, M =(0.5, 0.8, 1.0, 1.5, 2.0, 2.4, 2.5)$\times 10^{-6}$ A/V^2 for V_{GS} = 0, -10, -20, -30, -40, -50 and -60 V, respectively. b) Normalized values of the charge density in the channel, ρ, and free to total charge density ratio θ in the low conductivity region near the contact. The values of θ are extracted from the previous values of M and its definition in (2.6). The normalization values are: $\rho_{max} = 3.4 \times 10^{18}$ cm^{-3} and $\theta_{max} = 0.06$. The charge densities in the channel and in the contact region are correlated meaning that the values of M extracted by our procedure are acceptable.

value despite including the contact effects, $\gamma = -0.4$. In this situation, step 6*b* was followed instead of step 6*a*. The value of γ extracted by analysing the saturation region with the ideal $c - MOS$ model (2.1) in combination with the electric field degradation of the mobility (2.5) was used instead, γ= 0.118. The value of the threshold voltage was determined in step 5 by means of the H_{VG} function applied to the generic drift model (2.6). The parameters obtained after the fitting procedure are: $k_o = 7.78 \times 10^{-8}$ A/V^2, $\mu_o = 0.19$ cm^2/Vs, $V_T = 17.3$ V, $\gamma = 0.118$, M =(0.5, 0.8, 1.0, 1.5, 2.0, 2.4, 2.5)$\times 10^{-6}$ A/V^2 for V_{GS} = 0, -10, -20, -30, -40, -50, -60 V, respectively. Situations analysed in Fig. 2.6 and Fig. 2.11 shows the need to employ the advantages of simple models (although not exact ones) and to combine them in a precise sequence. The objective is to determine correct values for the transistor parameters that appear in a more compact and precise model, such as the one in (2.6).

Another feature of our model and its associated extraction procedure is that they allow us to determine the parameter M defined in (2.10). From this parameter, we can determine the evolution of the free to total charge-density ratio θ, with the gate voltage. Assuming the same value for the mobility in the transistor channel and in the low conductivity region at the contact, this ratio varies from 0.012 at $V_{GS} = 0\ V$ to 0.060 at $V_{GS} = -60\ V$. The values of θ, necessary to fit the experimental data with our model (Fig. 2.11(a)), are represented as a function of the gate voltage in Fig. 2.11(b) (circles). In this figure, we also represent the values of the charge density in the intrinsic channel, estimated according to the equation (solid line) [77],

$$\rho_{channel} = C_i(V_G - V_T)/t_o \tag{2.15}$$

where t_o is the thickness of the organic material.

The evolution of the ratio of free to total charge density with the gate voltage is in excellent agreement with the evolution of the charge density in the channel. This agreement validates the physical model we propose for the DC characteristics of organic $TFTs$ affected by contact effects.

The non-linear behaviour shown at low drain voltages in the experiments of Fig. 2.6 and Fig. 2.11 can also be reproduced by diodes in series with a resistance connected at the source and drain terminals (Fig. 2.3(b)). Good agreements between the experimental data and this model are obtained. For the experimental data in Fig. 2.6, the values of the

model parameters in Fig. 2.3(b) that achieve the best fit are $\gamma = -0.032$, $\mu_o = 2.65 \times 10^{-4}$ cm^2/Vs, $V_{AA} = 25.0$ V, $R_{D,S} = 10^4$ Ω, energy barrier at the interface $\phi_B = 0.65$ eV and non-ideality factor of the diode $\eta = 5$. For the experimental data in Fig. 2.11, the values of the model parameters that achieve the best fit are $\gamma = 0.118$, $\mu_o = 0.2$ cm^2/Vs, mobility evaluated at $V_{GS} = -60$ V, $\mu = 0.27$ cm^2/Vs, $V_{AA} = 5.70$ V, $R_{D,S} = 5$ kΩ, energy barrier at the interface $\phi_B = 0.65$ eV and non-ideal factor of the diode $\eta = 2.5$. Although the model in Fig. 2.3(b) can reproduce the experimental data, the values of the resulting parameters should be analysed with care, especially when high values of the non-ideal factor of the diodes and/or negative values of γ are extracted. The advantage of our model (Fig. 2.3(c)) is its physical approach to the real mechanisms affecting the low conductivity region near the contacts [35][4].

2.6.2. Linear contact current-voltage curves

Current-voltage $I_D - V_D$ curves showing linear responses at low drain voltages have also been studied in this work. Here, we apply the procedure from the previous section to extract the mobility, threshold voltage and the contact voltage drop from the output characteristics of poly($3 - hexadecylthiophene$)($P3HDT$) transistors [36] (symbols in Fig. 2.12(a)). The solid lines correspond to the evaluation of the generic drift model (2.6) in which the linear contact voltage-current model in (2.9) has been incorporated. The values of the contact resistances $R = R(V_G)$ and the rest of the model parameters are detailed in the same figure. A good agreement is observed between the experiments and the theoretical results. The extraction procedure followed with these data does not end in step 6a, but goes through step 6b. This is another example where the parameter γ is clearly affected by the contact effects (see Fig. 2.5). In step 5, $\gamma = -0.3$ and $V_T = -4.5$ V are obtained assuming an average value for the contact voltage in the saturation region $V_S = \overline{V_C(I_{D_{sat}})} = -1.5$ V. The value of γ is gradually increased and the value of k_o is modified until the extracted $I_D - V_C$ curves show a perfectly linear behaviour, as expected by the trend of the experimental data at low drain voltages. This occurs for $\gamma = 1.5$ (Fig. 2.12(b)). The value of the threshold voltage needs no modification.

In order to check, that this solution is unique, other pairs of values for γ and k_o are tested. As an example, Fig. 2.13 shows $I_D - V_C$ curves extracted from (2.6) for a lower γ, $\gamma = 0.15$, $V_T = -4.5$ V and different values of k_o, after equating I_D, V_G and

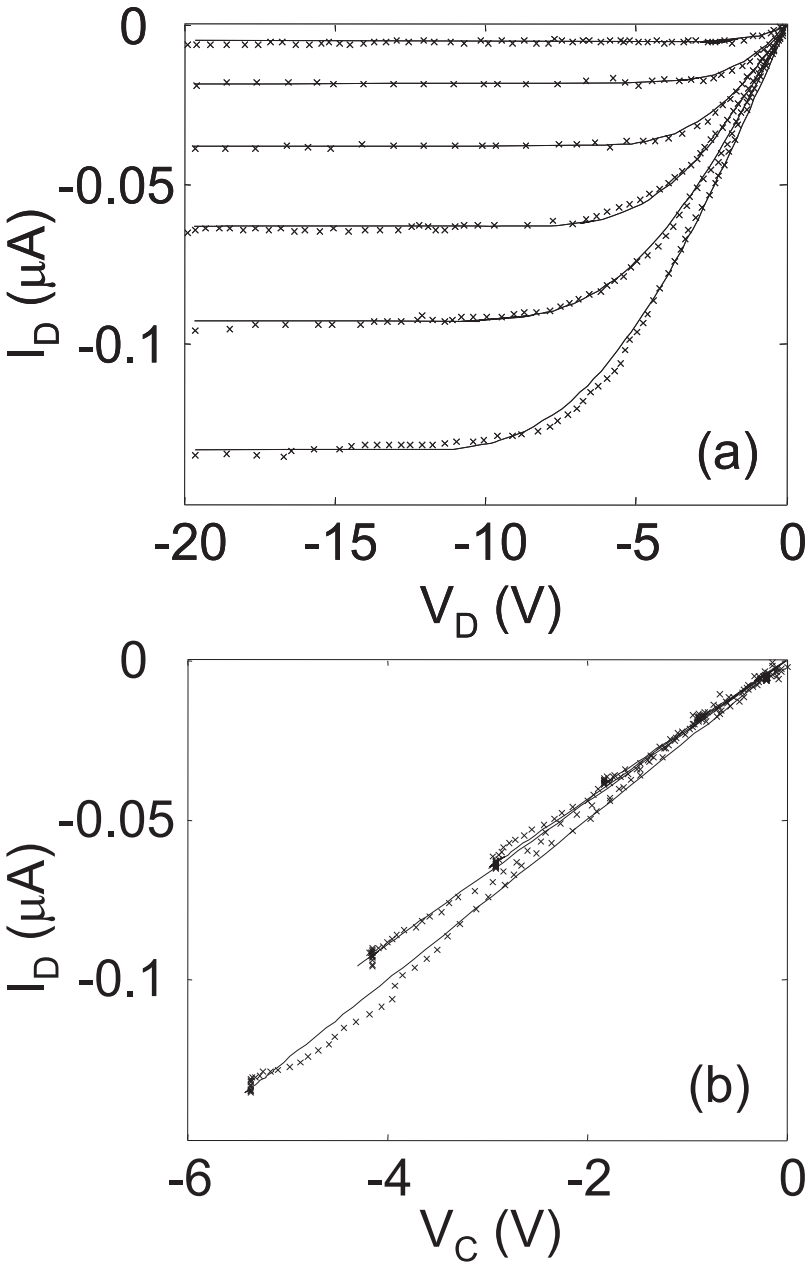

Figure 2.12: a) Output characteristics of an $Au-P3HDT\ BC$ transistor at V_G = -8, -10, -12, -14, -16, and -18 V from the top to the bottom. Symbols represent the experimental data [67] based on material described in [78][79]. Lines represent the fitting with the with the generic drift model (2.6) including linear contact effects (2.9). The details of the samples are: thermally grown SiO_2 ($\sim$ 200 nm), channel width $w = 0.5$ cm (multi-finger configuration), and channel length $L = 10$ μm. The polymer film is 7 nm thick and was deposited by spin coating. The parameters used in the model, determined according to the method detailed in this work, are $k_o = 3\times10^{-8}$ A/V^2, $\mu_o = 1.2\times10^{-5}$ cm^2/Vs, $V_T = -4.5$ V, $\gamma = 1.5$, R =(4.9 , 4.8, 4.7, 4.6, 4.5, 4.0)$\times10^7$ Ω for V_G = -8, -10, -12, -14, -16, and -18 V, respectively. b) Current voltage curves at the contact extracted from the experimental output characteristics at different gate voltages with our procedure (solid lines). The parameters employed in the calculation correspond to the final ones obtained in Fig. 2.12(a). The current voltage curves at the contact extracted directly from the generic drift model (2.6) are shown in symbols.

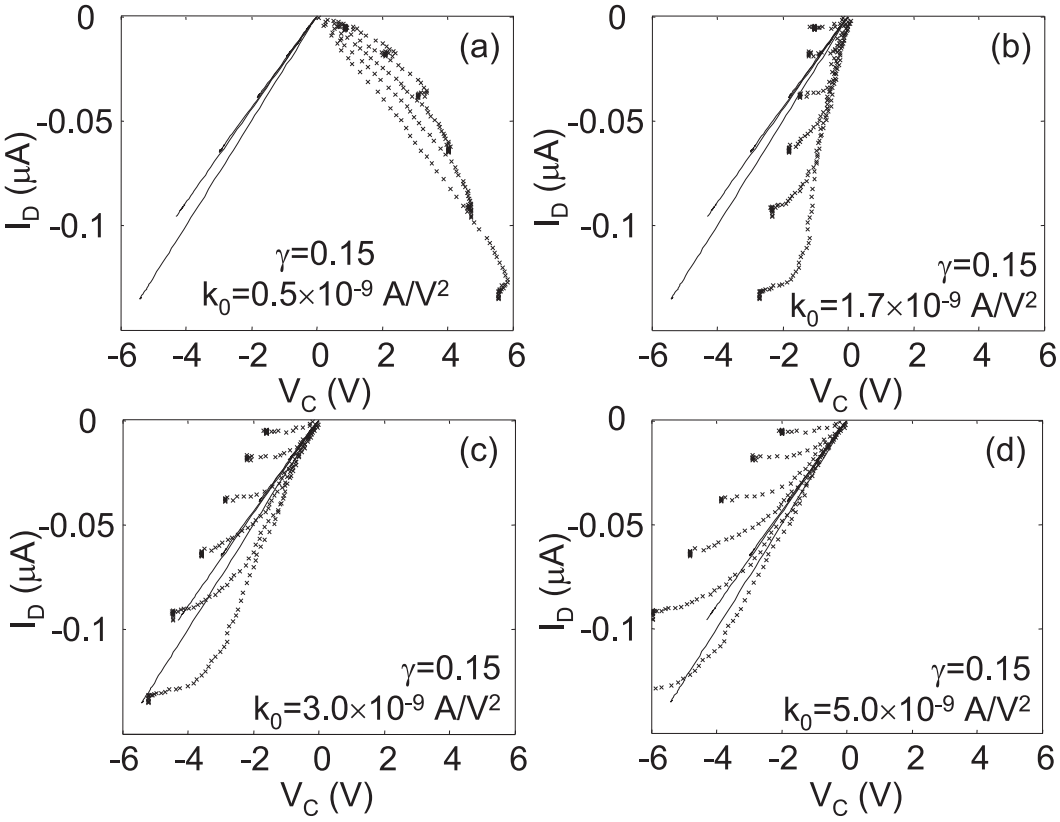

Figure 2.13: Contact current-voltage curves extracted from the experimental data of Fig. 2.12, directly from Eq. (2.6) (symbols) providing this model with the parameter values $V_T = -4.5$ V and γ and k_o given in the figures. The solid lines are used as a reference. They correspond to the final results obtained with our procedure for the $I_D - V_C$ curves (Fig. 2.12). No convergence to a physical acceptable solution is seen when varying the parameter k_o for $\gamma = 0.15$: figures (a) to (d). A similar lack of convergence towards a physical acceptable trend for the $I_D - V_C$ curves is seen for other values of γ, except for the actual solution depicted in Fig. 2.12

V_D to the experimental data (symbols). They are compared to the solution obtained in Fig. 2.12(b). The set of figures shows that there is no acceptable $I_D - V_C$ curve in any case. Fig. 2.13(a) shows positive values for V_C when negative ones are expected. Figs. 2.13(b)-(d) show linear responses at low values of V_C. However, the curves tend to saturate, reflecting the saturation response of the intrinsic channel, not the actual response of the contact region. A similar study was made with different values of γ, showing that the solution depicted in Fig. 2.12 is unique. As seen in these two subsections, the model distinguishes between linear responses and quadratic responses for

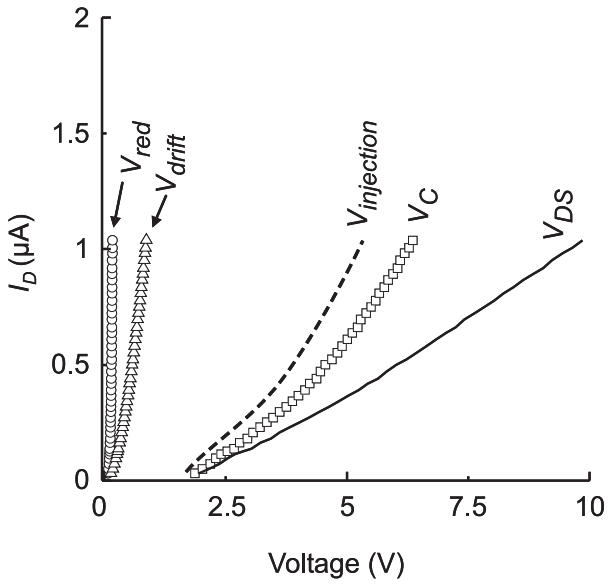

Figure 2.14: Measured output $I_D - V_{DS}$ characteristic in a $Cr/P3HT/Cr$ $OTFT$ [75](solid line). It is shown with the extracted $I_D - V_C$ curve (squares) and the three components of Eq. (2.7) [63], V_{red} (circles), V_{drift} (triangles), and $V_{injection}$ (dashed line).

the current voltage relation at the contact region. Both responses are included under the assumption that the energy barrier at the contact imposes no restriction to the current, *i.e.* under the assumption of space charge limited transport . Therefore, the model is limited to these situations. Outside these limits, when the energy barrier at the interface imposes a restriction to the current, non linear $I-V$ responses are also obtained, however not necessarily quadratic ones (thermionic emission or tunnel injection should be considered (2.7)). An example of this can be seen in Fig. 2.14, where the voltage drop at the contact of an $OTFT$ is the sum of the voltage drop at the space charge region and the voltage necessary to surpass the barrier at the contact (a combination of injection through the barrier and space charge transport). For these cases, the quadratic model can still be used by taking into account that we are working under a second order approximation, and no connection with the physical parameters appearing in (2.10) is possible. In any case, properly designed transistors are expected to use contacts with low energy barriers at the interface in order to reduce the injection-voltage term. Therefore, from this practical point of view, the model can be consider of full applicability.

3

Test of the extraction method

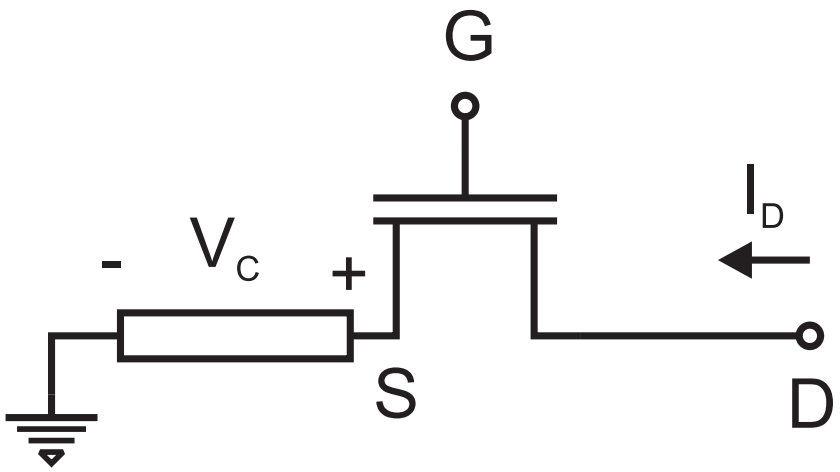

Figure 3.1: Proposed equivalent circuit of a TFT including the voltage drop at the source contact, $V_C \approx V_S$.

3.1. Introduction

The objective of this chapter is to test the procedure developed in Chapter 2 by applying it to output characteristics of a transistor with known parameters. The transistor under test is represented in Fig. 3.1. It consists of an ideal transistor plus contact effects where $V_{DS} = V_D - V_S$. The output characteristics are modelled by:

$$I_D \frac{L}{w} = \frac{\mu_o C_i}{\gamma + 2}[(V_G - V_T - V_S)^{\gamma+2} - (V_G - V_T - V_D)^{\gamma+2}] \tag{3.1}$$

$$I_D = MV_S^2, M = \frac{9}{8}\theta\frac{\varepsilon\mu S}{(x_c)^3} \tag{3.2}$$

We consider a p-type OTFT with the following parameters: $\mu_o = 5.0 \times 10^{-7}$ cm^2/Vs , $\gamma = 0.0$, $V_T = -2.5$ V, $L = 5$ μm, $w = 10$ mm, $C_i = 20.7$ nF we consider non linear contact effects modelled with the parameter M, and the following dependence with the gate voltage: $M(V_{GS}) = 10^{-11} - 3.5 \times 10^{-12} \times V_G(\mathrm{A/V^2})$. The resulting $I_D - V_D$ curves for different V_G are represented with symbols in Fig. 3.2. Our objective is to show that our method is able to recover the value of these parameters from these curves. We only assume as known parameters those associated to the geometry of the device (L, w, C_i).

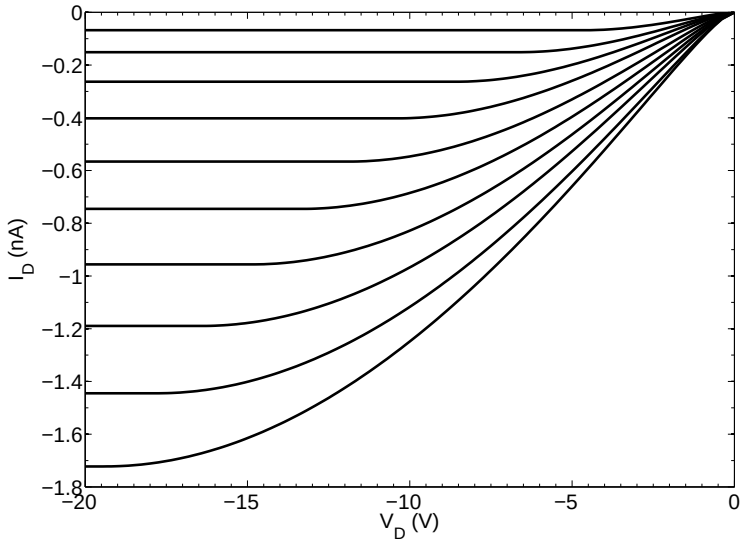

Figure 3.2: $I_D - V_D$ curves at V_G = -6.836, -8.533, -10.173, -11.770, -13.331, -14.797, -16.306, -17.795, -19.265 and -20.721 V, from top to bottom. These curves are calculated with the combination of (3.1) and (3.2) and the parameters defined in the text.

3.2. Test of the method

(i) In first place, we extract the value of μ_o and V_T from the $I_D - V_D$ curves in the saturation regime by using

$$\begin{aligned} I_D &= \frac{w\mu_o C_i}{L}(V_G - V_T)V_D - (\frac{V_D^2}{2}); V_D \leq (V_G - V_T) \\ I_D &= \frac{w\mu_o C_i}{2L}(V_G - V_T)^2; V_D \geq (V_G - V_T) \\ k &= \frac{w\mu_o C_i}{L} \\ C_i &= \frac{\varepsilon_i}{t_i} \end{aligned} \tag{3.3}$$

The result is $\mu_o = 2.7 \times 10^{-7}$ cm^2/Vs, and $V_T = -3.4$ V, clearly differing from the original ones, in particular the threshold voltage.

(ii) The second step consists of extracting the contact voltage from these curves. We combine the relation $V_D = V_{DS} - V_C$ (Fig. 3.1) with (3.2) and (3.3), and compare the result with the output characteristics. To determine the relation of the drain

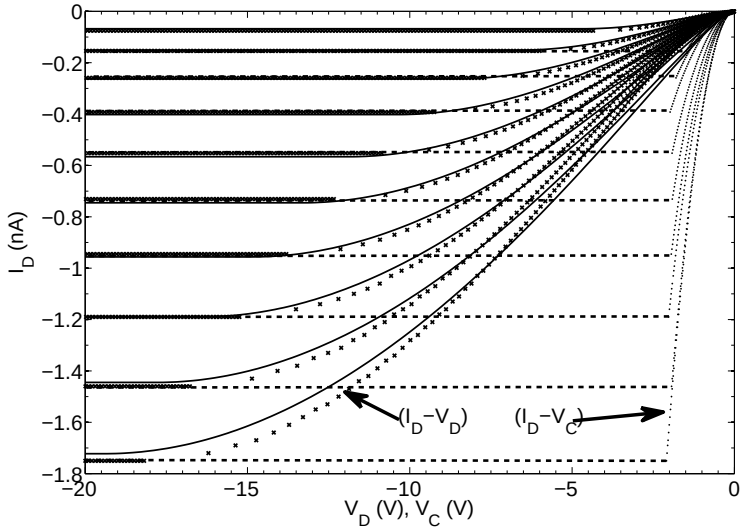

Figure 3.3: Left hand side: Comparison between the experimental curves of Fig. 3.2 (dotted lines on the left) and theoretical $I_D - V_D$ curves (solid lines) at V_G = -6.836, -8.533, -10.173, -11.770, -13.331, -14.797, -16.306, -17.795, -19.265 and -20.721 V, from top to bottom. The experimental data are assumed to be those of an ideal transistor with contact effects as shown in Fig.3.1. The theoretical ones correspond to the combination of (3.2) and (3.3), i.e. neglecting the effect of the contact voltage on V_G ($V_G \approx V_{GS}$). Right hand side: $I_D - V_C$ curves necessary to produce the best fitting between the experimental and theoretical $I_D - V_D$ curves. The parameters M associated to the $I_D - V_C$ curves are shown in the Table 3.1. The horizontal dashed lines indicate the value of the voltage drop at the contact in saturation

voltage with the contact voltage, we estimate the value of M parameters by an iterative procedure. The best agreement is shown in solid lines on the left, in Fig. 3.3. The resulting values of the M parameter are shown in the Table 3.1. The $I_D - V_C$ curves are shown in dotted lines on the right of Fig. 3.3. From the dotted lines in Fig. 3.3 , we can determine the value of V_C in the saturation region for different V_{GS}, V_C ($I_{D_{saturation}}$). Their average value is $V_{C_{average}} = -1.83$ V.

(iii) In a third step, we evaluate the H_{VG} function by integrating the drain current in the saturation regime from the output characteristics:

$$\begin{aligned} H_{VG}(V_G) &= \frac{\int_{<V_T}^{V_G} I_D dV_G}{I_D(V_G)} \\ H_{VG}(V_G) &= \frac{1}{\gamma+3} \frac{(V_G - V_T - V_S)^{(\gamma+3)} - (V_G - V_T - V_D)^{(\gamma+3)}}{(V_G - V_T - V_S)^{(\gamma+2)} - (V_G - V_T - V_D)^{(\gamma+2)}} \end{aligned} \tag{3.4}$$

In the saturation region, the H_{VG} function reduces to

$$H_{VG}(V_G) = \frac{(V_G - V_T - V_S)}{(\gamma + 3)}, V_D > (V_G - V_T) \tag{3.5}$$

Thus we can we can determine the values of γ and V_T, by assuming $V_S = V_{C_{average}}$ in (Eq-6.12). The resulting values are $\gamma = -0.14$ and $V_T = -2.52$ V. The value of the threshold voltage is clearly in agreement with the final result (only an error around 0.8 % is obtained). That means that the assumption made for V_S is appropriate. However, a lower value than expected is obtained for γ. When experimental data are analysed we cannot know whether this result is correct or not. Therefore, a next step is required.

(iv) Assuming this value of γ as correct, we proceed to determine the value of the mobility and M parameters. We use (3.1) and (3.2) to represent $I_D - V_D$ curves and we compare them with the experimental output characteristics. We know γ and V_T from step (iii). The values of parameters μ and M can be initially considered as the ones obtained in steps (i) and (ii), respectively. These two parameters are iteratively modified until a good fitting is obtained between the theoretical and experimental data (solid lines and symbols, respectively, in Fig. 3.4(a). The resulting values are $\mu = 5.8 \times 10^{-7}$ cm^2/Vs and M is given in Table. 3.2.

(v) Once the value of μ_o is determined, we can introduce it in (3.1) and obtain the

Table 3.1: Extracted values after step (ii) of M_{FS} and M_{BS} for the $OTFT$ with output characteristics in Fig. 3.3.

V_G (Volts)	M (A/V^2)
-6.836	50×10^{-12}
-8.533	70×10^{-12}
-10.173	80×10^{-12}
-11.770	100×10^{-12}
-13.331	150×10^{-12}
-14.797	200×10^{-12}
-16.306	250×10^{-12}
-17.795	290×10^{-12}
-19.265	390×10^{-12}
-20.721	400×10^{-12}

Table 3.2: Extracted values of M_{FS} and M_{BS} after step (iv) for the $OTFT$ with output characteristics in Fig. 3.4(a).

V_G (Volts)	M (A/V^2)
-6.836	330×10^{-13}
-8.533	380×10^{-13}
-10.173	420×10^{-13}
-11.770	480×10^{-13}
-13.331	550×10^{-13}
-14.797	600×10^{-13}
-16.306	700×10^{-13}
-17.795	820×10^{-13}
-19.265	930×10^{-13}
-20.721	1030×10^{-13}

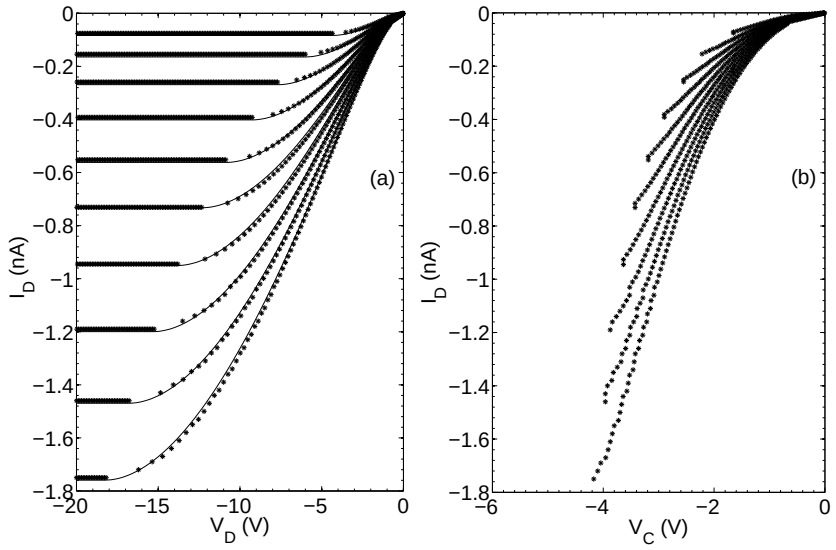

Figure 3.4: a) Comparison between experimental (x) and theoretical $I_D - V_D$ curves calculated with the generic drift model (3.1) (solid lines). $V_T = -2.52$ V, $\gamma = -0.14$ and μ_o and M are iteratively modified until a good agreement is obtained: $\mu_o = 5.8 \times 10^{-7}$ cm^2/Vs and M is in the Table 3.2. V_G is the same as in Fig. 3.2(b)): $I_D - V_C$ curves extracted from (3.1) with the values of the parameters used in (a).

relation $I_D - V_C$ for different gate voltages (Fig. 3.4(b)). We now proceed to test the solution. We expect a quadratic evolution of the drain current with the contact voltage, as seen in (3.2). That means that the slope should always increase when $|V_C|$ increases. In Fig. 3.4(b), we see that at high values of $|V_C|$ the slope starts decreasing and the $I_D - V_C$ curves turn in a clockwise direction, deviating from the physically expected behaviour.

(vi) To obtain a good physical behaviour for $I_D - V_C$ curves, the value of γ is modified. Lower values produce the same non-physical behaviour in the resulting $I_D - V_C$ curves as in Fig. 3.4(b). A higher value than expected one is also tested, $\gamma = 0.29$. The new value of μ_o to obtain a good fitting between experimental and numerical results (Fig. 3.5(a)) is $\mu_o = 2.9 \times 10^{-7}$ cm^2/Vs. The $I_D - V_C$ curves are extracted from (3.1) with the values of these parameters. In this case, the slope of the $I_D - V_C$ curves goes to infinity and then decreases at high values of $|V_C|$ (Fig. 3.5(b)). The $I_D - V_C$ curves turn in a counter-clockwise direction, again deviating from the physically expected behaviour.

Table 3.3: Extracted values of M_{FS} and M_{BS} for the $OTFT$ with output characteristics in Fig. 3.5.

V_G (Volts)	M (A/V^2)
-6.836	478×10^{-13}
-8.533	488×10^{-13}
-10.173	498×10^{-13}
-11.770	508×10^{-13}
-13.331	518×10^{-13}
-14.797	528×10^{-13}
-16.306	538×10^{-13}
-17.795	548×10^{-13}
-19.265	558×10^{-13}
-20.721	568×10^{-13}

The value of γ is iteratively modified until the slope in the $I_D - V_C$ curves always increases with $|V_C|$. In this case, this value is modified between -0.14 and 0.29. The solution is archived for $\gamma = 0$, as expected. The value of the mobility for the best fitting between experimental and numerical data (Fig. 3.6(a)) is $\mu_o = 4.8 \times 10^{-7}$ cm^2/Vs. This

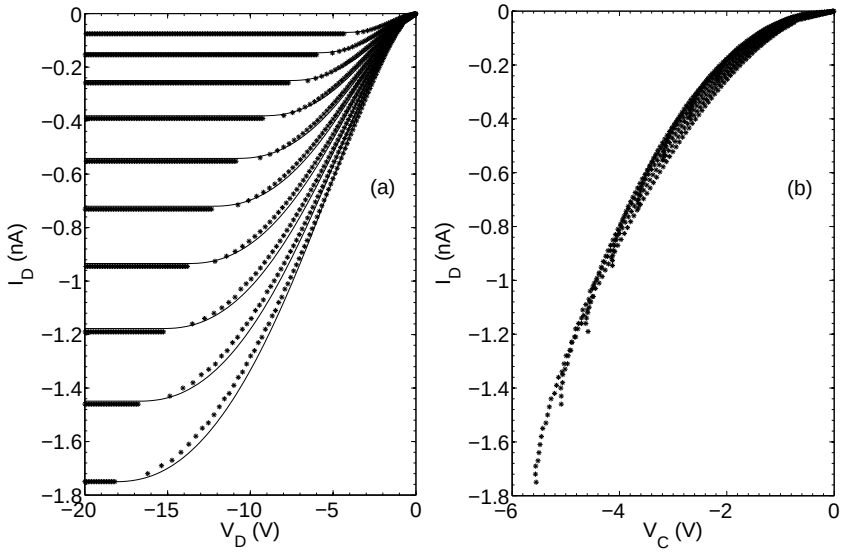

Figure 3.5: Comparison between experimental (x) and theoretical $I_D - V_D$ curves calculated with the generic drift model (3.1) (solid lines). $V_T = -2.52$ V, $\gamma = 0.29$ and μ_o and M are iteratively modified until a good agreement is obtained: $\mu_o = 2.9 \times 10^{-7}$ cm^2/Vs and M is in the Table. 3.2. V_G is the same as in Fig. 3.2(b)): $I_D - V_C$ curves extracted from (3.1) with the values of the parameters used in (a).

value differs only a 4 % in relation to the original one. In Fig. 3.6(b), we show the extracted $I_D - V_C$ curves from (3.1) by using these last values for γ and μ_o. In this case, the curves follow the trend expected in (3.2). Thus, we can conclude that the test to our method is positive.

Table 3.4: Extracted values of M_{FS} and M_{BS} for the $OTFT$ with output characteristics in Fig. 3.6.

V_G (Volts)	M (A/V^2)
-6.836	350×10^{-13}
-8.533	390×10^{-13}
-10.173	430×10^{-13}
-11.770	470×10^{-13}
-13.331	510×10^{-13}
-14.797	550×10^{-13}
-16.306	590×10^{-13}
-17.795	630×10^{-13}
-19.265	670×10^{-13}
-20.721	710×10^{-13}

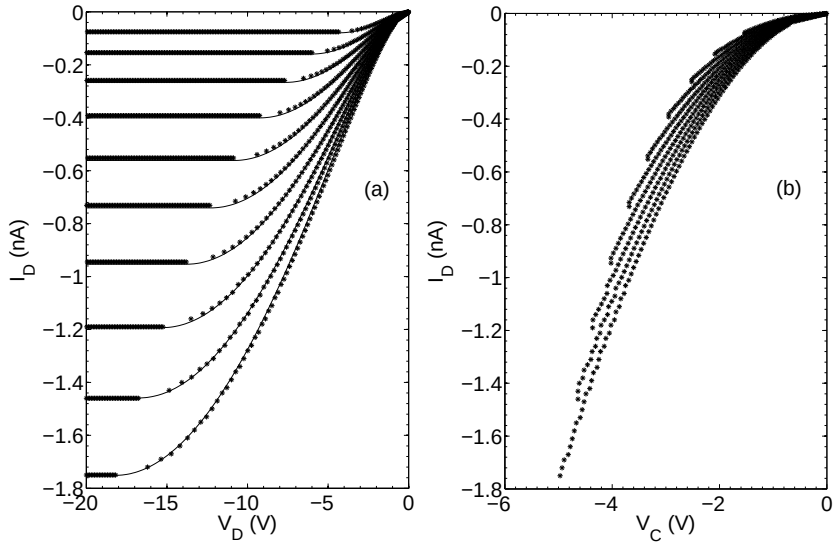

Figure 3.6: Comparison between experimental (x) and theoretical $I_D - V_D$ curves calculated with the generic drift model (3.1) (solid lines). $V_T = -2.52$ V, $\gamma = 0$ and μ_o and M are iteratively modified until a good agreement is obtained: $\mu_o = 4.7 \times 10^{-7}$ cm^2/Vs and M is in the Table 3.4. V_G is the same as in Fig. 3.2(b)): $I_D - V_C$ curves extracted from (3.1) with the values of the parameters used in a).

4

Characterization of $OTFTs$ with hysteresis and contact effects

4.1. Introduction

Trapping and de-trapping mechanisms can cause instabilities that produce changes in the threshold voltage of organic thin film transistors [1][10][80]. They are also the origin of hysteresis in current-voltage curves. The study of the hysteresis is important as it can provide information about the trapped charge in the organic material [10][45][48][50][81][82]. Subsequently, this information can be related to technological parameters with the objective of finding a better device design. Another problem that deteriorates the performance of the organic devices is the effect of the contacts. Part of the voltage applied in these devices is lost in the contact regions [83][84]. There are works devoted to control the barrier of the contact. The use of self-assembled monolayers is extended to achieve this objective [85].

In addition to controlling the barrier at the contacts, we have seen in the previous chapters that appropriate characterization techniques are necessary to determine how the contact region affects the electrical behaviour of the device. The combination of both hysteresis phenomenon and contact effects makes this characterization task more difficult. There are some previous studies that characterize the hysteresis in organic transistors from transfer and output characteristics. In some cases, contact effects are not considered [13]. In other cases, contact effects are eliminated from the experimental data by using techniques, like the four-terminal method, instead of the usual two-terminal one [14].

In this chapter, we propose a method to extract information on the traps influence on the hysteresis mechanisms in current voltage curves obtained with the two-terminal procedure. Moreover, the proposed method solves the difficulty of processing these curves when contact effects are present. The basis underlying this method is the compact model presented in the previous chapters [83][86]. In this part of the work, we analyse experimental current voltage curves taken from the literature that show both contact effects and hysteresis [13][14][87]. The characterization method based on this compact model is applied to these data and information is extracted for the trapped charge in the organic material. The results are compared with other values reported in the literature. The accuracy of our method is checked by comparing our results with the ones obtained from transient measurements [13] or the four-terminal method [14], which also considers the contact effects.

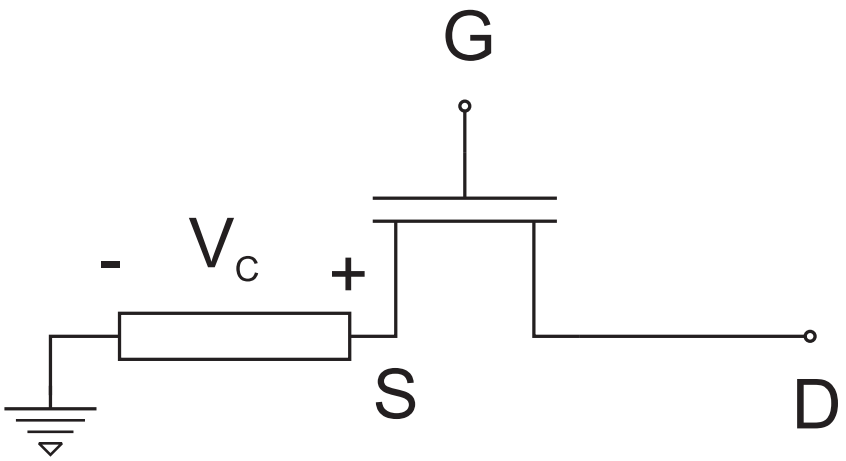

Figure 4.1: Proposed equivalent circuit of a TFT including a voltage drop at the source contact $V_C \equiv V_S$ [86].

4.2. Variation of trapped charge during hysteresis

The hysteresis phenomenon appears in output ($I_D - V_D$) and in transfer ($I_D - V_G$) curves of $OTFTs$. In case no contact effects are present ($V_C = 0$, $V_{GS} = V_G$, $V_{DS} = V_D$, see Fig. 4.1), a way to know the variation of trapped charge is by measuring the difference in drain current between forward (FS) and backward sweep (BS) curves, at certain values of the drain and gate voltages $\triangle I_D(V_{DS}, V_{GS}) = \triangle I_D(V_D, V_G)$, whereas an injection of holes occurs in FS current and the extraction of holes occurs in the BS current [13]. The relation between the variation of the trapped charge $\triangle P$ in the intrinsic channel of a transistor and the current displacement $\triangle I_D(V_{DS}, V_{GS})$ is given by [13]:

$$\Delta P = \frac{\Delta I_D(V_{DS}, V_{GS}) \times L}{q \times w \times V_{DS} \times \mu} \tag{4.1}$$

where q is the elementary charge, μ is the charge carrier mobility, L and w are the channel length and width of the transistor's organic material, respectively. In case contact effects are present ($V_C \neq 0$, $V_{GS} \neq V_G$, $V_{DS} \neq V_D$, see Fig. 4.1), the voltage drop at the contact must be extracted from the experimental values of V_G and V_D. Otherwise, the effect of the contact voltage can alter the results [88]. In the previous chapters , we proposed a method to extract the voltage drop at the contact from $I_D - V_D$ curves [83][86]. In this chapter, we apply this method to $I_D - V_D$ curves with hysteresis. Thus, the first objective is to determine current voltage curves in both forward and backward sweeps,

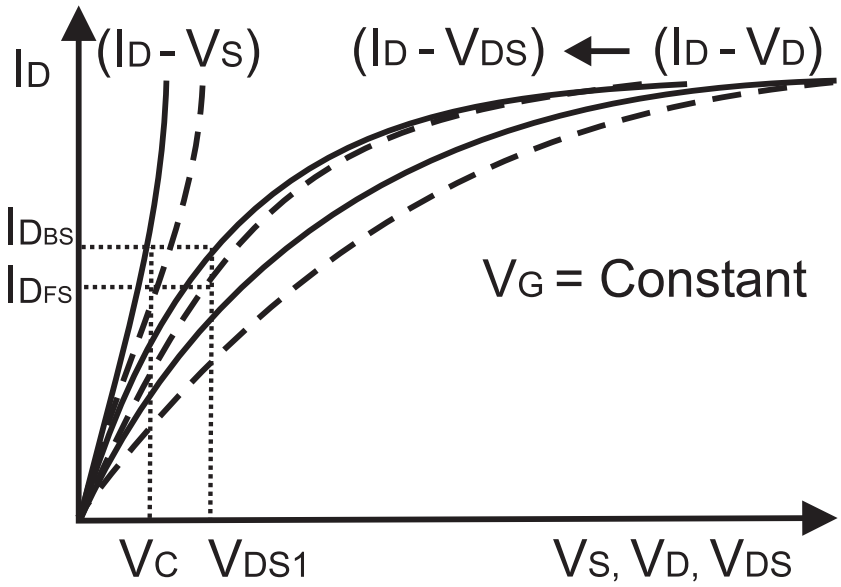

Figure 4.2: Schematic of current voltage curves of the intrinsic channel of an $OTFT$ ($I_D - V_{DS}$) and of the contact ($I_D - V_D$) extracted from a $I_D - V_D$ curve measured at the device terminals at $V_G = constant$. The dashed and the solid lines represent the FS and BS curves, respectively.

that depend exclusively on the voltage drops in the intrinsic transistor ($V_{DS} = V_D - V_S$ and $V_{GS} = V_G - V_S$, where $V_S = V_C$ is the voltage drop at the contact). Fig. 4.2 represents schematically the process of separation of experimental $I_D - V_D$ curves with hysteresis at a constant V_G into $I_D - V_S$ and $I_D - V_{DS}$ curves. This process is repeated at different values of V_G, so that finally, $\Delta I_D(V_{DS}, V_{GS})$ can be evaluated at different values of V_{GS} and V_{DS}. The procedure to separate the current voltage curves of the intrinsic transistor and of the contact region from the measured $I_D - V_D$ curves is detailed in the following section.

4.3. Parameter extraction from $(I_D - V_D)$ curves

4.3.1. Characterization method

To obtain the $I_D - V_{DS}$ curves for the intrinsic channel transistor, a model that incorporates the effect of the contacts is necessary [66][89][9]. We use the generic charge drift model presented in Chapter 2 [9] which includes a voltage drop at the contacts

$(V_S \equiv V_C)$ and an electric field dependent mobility $\mu = \mu_o(V_G - V_T)^\gamma$:

$$I_D \frac{L}{w} = \frac{\mu_o C_i}{\gamma + 2}[(V_G - V_T - V_S)^{\gamma+2} - (V_G - V_T - V_D)^{\gamma+2}] \tag{4.2}$$

where $C_i = \varepsilon_i / t_i$ is the gate insulator capacitance per unit area, ε_i is the insulator dielectric constant, t_i is the insulator thickness, V_T is the threshold voltage, μ_o is the mobility at zero electric field and γ is the mobility enhancement factor. This model reflects the fact that the voltage drop at the drain contact is small in comparison to the voltage drop at the source contact [35]. Also, this method is especially useful when combined with a characterization technique to extract its parameters. This is the so called H_{VG} function [73], also presented in Chapter 2. For the sake of clarity, the H_{VG} function is shown again:

$$\begin{aligned} H_{VG}(V_G) &= \frac{\int_{<V_T}^{V_G} I_D dV_G}{I_D(V_G)} \\ &= \frac{1}{\gamma + 3} \frac{(V_G - V_T - V_S)^{(\gamma+3)} - (V_G - V_T - V_D)^{(\gamma+3)}}{(V_G - V_T - V_S)^{(\gamma+2)} - (V_G - V_T - V_D)^{(\gamma+2)}} \end{aligned} \tag{4.3}$$

The H_{VG} function can be evaluated in the linear and saturation modes. In the saturation mode, H_{VG} is linear with V_G [83][86]:

$$H_{VG}(V_G) = (V_G - V_T - V_S)/(\gamma + 3) \tag{4.4}$$

The values of γ and V_T can be extracted easily from this relation if $V_S = 0$. However, it is more difficult when V_S is not zero and, in addition, depends on the current ($V_S = V_S(I_D) \neq 0$). In the previous two chapters, we showed how to solve this problem. For the sake of completeness, we provide a brief summary of this method in order to be applied later to $I_D - V_D$ curves with hysteresis. The method begins with an initial estimation of V_S in order to extract V_T and γ from (4.4). This estimation considers the ideal MOS model for the transistor of Fig. 4.1 and that the contact effects are introduced only in the drain-source voltage, $V_D = (V_{DS} + V_S)$:

$$I_D = \frac{w\mu_o C_i}{L}[(V_G - V_T)V_{DS} - \frac{V_{DS}^2}{2}] \tag{4.5}$$

In addition, our method considers a simple model for the current- voltage relation $I_D - V_C$ at the contact region controlled by a single parameter. It is observed experimentally, that output characteristics measured in $OTFTs$ with contact effects show linear or quadratic behaviours at low drain voltages [83][67]. Therefore, the $I_D - V_C$ relation can be approximated by a linear or Ohm's relation ($V_C = I_D R_C$), or a quadratic one ($I_D = MV_C^2$), respectively. They are simple expressions as they depend only on one parameter. These expressions are theoretically justified by a previously proposed model that considers injection and transport of charge in organic diodes [4][63][36]. For low contact barriers, the model reduces to the transport term:

$$\begin{aligned} V_C = V_{drift} &= \frac{2}{3}(\frac{2j}{\varepsilon\mu\theta})^{\frac{1}{2}}([x_C + x_p]^{\frac{3}{2}} - [x_p]^{\frac{3}{2}}) \\ x_p &\equiv \frac{j\theta\varepsilon}{2q^2\mu[\theta p(0)]^2} \end{aligned} \tag{4.6}$$

where $j = I_D/S$, S is the cross section of the channel where current flows, $p(0)$ is the free charge density at the metal-organic contact, x_p is a characteristic length (from the contact interface towards the organic film) at which the charge density $p(x_p)$ decays to $p(0)/\sqrt{2}$, ε is the organic dielectric constant, θ is the ratio of free to total charge density and x_C is the length of the contact region in the organic material. This equation (4.6) was demonstrated to have two asymptotical trends: a linear or ohmic behaviour if the characteristic length x_p is a few times larger than the contact length x_C,

$$I_D \approx qSp(0)\mu\theta V_C/x_C \equiv V_C/R_C \tag{4.7}$$

and a quadratic behavior (Mott-Gurney law) if the characteristic length x_p is much smaller than the contact length x_C [83][36],

$$I_D \approx (9/8)\varepsilon\mu\theta S V_C^2/x_C^3 \equiv M \times V_C^2 \tag{4.8}$$

The combination of equations (4.5) and (4.7) or (4.8) produce $I_D - V_D$ curves at diffe-

rent V_G. They are compared to the experimental data in order to obtain the parameters M or R_C, and the rest of parameters in equation (4.5). Once M or R_C are known for different gate voltages, an average value for the contact voltage ($\overline{V_C}$) can be determined and used as an estimation V_S in (4.4): $V_S \equiv \overline{V_C}$ [83][86]. With this estimation, V_T and γ can be extracted from (4.4). In the next step, these two parameters , V_T and γ are used in (4.2) and this equation is then evaluated for different values of M (or R_C) and μ_o until a good agreement with the experimental $I_D - V_D$ curves is achieved and an acceptable physical evolution for curves at the contact $I_D - V_C$ are also obtained (see Chapter 2 for more information about this procedure).

4.3.2. Trapped charge analysis of the intrinsic transistor

This method is now applied to current voltage curves with hysteresis in order to extract information on the trapping and de-trapping processes that occur during the hysteresis cycle. Before applying this method to the output characteristics with hysteresis, some conditions must be established regarding the parameters (V_T, γ, μ_o and M (or R_C)) in (4.2), (4.7) and (4.8).

(a) The trapping and de-trapping processes alter the charge present in the semiconductor. As the electric field is modified, the threshold voltage is assumed to be different in FS and BS.

(b) A variation of the trapped charge in the organic material also affects parameters M (or R_C) due to their dependence with the free to total charge ratio θ.

(c) The mobility (modelled by μ_o and γ) is the only variable assumed constant in both sweeps. With this in mind, the analysis of output characteristics with hysteresis will provide a value for μ_o and γ and different values for V_T and $M(V_G)$ (or $R_C(V_G)$) for the FS and BS. However, remember that M and R_C depend on the gate voltage.

Once these parameters are known, current-voltages curves for the intrinsic transistor, $I_D - V_{DS}$, can be evaluated with (4.2), considering $V_{DS} = V_D - V_C$, as detailed in Section 4.2. Finally, the variation of the trapped charge from forward to backward sweeps can be determined from (4.1), allowing for the variation of ΔP with V_{DS} for different values of V_{GS} , $\Delta P(V_{DS}, V_{GS})$, to be evaluated.

4.3.3. Trapped charge analysis of the contact region

An alternative way to estimate the trapped charge during the hysteresis cycle is to analyse the current voltage curves at the contact region $I_D - V_C$, taking into account the relation that parameters M or R_C have with the free charge density in this region (see equations (4.7) and (4.8) above). The mobile charge in the organic material can be divided in two parts: free charge density in the contact region $\rho_{contact}$ and free charge density in the intrinsic channel $\rho_{channel}$. The free charge density in the contact region can be considered a fraction of the last one: $\rho_{contact} = \rho_{channel}/K$, $K > 1$. Therefore, if we estimate the dependence with the gate voltage of $\rho_{contact}$ in both FS and BS ($\rho_{contact_{FS}}$ and $\rho_{contact_{BS}}$, respectively), and if we also know the fraction K in both FS and BS (K_{FS} and K_{BS}, respectively), the variation of the trapped charge density during the hysteresis cycle can be determined from:

$$\Delta P(V_G) = \rho_{channel_{FS}}(V_G) - \rho_{channel_{BS}}(V_G) = K_{FS}\rho_{contact_{FS}} - K_{BS}\rho_{contact_{BS}} \qquad (4.9)$$

Thus, the objective is to determine these constants K_{FS}, K_{BS} and the charge density at the contact.

Despite the difference in magnitude of the free charge density at the contact and in the intrinsic channel, the threshold voltage must be the same for both. There is no physical reason to believe that the charges in these two adjacent regions start appearing at different gate voltages. Therefore, during the characterization procedure we must look for solutions consistent with this condition.

The free charge density in the contact region is linked to parameters R_C or M by expressions (4.7) and (4.8), respectively. When a non-linear behaviour is observed in the output characteristics at low voltages, the $M(V_G)$ parameter can be extracted with our procedure of Sections 4.3.1 and 4.3.2 (see also Chapter 2). This parameter is proportional to the free to total charge ratio $\theta(V_G)$ at the contact region (4.8). The value of $\theta(V_G)$ for each sweep can be determined from $M(V_G)$, and introduced in (4.6), where the $p(0)$ variable can be extracted for every pair (V_C, j). The charge density at the contact can be estimated by considering $\rho_{contact} \approx qp(0)$ [90]. The variable $p(0)$ in (4.6) depends on the contact voltage V_C and the current density j. At the same time, the curves $(j - V_C)$ depend on the gate voltage. If we are searching for a dependence of $p(0)$ with V_G, we can

consider a critical value for the contact voltage, and analyse its evolution with the gate voltage. The result can be compared with the charge density in the intrinsic channel, usually expressed as [77]:

$$\rho_{channel} = C_i(V_{GS} - V_T)/t_o \tag{4.10}$$

where t_o is the thickness of the organic material. The value of the contact voltage is selected in such a way that the transistor is in the linear region, and we can assume $V_{GS} \approx V_G$. For a constant value of $V_{DS} = V_{DS1}$ and different values of V_G, I_D is extracted from the $I_D(V_G, V_{DS})$ curves (Fig. 4.2). From these values of I_D, V_C is obtained as a function of the gate voltage $V_C(V_G) = \sqrt{I_D(V_G, V_{DS1})/M(V_G)}$. This is repeated for the FS and BS (these values are named $I_{D_{FS}}$, $I_{D_{BS}}$ and V_C in Fig. 4.2). Finally, the charge density can be evaluated by substituting $V_C(V_G)$ and $I_D(V_G, V_{DS1})$ in (4.6), thus obtaining an estimation of the charge density at the contact as a function of the gate voltage $\rho_{contact}(V_G)$.

As we mentioned above, the charge density at the contact, obtained using the procedure described, is expected to be proportional to the charge density in the intrinsic channel. The value of the proportionality constant K can be determined by comparing $\rho_{contact}$ and $\rho_{channel}$. In case there is no hysteresis, the value of the charge density in the intrinsic channel can be estimated according to (4.10). In case experimental data show hysteresis, the way to extract the value of the charge density in the intrinsic channel becomes difficult, as the threshold voltage can vary during the voltage sweep. This means that (4.10) should be used with care.

Fig. 4.3 shows a scheme with different trends for the free charge density as a function of the gate voltage. Curves (1) represent (4.10) for constant values of V_T at FS and BS, $\rho_{contact}$ and $\rho_{channel}$, respectively. We also represent two different trends of $\rho_{channel}$ in case V_T changes with V_G. Depending on the variation of V_T with the gate voltage, we can expect curves (2) or (3), separating from the straight line given by (4.10). As the charge density in the contact is a proportional to $\rho_{channel}$, curves (4) or (5) should be expected, respectively. We recognize that there is an initial region at low gate voltages where trapping effects are not noticeable and V_T can be assumed as constant. We have described above how to estimate the evolution of the free charge density at the contact with V_G. From this estimation, we can know whether curve (4) or curve (5) is the actual

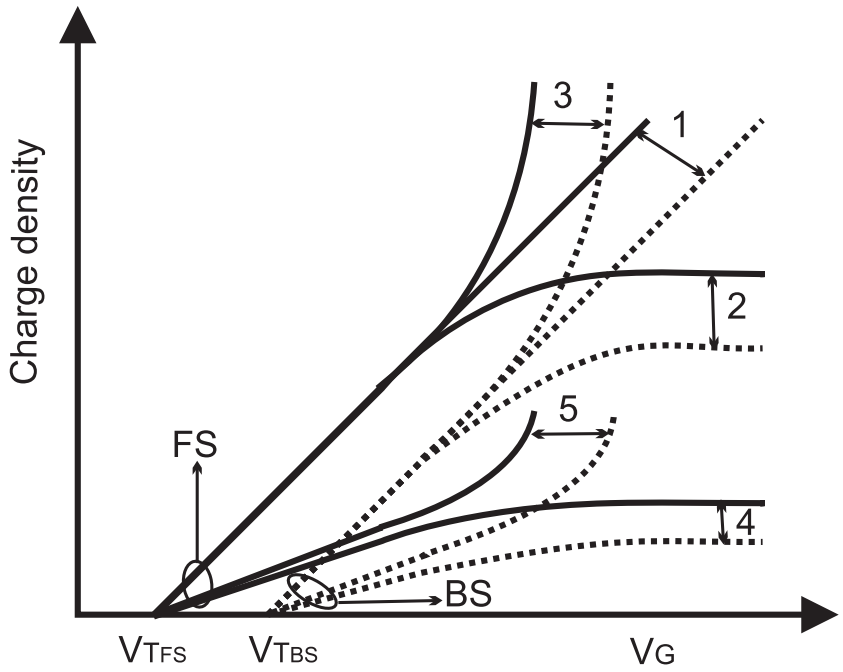

Figure 4.3: Schematics for the free charge density in the intrinsic channel and in the contact region for forward (solid lines) and backward sweeps (dotted lines): (1) Free charge density density in the channel according to (4.10) and V_T constant; (2) and (3) expected free charge density in the channel assuming V_T as a function of V_G; (4) and (5) expected free charge density in the contact region, proportional to the free charge density in the channel, (2) and (3), respectively.

case. In order to obtain K_{FS} and K_{BS}, we analyse the region of the $\rho_{contact}$ curve that shows a linear trend with V_G and compare it with (4.10).

This procedure has been described and applied to the output characteristics showing a non-linear trend caused by the contact effects at low V_D (Ohmic region). A similar procedure is followed when the contact effects show a linear $I_D - V_C$ behaviour, and the output characteristics show accordingly a linear trend in this Ohmic region. In this case, the values of R_C extracted for different V_G are analysed, and the product $\theta p(0)$ is extracted from (4.7). A lower limit of $p(0)$ can be obtained by assuming $\theta \approx 1$.

4.4. Results and Discussion

To check the validity of the procedure described in the previous section, we analyse measurements of output characteristics taken by other authors in transistors showing linear or non-linear trends at low drain voltages V_D [14][87][13].

4.4.1. Non-linear contact current-voltage curves

Fig. 4.4 shows output characteristics with hysteresis measured in a rubrene single crystal TFT (symbols) [14]. In this transistor, the gate dielectric thickness is t_o=5 μm, the channel length L =16 μm, the transistor width w=500 μm and the organic-film thickness t_i=0.3 μm. These current voltage curves in the FS and BS are compared with the compact model (4.2) with parameters obtained by our characterization method (solid line). The parameters obtained from the fitting procedure are: μ_o=0.38 cm^2/(Vs) , γ=0, $V_{T_{FS}}$=-0.36 V and $V_{T_{BS}}$=-0.40 V. The output characteristics show a non-linear trend at low V_D. For this reason, we analyse the current-voltage curves at the contact with (4.8). Parameter M in (4.8) for forward and backward sweeps for each V_G is given in Table. 4.1.

Table 4.1: Extracted values of M_{FS} and M_{BS} for the rubrene single-crystal sample with output characteristics in Fig. 4.4.

V_G (Volts)	M_{FS} (A/V^2)	M_{BS} (A/V^2)
-8	0.90×10^{-6}	0.90×10^{-6}
-12	1.00×10^{-6}	1.00×10^{-6}
-16	1.10×10^{-6}	1.15×10^{-6}
-20	1.41×10^{-6}	1.46×10^{-6}
-24	1.42×10^{-6}	1.47×10^{-6}
-28	1.43×10^{-6}	1.48×10^{-6}
-32	1.44×10^{-6}	1.49×10^{-6}

We would like to remind that the fitting procedure requires three conditions to be satisfied.

(i) A good agreement between experimental and numerical results. The existence of some fitting parameters can produce different agreements for different combinations of these parameters. In this regard, two other conditions are imposed.

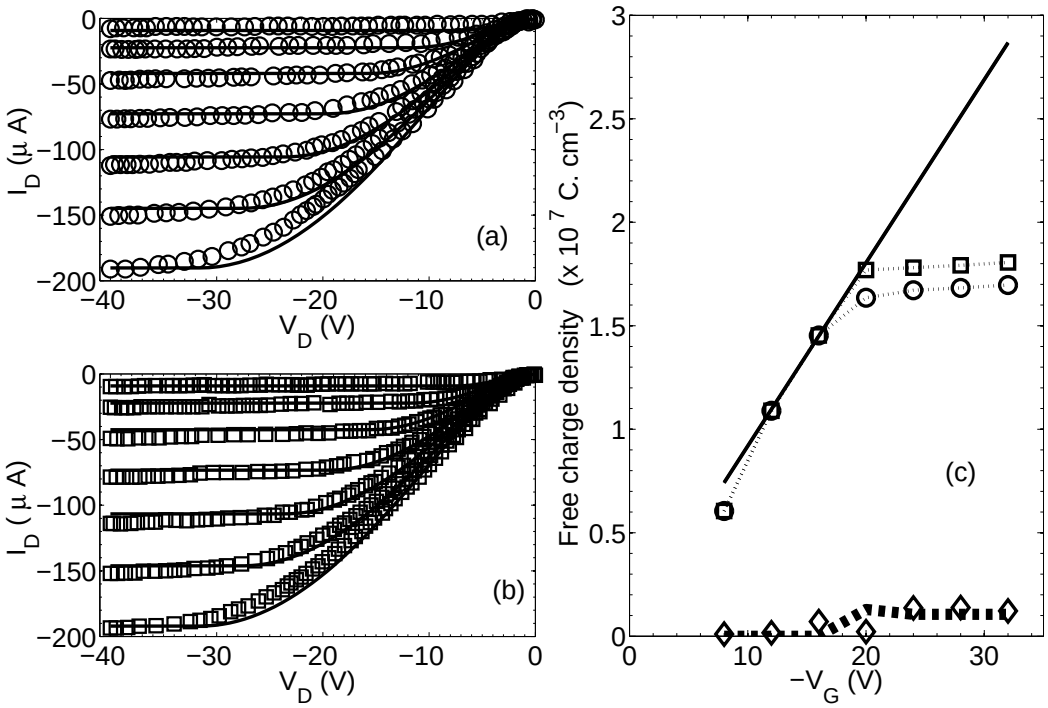

Figure 4.4: (a), (b) Comparison of experimental output characteristics (FS, circles; and BS, squares)of a rubrene single crystal field effect device measured [14], with our compact model (solid line). $V_G = -8$ to -32 V from top to bottom with a -4 V step. (c) Free charge density in the device as a function of V_G: evaluated from (4.10) with $V_{T_{FS}} = -0.36$ V and $V_{T_{FS}} = -0.40$ V constant (Superimposed solid line); $K_{FS}\rho_{contact_{FS}}$ with $K_{FS} = 170$ (circles); and $K_{BS}\rho_{contact_{BS}}$ with $K_{BS} = 170$ (Squares); $\Delta P = K_{BS}\rho_{contact_{BS}} - K_{FS}\rho_{contact_{FS}}$ (dotted line); ΔP evaluated from (4.1) (diamonds),

(II) The current voltage curves at the contact, extracted from (2) by using the values of the parameters γ, μ_o, V_T , must show continuous increment of I_D with increasing V_C , according to the expected physical behaviour [83][86].

(III) The evolution of the free charge density of the contact with the gate voltage, estimated with the procedure described in the previous section, must be consistent with the values of the threshold voltage $V_{T_{FS}}$ and $V_{T_{BS}}$. This means that the free charge density must appear at the contact region and in the intrinsic channel simultaneously. In the iterative procedure, if different threshold voltages are obtained for the free charge density at the contact and in the intrinsic channel, then a new threshold voltage is used in (4.2) consisting on the mean value of both. Parameters

γ and μ_o are maintained equal to the previous solution, and parameters M or R_C are varied in order to get a good agreement between the experimental data and our compact model prediction.

For the experimental data of Fig. 4.4(a) and (b), the free charge density at the contact and in the intrinsic channel are determined as a function of V_G in the FS and BS. The results are represented in Fig. 4.4(c). The charge density at the contact, estimated as $\rho_{contact} = qp(0)$, is determined at $V_{DS} =$ –6 V, following the procedure described in Section 4.3.3. The charge densities at the contact, $\rho_{contact_{FS}}$ and $\rho_{contact_{BS}}$, are multiplied by the factors $K_{FS} = 170$ and $K_{BS} = 170$ (circles and squares for the FS and BS, respectively). They are multiplied by these factors in order to compare the result with (4.10) evaluated for $V_{T_{FS}}$ and $V_{T_{BS}}$ (straight solid line). Only one curve is seen for both $V_{T_{FS}}$ and $V_{T_{BS}}$ because $V_{T_{FS}} \approx V_{T_{BS}}$. Fig. 4.4(c) shows the fulfilment of another condition of our fitting produce: the same threshold voltage for the charge density in the intrinsic channel and in the contact region. The third condition of acceptable $I_D - V_C$ curves at the contacts is also fulfilled, although it is not shown in the figure.

Once the solution exists and is physically acceptable, information of the trapping processes during the hysteresis cycle can be extracted from the two procedures described in Sections 4.3.2 and 4.3.3. In Fig. 4.4(c), the difference ($K_{FS}\rho_{contact_{FS}} - K_{BS}\rho_{contact_{BS}}$) between the circles and squares, is represented as a dotted line. The variation of the trapped charge extracted from the output characteristics of the intrinsic transistor is also represented with open diamonds in Fig. 4.4(c). This curve shows the result of evaluating (4.1) at $V_{DS} =$ –6 V and different gate voltages. A good agreement between these two different procedures is observed. It demonstrates that information of the trapping process during hysteresis can be obtained, first by separating contact effects from the output characteristic of a transistor, and second, by analysing separately the current voltage curves at the contact or the current voltage curves in the intrinsic channel, obtaining similar results. This agreement allows us to identify $K_{FS}\rho_{contact_{FS}}$ and $K_{BS}\rho_{contact_{BS}}$ (circles and squares in Fig. 4.4(c), respectively) as the charge density in the channel in both sweeps. They do not follow the linear trend of (4.10) at high V_G because V_T is modified due to the variation in the trapped charge. The difference between the curve in solid line and any of the curves with circles or squares can give information about the traps present in the organic semiconductor. The fact that the $\rho_{contact}$ curves are located

under the solid line (4.10) means that positive charge is trapped, increasing the absolute value of the threshold voltage above the extracted values $V_{T_{FS}}$ and $V_{T_{BS}}$. The inequality $K_{FS}\rho_{contact_{FS}} > K_{BS}\rho_{contact_{BS}}$ means that some positive charges are released from the traps, but not all that were initially trapped. As V_G increases, more free charges are trapped but only a fraction is de-trapped, the same quantity for different V_G, as shown in the dotted line or the diamonds. On average, the variation of trapped particles per unit area is 4×10^{10} cm^{-2}. The experimental data in Fig. 4.4(a) and (b) were treated in the past by the four terminal method [14], in order to eliminate the contact effects. In this technique, two probes are connected at the source and drain terminal and other two probes are separated at such a distance from the terminals as to eliminate the voltage drop in the contact region [14]. They obtained a larger value for the variation of trapped charges per unit area, $\Delta P = 10 \times 10^{10}$ cm^{-2}, but this value is of the same order of magnitude as we obtained.

This difference may be explained by some of the suggestions the authors left open for future consideration. One of them was the calculation of the threshold voltage where the contact effects were not eliminated. The other one was the extraction of the mobility by the four probe method, which showed a questionable dependence on the drain voltage. Our compact model solves all these open questions as it incorporates the contact effects in the determination of these variables. Moreover, it is based on easier-to-implement-measurements such as the two-probe technique. In any case, the study of this difference is treated in detail in the next chapter.

4.4.2. Linear contact current-voltage curves

Fig. 4.5 shows a set of output characteristics with hysteresis measured in a pentacene single crystal TFT (symbols) [13]. In this transistor, the gate dielectric thickness is $t_i = 0.3$ μm , the channel length $L = 26$ μm, the transistor width w=2000 μm and the organic-film thickness t_o=120 nm. These current voltage curves in the FS and BS are compared with the compact model (4.2) in combination with the linear model (4.7) for the current-voltage curves at the contact, as the output characteristics show a linear trend at low V_D . Our numerical results are shown in solid lines in Fig. 4.7a and b. The parameters obtained from the fitting procedure are: $\mu_o = 0.191$ cm^2/(Vs), $\gamma = 0.004$, $V_{T_{FS}} = 9.09$ V and $V_{T_{BS}} = 7.95$ V. The parameter R_C in (4.7) for forward and backward

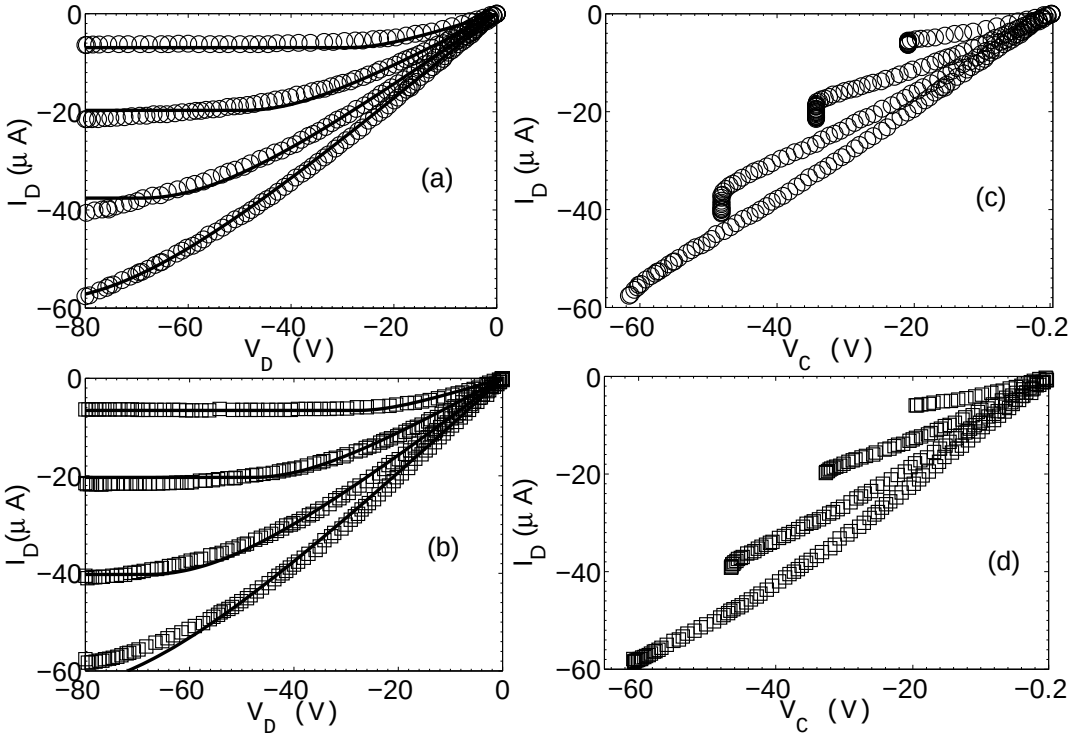

Figure 4.5: (a), (b) Comparison of experimental output characteristics (FS , circles; and BS, squares) of a pentacene single crystal field effect device [13], with our compact model (solid line). V_G is swept from 0 to - 80 V (OFF-to-ON) with a -20 V step. (c), (d) Extracted current voltage curves at the contact region from (a) and (b), respectively.

sweeps for each V_G is given in Table. 4.2.

Table 4.2: Extracted values of $R_{C_{FS}}$ and R_{C-BS} for the pentacene single-crystal sample with output characteristics in Fig. 4.5.

V_G (Volts)	$R_{C_{FS}}$ (Ω)	$R_{C_{BS}}$ (Ω)
-20	2.90×10^6	2.90×10^6
-40	1.72×10^6	1.60×10^6
-60	1.28×10^6	1.15×10^6
-80	1.08×10^6	0.95×10^6

Combining in (4.2) the above values of μ_o, γ and with the experimental values (I_D, V_D) of Fig. 4.5(a), then the current-voltage curves at the contact in the FS can be obtained. The result is seen in Fig. 4.5(c), where an almost perfect linear trend is observed, as expected. Repeating the same procedure with the experimental values (I_D, V_D) of Fig.

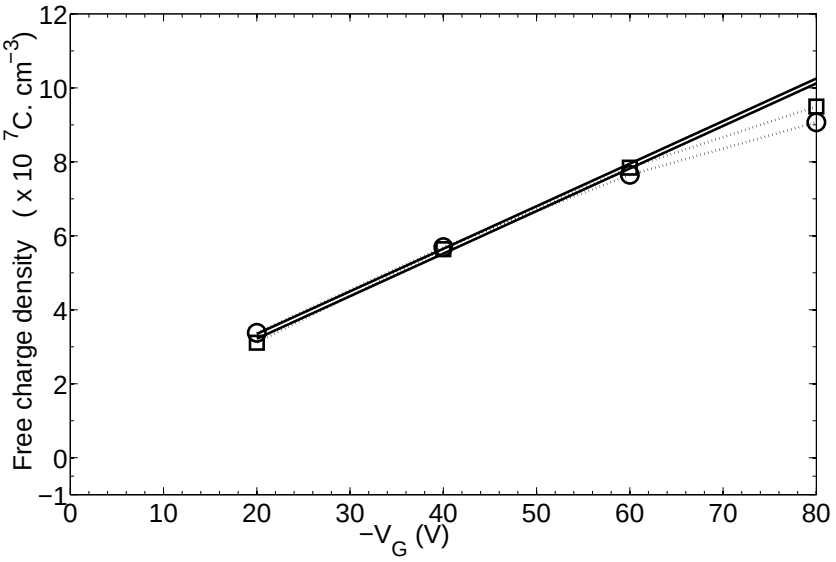

Figure 4.6: Free charge density in the intrinsic channel of the transistor with output characteristics in Fig. 4.5 as a function of V_G: evaluated from (4.10) with $V_{T_{FS}}$=9.09 V and $V_{T_{FS}}$=7.95 V (solid lines); $\theta K_{FS}\rho_{contact_{FS}}$ with θK_{FS} =38×10^2 (circles); and $\theta K_{BS}\rho_{contact_{BS}}$ with θK_{BS}=35×10^2 (squares).

4.5(b), then the current-voltage curves at the contact in the BS can be obtained (Fig. 4.5(d)). The third condition of our fitting procedure aims at the threshold voltages of the charge density in the intrinsic channel and in the contact region, which must be the same. As in the case of the non-linear $I_D - V_C$ curves in the contact, the charge density in this region can be estimated as $\rho_{contact} = qp(0)$. Introducing the fitting values for and in (4.7), values of $\theta p(0)$ can be obtained. If θ is unknown, $\rho_{contact}$ is not completely determined. However, this is no obstacle for the purpose of finding the threshold voltage. Fig. 4.6 shows with symbols the charge density at the contact as a function of the gate voltage for the FS and BS, multiplied by the factors θK_{FS}=38×10^2 (circles) and θK_{BS}=35×10^2 (squares), respectively. This calculation is made at a low drain voltage (V_{DS} = −6 V) following the procedure of Section 4.3.3. These two curves are compared with the free charge density evaluated with (4.10) for $V_{T_{FS}}$ and $V_{T_{BS}}$ (straight solid lines). These are almost superimposed due to the similar values of $V_{T_{FS}}$ and $V_{T_{BS}}$ and the scale factor used in the figure. From this comparison, we observe that the charge density in the contact region starts appearing at the same values of $V_{T_{FS}}$ and $V_{T_{BS}}$.

Once the three conditions of our fitting procedure are fulfilled, the variation of the

trapped particles per unit area can be evaluated from (4.1). However, prior to the analysis of the data in Fig. 4.5, we show a case where one of the conditions of our fitting method are not fulfilled, and how our method solves this problem. Fig. 4.7 shows output characteristics with hysteresis measured in the same transistor as in Fig. 4.5 (symbols) [13]. In Fig. 4.5, the gate voltage sweeps from –20 to –80 V with a −20 V step (OFF-to-ON). In Fig. 4.7, the gate voltage sweeps from ON-to-OFF (-80 to -20 V) with a 20 V step. These current voltage curves in the FS and BS are compared with the compact model (4.2). The parameters used in the fitting are the same as in Fig. 4.5 except the parameter R_C. The values of this parameter for forward and backward sweeps for each V_G are given in Table 4.3.

Table 4.3: Extracted values of $R_{C_{FS}}$ and R_{C-BS} for the pentacene single-crystal sample with output characteristics in Fig. 4.7.

V_G $(Volts)$	$R_{C_{FS}}$ (Ω)	$R_{C_{BS}}$ (Ω)
-20	7.0×10^6	7.0×10^6
-40	2.9×10^6	2.6×10^6
-60	1.7×10^6	1.4×10^6
-80	1.1×10^6	1.0×10^6

For the experimental data of Fig. 4.7(a) and (b), the evaluation of the free charge density in the device with V_G in the FS and BS can be seen in Fig. 4.7(c). The charge density at the contact during the FS and BS ($\rho_{contact_{FS}}$ and $\rho_{contact_{BS}}$, respectively), estimated as $\rho_{contact}$=$qp(0)$, is evaluated at $V_{DS} = -6$ V and following the procedure described in Section 4.3.3. These charge densities are multiplied by the factors θK_{FS}=11×10^3 and θK_{BS}=11×10^3 (circles and squares, respectively). The resulting curves are compared with (4.10) evaluated at $V_{T_{FS}}$ and $V_{T_{BS}}$ (straight solid lines). According to Fig. 4.7(c), the charge density in the intrinsic channel and in the contact region starts appearing at different threshold voltages: ≈+9 V and ≈-8.5 V, respectively. This result means that the set of fitting parameters do not provide a good physical solution, despite the good agreement between the experimental data and the results of the compact model (4.2). Under this circumstance, the iterative procedure must be repeated using the average values of the threshold voltages obtained for the intrinsic channel and contact regions in FS and BS:$V_{T_{FS}}$=0 V and $V_{T_{BS}}$=-1 V, respectively. Parameters γ and μ_o are maintained equal to the previous solution, and parameters R_C are searched in order to get a new

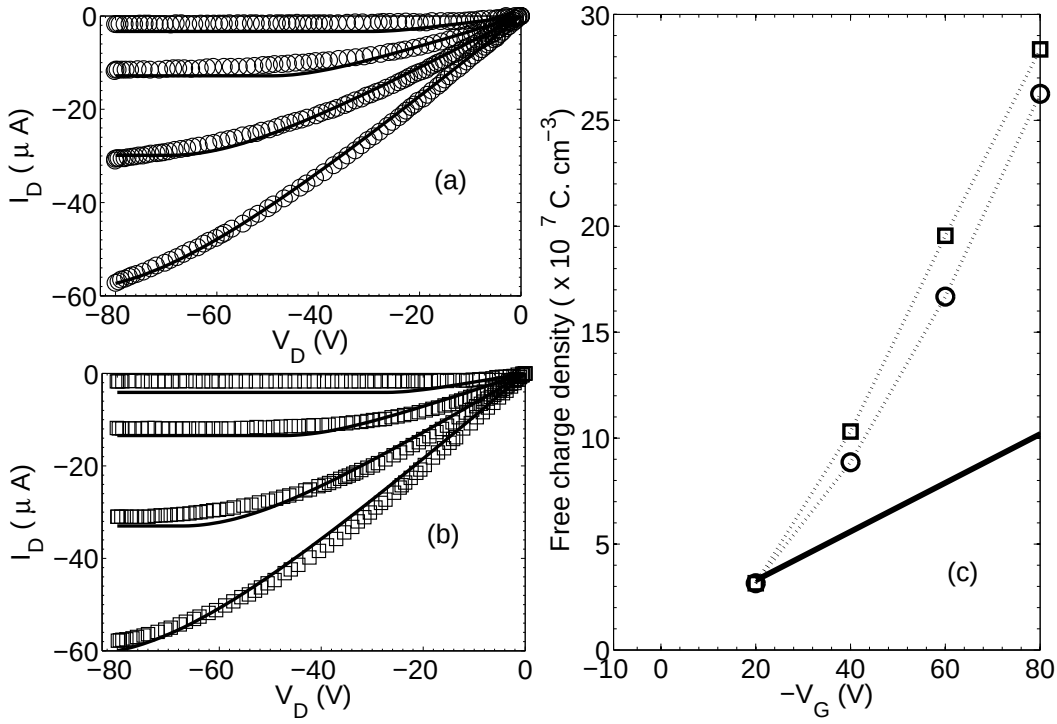

Figure 4.7: (a), (b) Comparison of experimental output characteristics (FS , circles; and BS, squares) of a pentacene single crystal field effect device [13], with our compact model (solid line). V_G is swept from - 80 to 0 V (ON-to-OFF) with a 20 V step. The values of the fitting parameters $R_{C_{FS}}$ and $R_{C_{BS}}$ are in Table. 4.3. (c) Free charge density in the intrinsic channel as a function of V_G: evaluated from (4.10) with $V_{T_{FS}} = 9.09\ V$ and $V_{T_{BS}} = 7.95\ V$ (superimposed solid lines); $\rho_{contact_{FS}}$ with $\theta K_{FS} = 11 \times 10^3$ (circles) and $\rho_{contact_{BS}}$ with $\theta K_{BS} = 11 \times 10^3$ (squares).

agreement between the experimental data and our compact model. This is shown in Fig. 4.8(a) and (b). The new set of values for the parameter R_C in (4.7) for forward and backward sweeps for each V_G are given in Table 4.4.

Table 4.4: Extracted values of $R_{C_{FS}}$ and R_{C-BS} for the pentacene single-crystal sample with output characteristics in Fig. 4.7.

$V_G\ (Volts)$	$R_{C_{FS}}\ (\Omega)$	$R_{C_{BS}}\ (\Omega)$
-20	5.00×10^6	5.00×10^6
-40	2.45×10^6	2.20×10^6
-60	1.55×10^6	1.35×10^6
-80	1.05×10^6	0.95×10^6

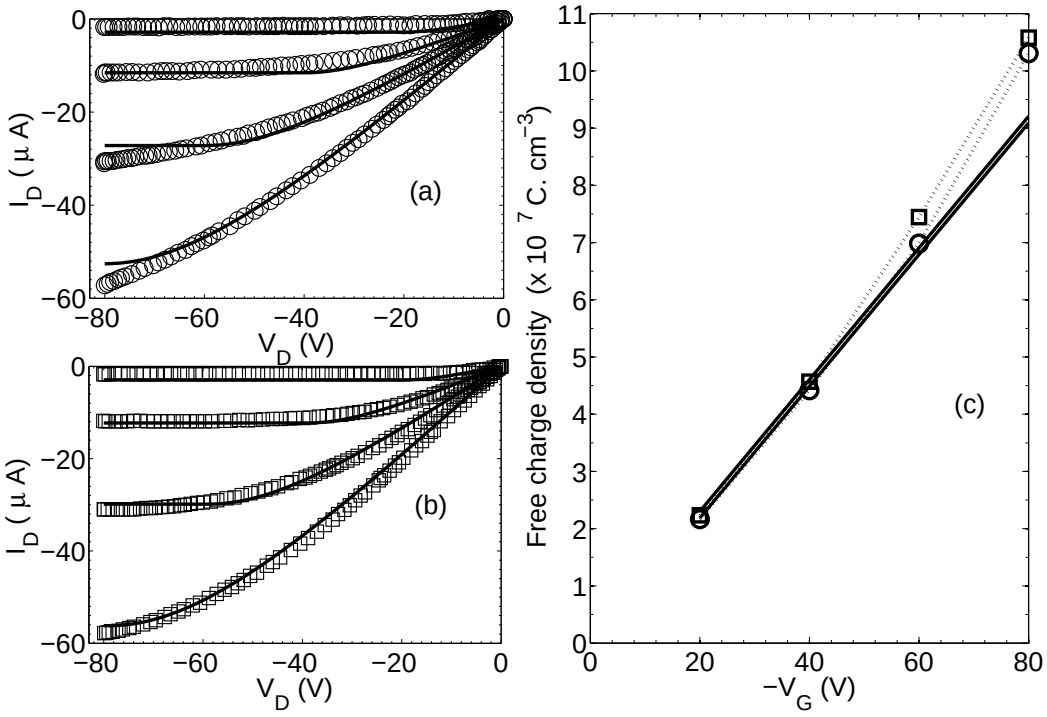

Figure 4.8: (a), (b) Comparison of experimental output characteristics (FS , circles; and BS, squares) of a pentacene single crystal field effect device [13], with our compact model (solid line). V_G is swept from - 80 to 0 V (ON-to-OFF) with a 20 V step. The values of the fitting parameters $R_{C_{FS}}$ and $R_{C_{BS}}$ are in Table. 4.4. (c) Free charge density in the intrinsic channel as a function of V_G: evaluated from (4.10) with $V_{T_{FS}} = 0$ V and $V_{T_{BS}} = -1$ V (superimposed solid lines); $\rho_{contact_{FS}}$ and $\rho_{contact_{BS}}$ with $\theta K_{FS} = 42 \times 10^3$ (circles) and $\theta K_{BS} = 39 \times 10^3$ (squares).

For this solution, the evaluation of the free charge density in the device with V_G in the FS and BS can be seen in Fig. 4.8(c). The charge densities at the contact during the FS and BS ($\rho_{contact_{FS}}$ and $\rho_{contact_{BS}}$, respectively), estimated as $\rho_{contact}$=$qp(0)$, are evaluated at V_{DS} = –6 V following the procedure described in Section 4.3. The charge density at the contact is multiplied by the factors θK_{FS}=42×10^2 and θK_{BS}=39×10^2 (circles and squares, respectively). This solution shows how the threshold voltages of the charge density in the contact and in the intrinsic channel coincide.

Once a physical solution has been obtained, the variation of trapped particles per unit area can be extracted from the output characteristics of the intrinsic transistor. The variation ΔP is obtained from (4.1) evaluated at V_{DS} = –6 V and different gate voltages. The equivalent drain-terminal voltage is $V_D = V_{DS}+V_S \approx$ –10 V. Fig. 4.9 shows,

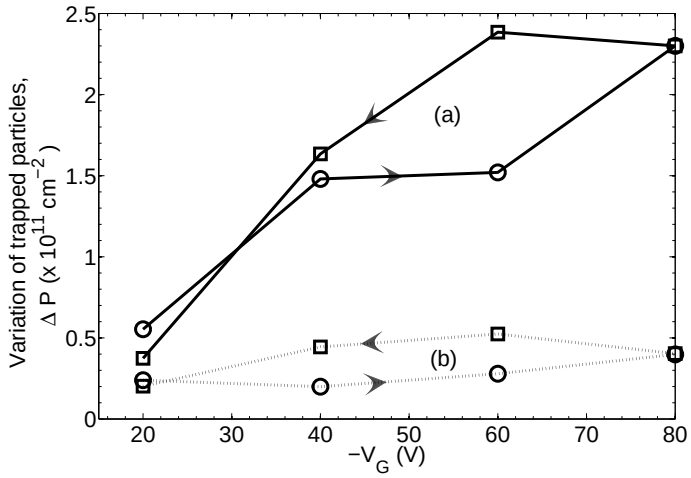

Figure 4.9: Variation of the concentration of trapped particles per unit area as a function of the gate voltage. (a) ΔP is extracted from (4.1) at V_{DS} =–6 V ($\Delta(I_D(V_{DS}, V_G))$. (b) ΔP is extracted from (4.1) at V_D = –10 V ($\Delta(I_D(V_D, V_G))$; V_{DS} and V_D are related by the contact voltage $V_S \approx -4$ V. Circles and squares represent the OFF-to-ON case of Figs. 4.5(a) and (b), and the ON-to-OFF case of Figs. 4.8(c) and (d), respectively.

in solid lines with symbols, the result of this calculation as a function of gate voltage for the OFF-to-ON case (circles) and the ON-to-OFF case (squares). On average, the variation of the concentration of trapped particles per unit area is $\Delta P = 1.24 \times 10^{11}$ cm^{-2} and $\Delta P = 2.1 \times 10^{11}$ cm^{-2} for the FS and BS, respectively. These values are in agreement with the values obtained for the same transistors by transient experiments [13].

The advantage of our procedure is the use of a compact model that describes the output characteristics of the transistor measured with the two-terminal method. Essential parameters such as the threshold voltage and the mobility, the contact voltage and a solution of the variation of trapped charge during a hysteresis cycle are determined with these experimental and modelling tools. Other techniques, such as the transient experiments need to be complemented with other measurements (transfer or output curves) in order to determine all this information. The use of other models that do not consider the contact effects properly may alter the results significantly. Fig. 4.9 shows, in dotted line with symbols, the results of evaluating the concentration of the trapped particles per unit area by considering the output characteristics of the transistors referred to its terminal voltages $I_D(V_D, V_G)$, instead of using the intrinsic transistor response.

They are evaluated for V_D = –10 V, which is related to V_{DS} = –6 V by the contact voltage ($V_S \approx 4$ V). We observed a decrease of one order of magnitude compared to the results obtained by the analysis of the intrinsic transistor (i.e. by eliminating the contact effects). This difference in the results obtained by considering the contact region or not are treated in detail in the next chapter.

5

Variation of the Trapped Charge in OTFTs during Hysteresis

5.1. Introduction

In Chapter 2, we proposed a method to extract the voltage drop at the contact region from the output characteristics of the transistor [86][83]. The basis of this method is the combination of a characterization technique [73] with a compact model that incorporates the effect of the contacts in both the drain and gate voltages, and the mobility and the threshold voltage [9]. In Chapter 4, we applied this method to curves with hysteresis. Hysteresis adds the problem of working with a variable threshold voltage from the forward sweep (FS) to the backward sweep (BS), and even during each sweep. We proposed a solution to overcome this inconvenience during the extraction process [91].

In the literature, we can find studies that characterize the hysteresis in $OTFTs$ from transfer and output characteristics. In some cases, contact effects are not considered [13]. In other cases, contact effects are eliminated from the experimental data by using elaborate experimental procedures such as the four-terminal method, instead of the usual two-terminal one [14]. Different results are obtained depending on the characterization method and the importance given to the contact region of the transistor. The complete isolation of the intrinsic transistor from the contact region should be essential to obtain accurate results. Other studies analysing different properties of $OTFTs$, such as the low-frequency noise, showed the importance of determining the correct voltage across the intrinsic channel by removing previously the contact resistance [88].

In this chapter, we propose a precise way to remove the contact voltage from the output characteristics of an OTFT. The objective is to determine accurately the variation of trapped charge produced during voltage cycling in the output characteristics of the transistor.

In the previous chapters, we have developed and checked a method to extract the current-voltage curves at the contact ($I_D = I_D(V_S)$) and the output characteristics of the intrinsic transistor ($I_D = I_D(V_{DS}, V_{GS})$) from the experimental curves ($I_D = I_D(V_D, V_G)$) (Fig. 5.1). Once these curves are extracted, the variation of the trapped charge during a hysteresis cycle can be determined considering the variations of the drain current during a hysteresis cycle. In the previous chapter, we determined the variation of the trapped charge by analysing the variation of the curves $I_D(V_{DS}, V_G)$. In that case, we assumed $V_{GS} \approx V_G$. In this chapter, we determine this variation of the trapped charge by analysing the intrinsic transistor, described by the $I_D = I_D(V_{DS}, V_{GS})$ curves (Fig. 5.1). We also

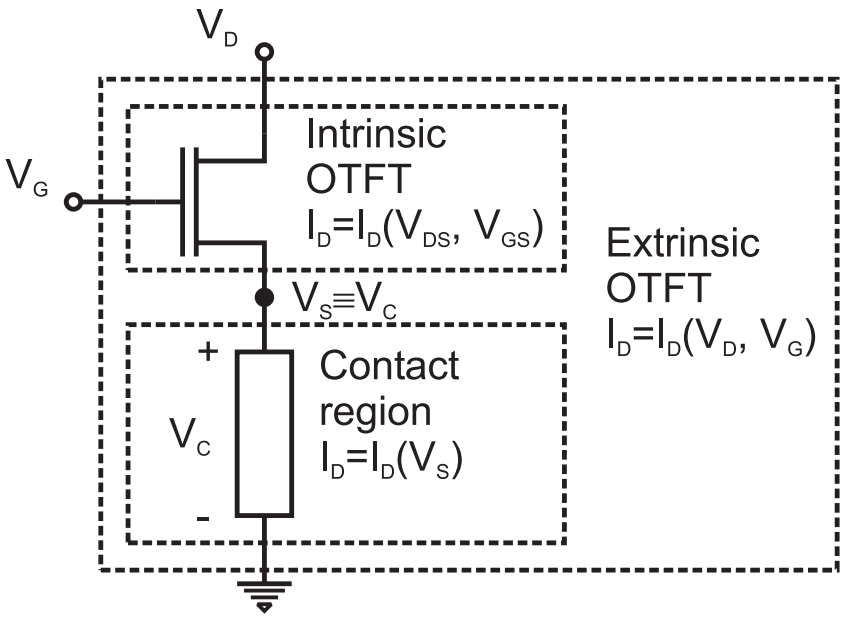

Figure 5.1: The proposed equivalent circuit of a TFT including a voltage drop at the source contact $V_C \equiv V_S$ [83].

evaluate this variation directly from the experimental $I_D = I_D(V_D, V_G)$ curves. All these cases intend to reproduce characterization methods found in the literature where the contacts are treated in different ways [13][14].

Other situations can be analysed, as the contact effects have been treated and modelled extensively in the past. There are models that remove the contact effects mainly from the drain-terminal voltage, provide excellent fittings with the experimental data, and extract the contact I-V curves from the experimental ones [59][67][36]. It is our objective to determine the variation of the trapped charge produced during a hysteresis cycle under the conditions imposed by all these models and to compare their results. Even the classical MOS model is analysed, in order to quantify the effect of neglecting the contact effects completely. The objective is to find out whether it is worth dealing with a more elaborate and precise characterization procedure instead of working with a simpler but less precise one; or whether it is worth extracting the intrinsic current voltage curves of the $OTFT$ instead of working directly with the experimental data. This is discussed in this chapter.

5.2. Variation of the trapped charge in voltage cycling

Hysteresis phenomena can appear in output (I_D–V_D) and in transfer (I_D–V_G) curves of $OTFTs$. In case no contact effects are present ($V_C = 0$ in Fig. 5.1), a way to determine the variation of the trapped charge is by measuring the displacement current or difference in the drain current between forward- (FS) and backward-sweep (BS) curves, at certain values of the drain and gate voltages, $\Delta I_D = \Delta I_D(V_D, V_G)$. The relation between the variation of the trapped particles ΔP in the intrinsic channel of a transistor and the current displacement $\Delta I_D = \Delta I_D(V_D, V_G)$ is given by [13]:

$$\Delta P = \frac{\Delta I_D \times L}{q \times w \times V_D \times \mu} \tag{5.1}$$

where q is the elementary charge, μ is the charge carrier mobility, L and w are the channel length and width of the transistor's organic material, respectively. In case contact effects are present, ($V_C \neq 0$), we propose to determine the variation of the trapped particles by measuring the difference in the drain current between the FS and BS that occurs in the intrinsic channel of the transistor, $\Delta I_D = \Delta I_D(V_{DS}, V_{GS})$, (Fig. 5.1):

$$\Delta P = \frac{\Delta I_D \times L}{q \times w \times V_{DS} \times \mu} \tag{5.2}$$

The results obtained by substituting $\Delta I_D(V_{DS}, V_{GS})$ in (5.2) are expected to be free of contact effects, and thus, close to the actual results.

The process of extraction of the output characteristics of the intrinsic transistor $I_D(V_{DS}, V_{GS})$ begins by extracting the curves $I_D = I_D(V_{DS})$ and $I_D(V_S)$ from the measured output characteristics $I_D(V_D)$ at $V_G =$ constant. The process of extraction considers that $I_D = I_D(V_S) = I_D(V_{DS}) = I_D(V_D)$ and $V_D = V_{DS} + V_S$ at $V_G =$ constant. 5.2 shows two examples of this procedure applied to transistors analysed in this work [87][14]. Subsequently, a simple numerical treatment of the curves $I_D = I_D(V_{DS})$ and $I_D(V_S)$ at $V_G =$ constant provides a set of curves for the intrinsic transistor: $I_D(V_{DS})$ at $V_{GS} =$ constant.

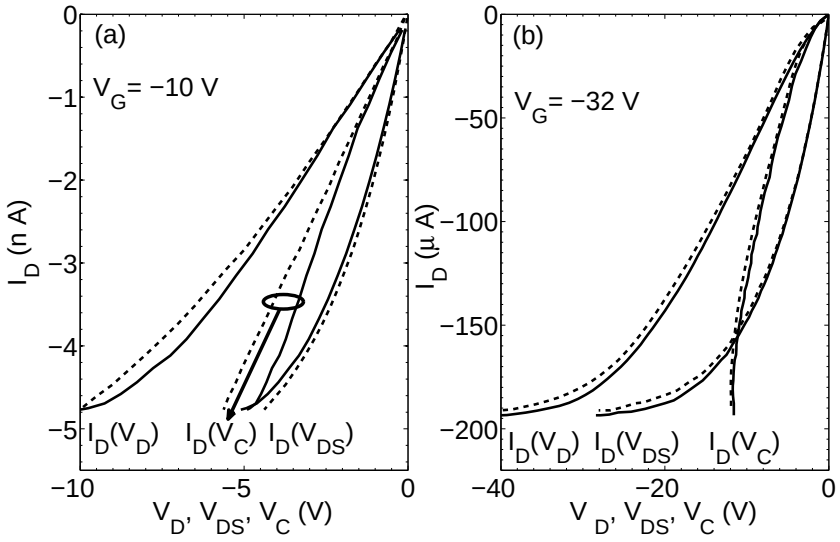

Figure 5.2: Extraction of current-voltage curves of the intrinsic channel, $I_D(V_{DS})$, and the contact, $I_D(V_S)$, from experimental curves measured at the external terminals of $OTFTs$, $I_D(V_D)$. $I_D = I_D(V_S) = I_D(V_{DS}) = I_D(V_D)$ and $V_D = V_{DS} + V_S$. The transistors show (a) linear [87] and (b) non-linear $I_D(V_S)$ curves at the contacts [14]. In a second step, curves $I_D(V_{DS})$ at V_{GS} = constant can be obtained. The dashed and solid lines represent the forward (FS) and backward sweeps (BS), respectively.

5.3. Transistor models

The process of separating the contact and intrinsic contributions in the OTFT, requires a model that incorporates the contact effects. As the basis of this work, we consider the compact model that presented in Chapter 2. It describes the output characteristics in a transistor as [83][73]:

$$\begin{aligned} I_D\frac{L}{w} &= \frac{\mu_o C_i}{\gamma+2}[(V_G - V_T - V_S)^{\gamma+2} - (V_G - V_T - V_D)^{\gamma+2}] \\ I_D &= \frac{V_S}{R_C}, \text{or } I_D = MV_S^2 \end{aligned} \tag{5.3}$$

where C_i is the gate insulator capacitance per unit area, V_T is the threshold voltage, μ_o is the mobility at zero electric field ($\mu = \mu_o(V_G - V_T)$) and μ is the mobility enhancement factor. The contact voltage V_S is modelled by a linear or non-linear relation with I_D

depending on the behaviour of the output characteristics at low drain voltage. The advantages of this method is that it clearly distinguishes the contact voltage V_S from the terminal voltages V_G and V_D.

There are models that eliminate the contact voltage only from the drain-terminal voltage [59][67][36]. They can be used instead of our compact model to obtain the intrinsic and contact contributions. However, they represent an intermediate situation between a compact model that eliminates the effect of the contacts from both the drain and gate terminals, and the classical MOS model that neglects all these effects:

$$\begin{aligned} I_D &= \frac{w\mu_o C_i}{L}[(V_G - V_T)V_D - \frac{V_D^2}{2}], V_D < V_G - V_T \\ I_D &= \frac{w\mu_o C_i}{2L}[(V_G - V_T)^2], V_D \geq V_G - V_T \end{aligned} \tag{5.4}$$

In order to consider the effect of analysing an $OTFT$ under a generic intermediate situation, we consider a modification of (7.1), while maintaining the model of the contact region of (5.3). It assumes that the contacts affect only on the drain voltage ($V_{DS} = V_D – V_S$) while $V_{GS} \approx V_G$. Thus, this modification affects only the triode region in (7.1):

$$\begin{aligned} I_D &= \frac{w\mu_o C_i}{L}[(V_G - V_T)V_{DS} - \frac{V_{DS}^2}{2}] \\ I_D &= \frac{w\mu_o C_i}{2L}[(V_G - V_T)^2], V_D \geq V_G - V_T \\ I_D &= \frac{V_S}{R_C}, \text{or } I_D = MV_S^2 \end{aligned} \tag{5.5}$$

In the following section, we determine the variation of the trapped particles (ΔP) from output characteristics with hysteresis taken from the literature [14][87], using the models (5.3)-(5.5) (Table 5.1). The objective is to determine which parameter or variable is affected the most by the contact region: the mobility or the gate- and drain-terminal voltages.

In procedures # 1, # 2 and # 3 of Table 5.1, the transistor is modelled with the compact model (5.3). ΔP is extracted from variations in the drain current referred to: the intrinsic voltages (V_{DS} and V_{GS}) (procedure # 1); the intrinsic V_{DS} and the external V_G (procedure # 2); and the external V_G and V_D (procedure # 3). The mobility in these

three cases is assumed free of contact effects and the same in all of them, as the compact model is used to reproduce the experimental output characteristics.

To analyse the effect of the mobility on the determination of ΔP, model (5.5) is also used to fit the experimental data (procedures # 4 and # 5). Basically, the mobility and the threshold voltage are extracted from the saturation region. Therefore, no relation to the contact region is established. The contact parameters, R_C or M, are extracted from the triode region. In procedure # 4, the variation of the drain current is referred to the intrinsic V_{DS} and the external V_G. In procedure # 5, ΔP is referred to the external voltages V_D and V_G. This last case represents the worst scenario as contact effects are neglected in both the mobility and terminal voltages. Procedures # 2, # 3 and # 4 represent intermediate situations between the best and worst scenarios. In any case, we aim to find out how far these situations are among each other, and whether a good approximation to case # 1 exists or not, in order to obtain more simple calculations.

These procedures are applied to the linear regime of the transistor, where the variation of the trapped charge is evaluated at different gate and drain voltages. The output characteristics affected by contact effects show typically two different trends at low drain voltages. Non-linear [75][60][59], and linear relations [75][22][92] can be observed in this low drain voltage region. In this work, we analyze output characteristics taken by different authors showing both trends (Fig. 5.2) [14][87].

Table 5.1: Procedures to determine the variation of the trapped particles (ΔP) during a hysteresis cycle in the transistor. The ΔP is extracted analysing the variations of the drain current referred to the voltages at the external terminals (5.1) or at the intrinsic transistor (5.2). The intrinsic voltages are extracted employing the compact model (5.3) or model (5.5). The effect of the contact voltage on the mobility is also checked. Two different values for the mobility are extracted: one extracted from the compact model (5.3) and another from model (5.5).

Procedure	ΔP Model	$I-V$ Model	Correction of contact effects on terminals	Mobility model	Correction of contact effects on μ
# 1	(5.2)	(5.3)	V_D, V_G	(5.3)	Yes
# 2	(5.2)	(5.3)	V_D	(5.3)	Yes
# 3	(5.1)	(5.3)	$none$	(5.3)	Yes
# 4	(5.2)	(5.5)	V_D	(5.5)	No
# 5	(5.1)	(5.5)	$none$	(5.5)	No

5.4. Results and discussion

5.4.1. Transistors with linear contacts

Figs. 5.3(a) and (b) show with symbols output characteristics with hysteresis measured in a pentacene single crystal TFT [87]. In this transistor, the gate dielectric thickness is $t_i = 1\mu$m , the channel length L=100 μm, the transistor width $w = 1$ mm, the organic-film thickness $t_o = 100$ nm. The drain-source electrodes are deposited through a shadow mask and the metal thicknesses are $Cr = 5$ nm and $Au = 40$ nm. These current voltage curves in the FS and BS are compared with the compact model (5.3) in combination with the linear model (5.6) for the current-voltage curves at the contact, as the output characteristics show a linear trend at low V_D values. Our numerical results are shown in solid lines in Fig. 5.3(a) and (b). The parameters obtained from the fitting procedure are: $\mu_o = 0.0041$ cm^2/(Vs), $\gamma = 0.05$, $V_{T_{FS}} = 5.18$ V and $V_{T_{BS}} = 3.55$ V. Parameter R_C in (5.6) for forward and backward sweeps for each V_G is given in Table. 5.2.

$$I_D \approx qSp(0)\mu\theta V_C/x_C \equiv V_C/R_C \tag{5.6}$$

Table 5.2: Extracted values from model (5.3) of $R_{C_{FS}}$ and R_{C-BS} for the pentacene single-crystal sample with output characteristics in Fig. 5.3.

V_G (Volts)	$R_{C_{FS}}$ (Ω)	$R_{C_{BS}}$ (Ω)
0	14×10^9	10×10^9
-2	10×10^9	6.0×10^9
-4	6.0×10^9	3.8×10^9
-6	3.0×10^9	2.1×10^9
-8	1.8×10^9	1.3×10^9
-10	1.2×10^9	1.0×10^9

Combining in (5.3) the above values of μ_o, γ and $V_{T_{FS}}$ with the experimental values (I_D, V_D) of Fig. 5.3(a), then the current-voltage curves at the contact in the FS can be obtained. The result is seen in Fig. 5.3(c), where an almost perfect linear trend is observed, as expected. Repeating the same procedure with the experimental values (I_D, V_D) of Fig. 5.3(b), then the current-voltage curves at the contact in the BS can be obtained (Fig. 5.3(d)). The third condition of our fitting procedure aims at the threshold

voltages of the charge density in the intrinsic channel and in the contact region, which must be the same. The charge density in this region can be estimated as $\rho_{contact} = qp(0)$. Introducing the fitting values for $R_{C_{FS}}$ and $R_{C_{BS}}$ in (5.6), values of $\theta p(0)$ can be obtained. If θ is unknown, $\rho_{contact}$ is not completely determined. However, this is no obstacle for the purpose of finding the threshold voltage. Fig. 5.4 shows with symbols the charge density at the contact as a function of the gate voltage for the FS and BS, multiplied by the factors $\theta K_{FS} = 1 \times 10^4$ (circles) and $\theta K_{BS} = 5 \times 10^4$ (squares), respectively. This calculation is made at a low drain voltage (V_{DS} = -2 V) following the procedure of Section 4.3.3. These two curves are compared with the free charge density evaluated as

$$\rho_{channel} = C_i(V_{GS} - V_T)/t_o \tag{5.7}$$

for $V_{T_{FS}}$ and $V_{T_{BS}}$. From the comparison in Fig. 5.4, we observe that the charge density in the contact region starts appearing at the same values of $V_{T_{FS}}$ and $V_{T_{BS}}$.

Once the results of these tests have physical meaning, the current voltage curves of the intrinsic transistor and of the contact region can be extracted following the procedures described in Sec. 5.3. From these curves, the variation of the trapped charge can be determined. Fig. 5.5 illustrates some steps of these extraction procedures.

- **Procedure #1**. Fig. 5.5(a) shows the drain current as a function of the gate voltage V_{GS} at $V_{DS} = 2$ V. The variation of the drain current from Fig. 5.5(a) can be introduced in (5.2) to determine ΔP as a function of V_{GS}. The average value over V_{GS} is $\overline{\Delta P} = 2 \times 10^{10}$ cm^{-2}. This procedure is repeated at different values of V_{DS} in the linear region. The result is represented with circles in Fig. 5.6. The average value over V_{DS} and V_{GS} in this region is $\overline{\Delta P}(\#1) = 2.47 \times 10^{10}$ cm^{-2}. By referring ΔP to the intrinsic voltages V_{DS} and V_{GS}, we eliminate any relation to the contact region. The mobility is also free from contact effects as the experimental data have been reproduced by (5.3). To analyse the difference of working with the intrinsic voltages or with terminal voltages, we study the following two procedures.

- **Procedure #2**. This case considers the effect of the contact region on the gate terminal. The variation of the trapped charge is analysed as a function of V_{DS} and V_G. Solid lines in Fig. 5.5(b), show the drain current as a function of V_G at $V_{DS} = 2$ V. By introducing the variation of the drain current $\Delta I_D(V_{DS}, V_G)$ in

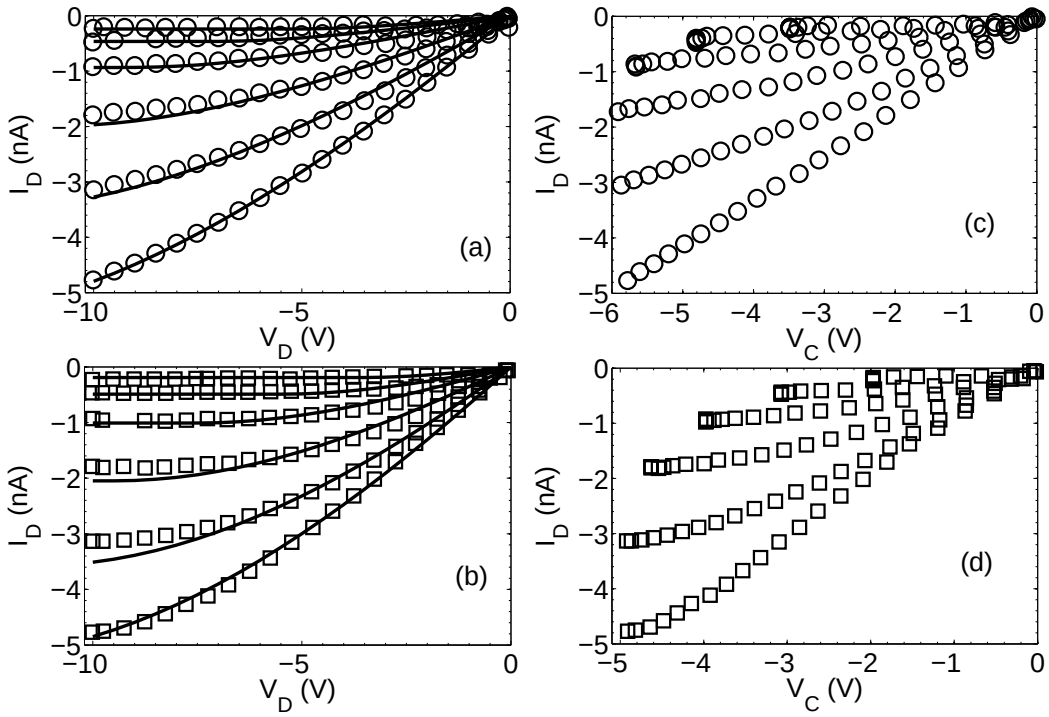

Figure 5.3: (a), (b) Comparison of experimental output characteristics of a top gate coplanar PVA / pentacene / Au $OFET$ [87], with our compact model (solid line); (c), (d) Extracted current voltage curves at the contact region. $V_G = 0$ to -10 V from top to bottom with a -2 V step (FS, circles; and BS, squares).

(5.2), the variation ΔP can be obtained. The average value over V_G evaluated at $V_{DS} = -2$ V is $\overline{\Delta P} = 0.6 \times 10^{10}$ cm^{-2}, lower than in procedure #1. Repeating this calculation at different values of V_{DS} in the linear region, we obtain the squares in Fig. 5.6. The average value over V_{DS} and VG is $\overline{\Delta P}(\#2) = 0.3 \times 10^{10}$ cm^{-2}. The relative difference between procedure #1 and #2 is 88 %.

- **Procedure #3**. In this case, the variation of the trapped charge is extracted directly from the experimental data $I_D = I_D(V_D, V_G)$. We analyse the effect of working with the terminal voltages instead of the intrinsic ones. However, the mobility is extracted from the fitting of the experimental data with (5.3). This situation might be interesting if these results were close to the ones in procedure #1, since no computational time is needed to determine I_D as a function of the intrinsic voltages. The dotted lines in Fig. 5.5(b) show the drain current as a

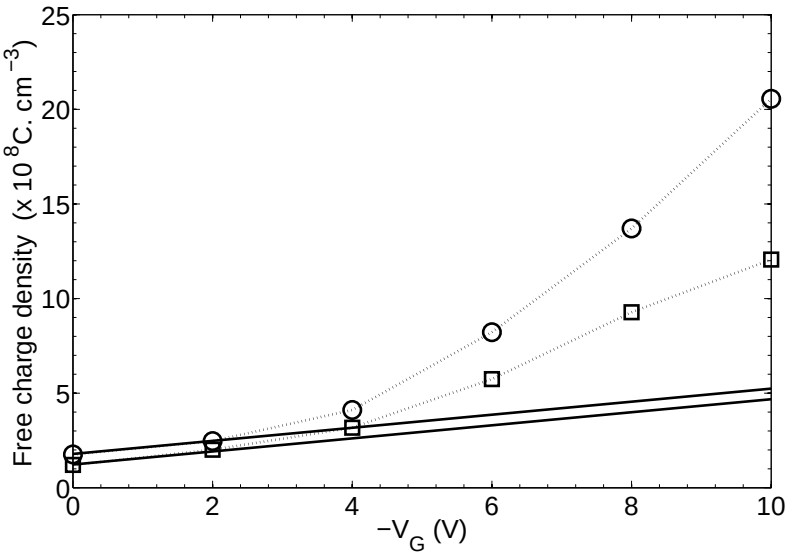

Figure 5.4: Free charge density in the intrinsic channel of the transistor with output characteristics in Fig. 5.3 as a function of V_G: evaluated from (4.10) with $V_{T_{FS}} = 5.18$ V and $V_{T_{BS}} = 3.55$ V (solid lines); $\theta K_{FS}\rho_{contact_{FS}}$ with $\theta K_{FS} = 1 \times 10^4$ (circles); and $\theta K_{BS}\rho_{contact_{BS}}$ with $\theta K_{FS} = 5 \times 10^3$ (squares).

function of V_G at $V_D = -2$ V. By introducing the variation of the drain current $\Delta I_D(V_D, V_G)$ in (5.1), ΔP can be obtained. The average value over V_G evaluated at $V_D = -2$ V is $\overline{\Delta P} = 0.93 \times 10^{10}$ cm^{-2}, lower than in procedure #1. Repeating this calculation at different V_{DS}, we obtain the crosses in Fig. 5.6. The average value of ΔP over V_D and V_G is $\overline{\Delta P}(\#3) = 0.77 \times 10^{10}$ cm^{-2}. The relative different between procedure #1 and #3 is 68 %. This relative variation is better than in procedure #2, however this result disregards the possibility of using directly the experimental data to obtain an accurate value of ΔP. Otherwise, we have to be conscious of the error we manage with.

- **Procedure #4**. In procedures #4 and #5, we consider the effect of the contacts on the mobility and how this variable affects the determination of ΔP. We consider model (5.5) with $I_D = V_C/R_C$ to fit the same experimental data of Fig. 5.3. The fitting of the experimental data with model (5.5) can be seen in Figs. 5.7(a) and (b). In this case, another set of fitting parameters is obtained: $\mu_o = 0.0024$ cm^2/ Vs and $V_T = 0.6$ V for both FS and BS. The parameter R_C in (5.5) for forward

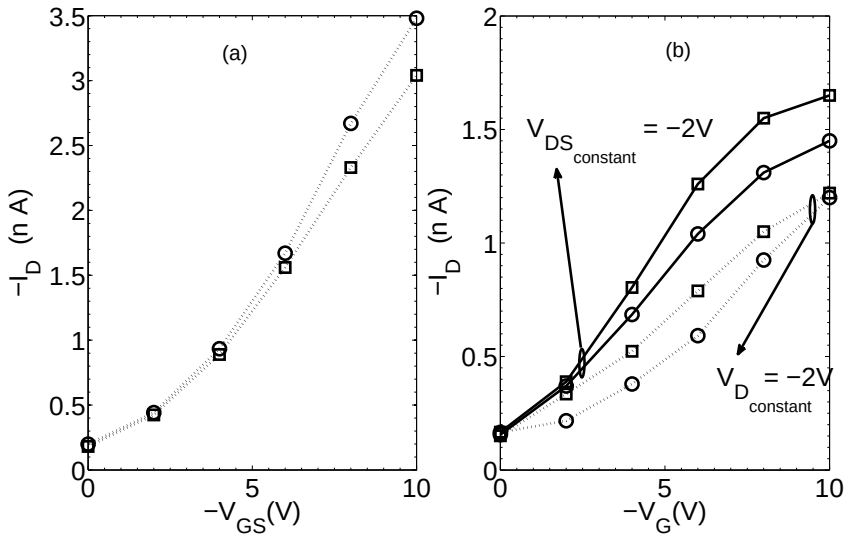

Figure 5.5: Transfer characteristics corresponding to the transistor in Fig. 5.3 [87]. (a) Procedure #1, intrinsic transistor, $I_D(V_{GS})$ at $V_{DS} = -2$ V. (b) Procedure # 3, external terminals, $I_D(V_G)$ at $V_D = -2$ V (dotted lines); and procedure # 2, intermediate situation, $I_D(V_G)$ at $V_{DS} = -2$ V(solid lines). (FS, circles; and BS, squares).

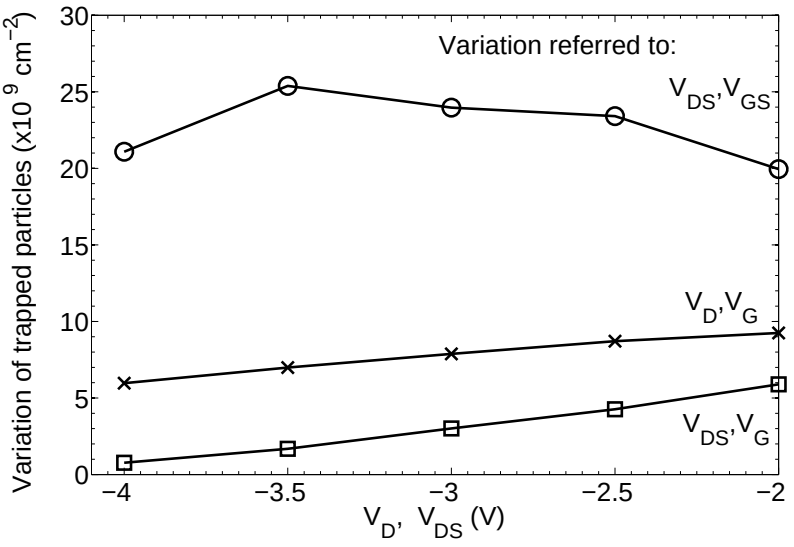

Figure 5.6: Variation of trapped particles obtained from the hysteresis cycles in Fig. 5.3. Intrinsic transistor, #1, (circles); intermediate situation, #2, (squares); external terminals, #3, (crosses).

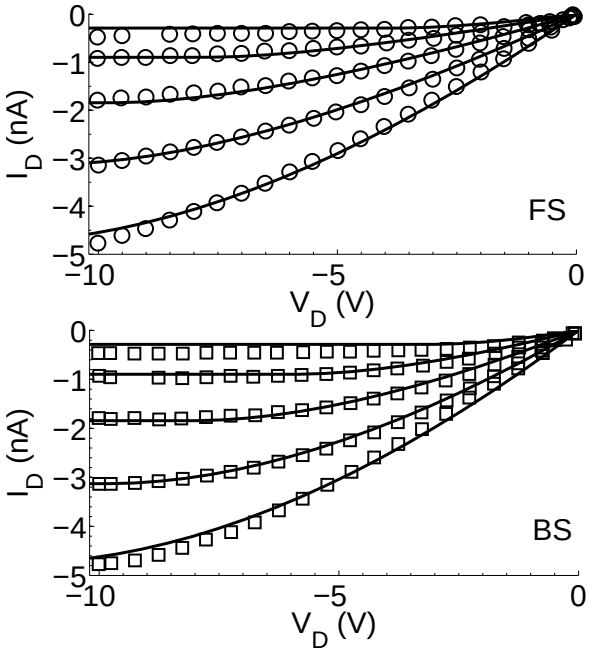

Figure 5.7: Comparison of the same experimental output characteristics of Fig. 5.3 (circles FS; and squares BS) with model (5.5) (solid lines). V_G = (-2, -4, -6, -8, -10) V from top to bottom

and backward sweeps for each V_G is given in Table 5.3. Although a good fitting is obtained, it does not mean that the fitting parameters have a good physical meaning, as has been checked positively with the ones extracted from model (5.3). An extensive discussion on how to select a proper value for the threshold voltage from curves with hysteresis was done in Chapter 4 [91].

Table 5.3: Extracted values from model 5.5 of $R_{C_{FS}}$ and $R_{C_{BS}}$ for the pentacene single-crystal sample with output characteristics in Fig. 5.7.

$V_G\ (Volts)$	$R_{C_{FS}}\ (\Omega)$	$R_{C_{BS}}\ (\Omega)$
0	55×10^8	20×10^8
-2	40×10^8	18×10^8
-4	35×10^8	15×10^8
-6	17×10^8	8.0×10^8
-8	8.0×10^8	4.0×10^8
-10	3.5×10^8	2.5×10^8

Once this agreement is achieved, the curves $I_D(V_{DS})$ for V_G = constant can be

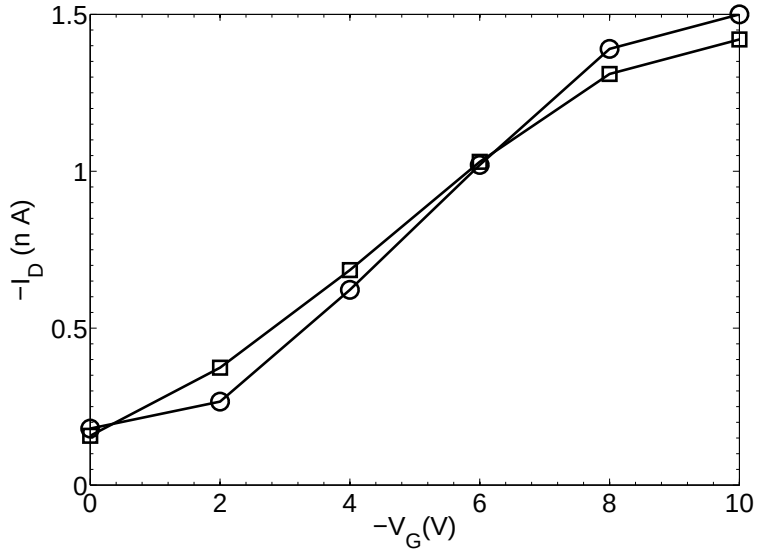

Figure 5.8: Transfer characteristics, $I_D(V_G)$ at $V_{DS} = -2$ V, after the fitting of the experimental data [87] in Figs. 5.7(a) and (b) with model (5.5). (FS, circles, and BS, squares).

extracted from the experimental data, as detailed in Sec. 5.3. One of the results the extraction process is shown in Fig. 5.8, where I_D is represented as a function of V_G at $V_{DS} = -2$ V. The variation of the drain current from Fig. 5.8, $\Delta I_D = \Delta I_D(V_{DS}, V_G)$, can be inserted in (5.2) to determine ΔP as a function of V_G. At $V_{DS} = -2$ V, the average value over V_G is $\overline{\Delta P} = 0.09 \times 10^{10}$ cm^{-2}. This procedure is repeated at different values of V_{DS} in the linear region. The average value over V_{DS} and V_G in this region is $\overline{\Delta P}(\#4) = 0.74 \times 10^{10}$ cm^{-2}. In order to analyze the effect of the contact region on the mobility, we can compare this result with the one in procedure #2, as ΔI_D is referred to the voltages V_{DS} and V_G, in both cases. Despite using different models, the ratio of ΔP between procedures #2 and #4 is similar to the ratio of the values of the mobility obtained with the models (5.3) and (5.5): μ (model (5.3)) /μ (model (5.5)) (=ratio of the values of the mobility extracted from the models (5.3) and (5.5)).

- **Procedure #5**. In this procedure, we consider the external voltages of the transistor (V_D, V_G), not the intrinsic ones. The variation of the trapped particles is determined by introducing $\Delta I_D = \Delta I_D(V_D, V_G)$ in (5.1). At $V_D = -2$ V, the average value of ΔP over V_G is $\overline{\Delta P} = 0.16 \times 10^{10}$ cm^{-2}. This calculation is repeated

at different values of V_D in the linear region. The averaged result over V_D and V_G in this region is $\overline{\Delta P} = 1.44 \times 10^{10}$ cm^{-2}. This result can be compared with the one in procedure #3. Both procedures use (5.1) to determine ΔP. Thus, ($\overline{\Delta P}$(#5)) / ($\overline{\Delta P}$(#3)) $\approx \mu$ (model (5.3)) /μ (model (5.5)).

By comparing the result of procedure #1 with the rest, we observe that neglecting the effect of the contact region on the terminal voltages reduces the value of ΔP. ΔP is also reduced when the contact region is not considered in the determination of the mobility. Both reductions are similar. In the case studied above, the factor γ, that represents the dependence of the mobility on the gate voltage, is close to zero. A greater value of γ would enhance the difference of results among the procedures. The relative variation of ΔP among the different procedures ranges from 70 % to 98 % . A summary of these results is seen in Table 5.4.

Table 5.4: Average variation of the trapped charge ($\triangle\ \overline{P}$) in the linear region during a hysteresis cycle in two kinds of $OTFT$ (showing linear and non-linear contact current-voltage curves).

	Linear $I_D - V_C$ curves		Non-Linear $I_D - V_C$ curves	
Procedure	$\overline{\Delta P}$ (cm^{-2})	μ (cm^2/Vs)	$\overline{\Delta P}$ (cm^{-2})	μ (cm^2/Vs)
#1	2.47 $\times 10^{10}$	0.0041	2.21 $\times 10^{11}$	0.38
#2	0.30 $\times 10^{10}$	0.0041	0.32 $\times 10^{11}$	0.38
#3	0.77 $\times 10^{10}$	0.0041	1.52 $\times 10^{11}$	0.38
#4	0.06 $\times 10^{10}$	0.0245	0.27 $\times 10^{11}$	1.80
#5	0.13 $\times 10^{10}$	0.0245	0.32 $\times 10^{11}$	1.80

5.4.2. Transistors with non-linear contacts

In this section, we repeat the previous analysis on $OTFTs$ showing a non-linear response at low values of the drain voltage. The objective is to analyse whether different behaviours of the current voltage curves at low values of the drain voltage affect the results. Fig. 5.9 shows output characteristics with hysteresis measured in a rubrene single crystal TFT [14] (symbols).

In this transistor, the gate dielectric thickness is $t_i = 0.3\mu$ m, the channel length L=16 μ m, the transistor width w=500 μ m and the organic-film thickness t_o=5 μ m.

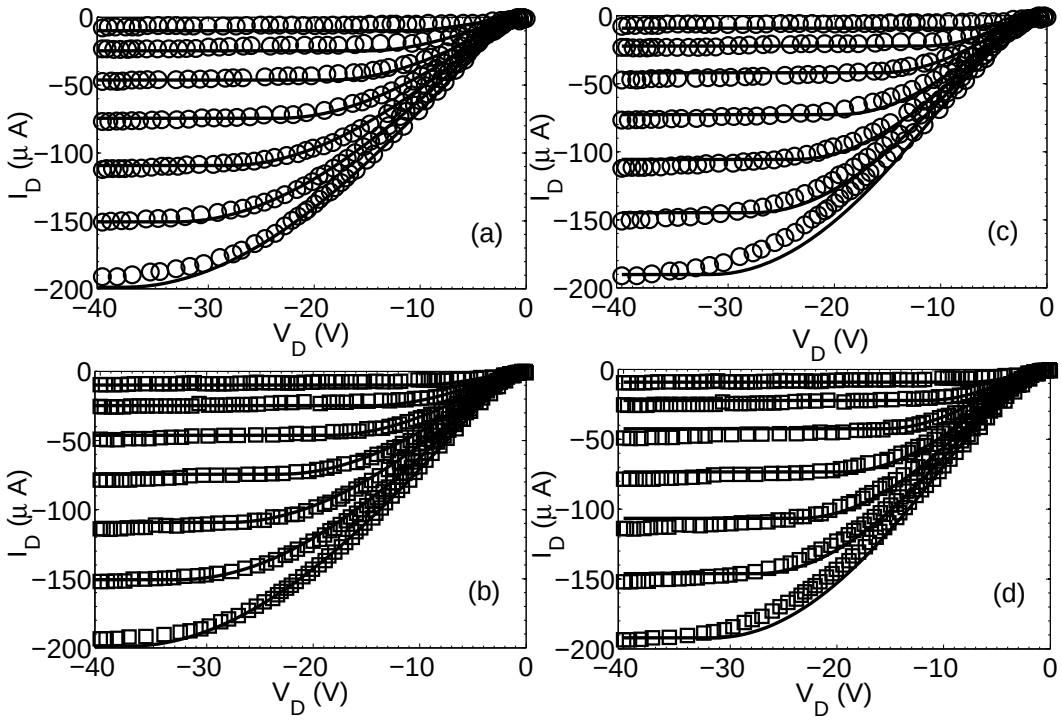

Figure 5.9: Comparison of the experimental (circles FS; and squares BS) output characteristics of a rubrene transistor in [14] , (a) and (b) with model (5.5) (solid lines), (c) and (d) with model (5.3) (solid lines). V_G = (-8, -12, -16, -20, -24, -28, -32) V from top to bottom.

The experimental $I - V$ curves in the FS and BS are compared with the compact model (5.3) (solid lines in 5.9(c) and (d)) and with the model (5.5) (solid lines in Fig. 5.9(a) and (b). The output characteristics show a non-linear trend at low V_D. In this case, $I_D = MV_C^2$ is employed in (5.3) and (5.5) to model the contact region. The fitting parameters from model (5.3) are extracted following the procedure developed in Chapter 4 [91]: $\mu_o = 0.38$ cm^2 / (Vs), $\gamma = 0$, $V_{T_{FS}}$=- 0.36 V and $V_{T_{BS}}$ = -0.4 V for the FS and BS. The parameter M in (5.3) for forward and backward sweeps for each V_G is given in Table 5.5.

In the case of model (5.5) the fitting parameters are: $\mu_o = 1.8$ cm^2/Vs, $V_T = -1$ V for both FS and BS. The parameter M in (5.5) for forward and backward sweeps for each V_G is given in Table 5.5.

Once the experimental data have been reproduced with models (5.3) and (5.5) and all fitting parameters are known, the current voltage curves of the intrinsic transistor and of the contact region can be extracted in both situations, and from them, the variation

of the trapped charge. Procedures #1, #2 and #3 analyse the curves extracted with model (5.3) and procedures #4 and #5 the curves extracted with model (5.5).

- **Procedure #1**. Fig. 5.10(a) shows the drain current as a function of the gate voltage V_{GS} at $V_{DS} = -6$ V. The variation of the drain current from Fig. 5.10(a) can be introduced in (5.2) to determine $\overline{\Delta P}$ as a function of V_{GS}. The average value over V_{GS} is 2.34×10^{11} cm^{-2}. This procedure is repeated at different values of V_{DS} in the linear region. The result is represented with circles in Fig.5.11(a). The average value over V_{GS} and V_{DS} is $\overline{\Delta P}(\#1) = 2.21 \times 10^{11}$ cm^{-2}. As in the previous case (section. 5.4.1), this procedure represents a situation where the ΔP is free from contact effects. The effect of the contact region on the terminal voltages and in the mobility is treated in the following procedures.

- **Procedure #2**. This case considers the effect of the contact region on the gate terminal. The variation of the trapped particles is analysed as a function of V_{DS} and V_G. Solid lines in Fig. 5.10(b), show the drain current as a function of V_G at $V_{DS} = -6$ V. By introducing the variation of the drain current $\Delta I_D(V_{DS}, V_G)$ in (5.2), the variation ΔP can be obtained. Its average value, evaluated over V_G at $V_{DS} = -6$ V, is $\overline{\Delta P} = 0.45 \times 10^{11}$ cm^{-2}, lower than in procedure #1. Repeating this calculation at different values of V_{DS}, we obtain the squares in Fig. 5.11. The average value over V_{DS} and V_G is $\overline{\Delta P}(\#2) = 0.32 \times 10^{11}$ cm^{-2}. The relative difference between the procedures #1 and #2 is 85 %.

- **Procedure #3**. In this case, the variation of the trapped charge is extracted

Table 5.5: Extracted values of M_{FS} and M_{BS} for the rubrene single-crystal sample with output characteristics in Fig. 4.4.

	Model (5.3)		Model (5.5)	
V_G (Volts)	M_{FS} (A/V^2)	M_{BS} (A/V^2)	M_{FS} (A/V^2)	M_{BS} (A/V^2)
-8	0.90×10^{-6}	0.90×10^{-6}	0.50×10^{-6}	1.00×10^{-6}
-12	1.00×10^{-6}	1.00×10^{-6}	1.50×10^{-6}	2.00×10^{-6}
-16	1.10×10^{-6}	1.15×10^{-6}	3.60×10^{-6}	3.50×10^{-6}
-20	1.41×10^{-6}	1.46×10^{-6}	3.90×10^{-6}	4.30×10^{-6}
-24	1.42×10^{-6}	1.47×10^{-6}	4.00×10^{-6}	4.50×10^{-6}
-28	1.43×10^{-6}	1.48×10^{-6}	4.03×10^{-6}	4.60×10^{-6}
-32	1.44×10^{-6}	1.49×10^{-6}	4.08×10^{-6}	4.70×10^{-6}

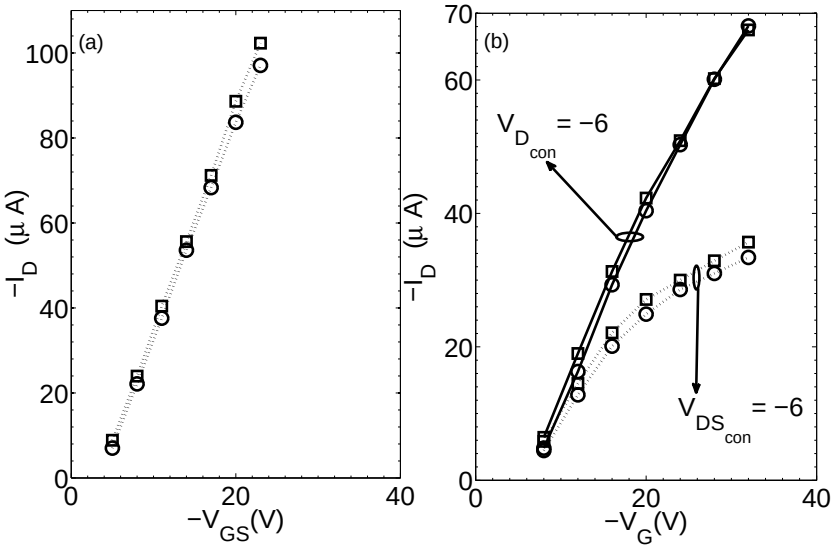

Figure 5.10: Transfer characteristics corresponding to the transistor in Fig. 5.9 [14]. (a) Procedure #1, intrinsic transistor, $I_D(V_{GS})$ at $V_{DS} = -6$ V. (b) Procedure # 3, external terminals, $I_D(V_G)$ at $V_D = -6$ V (dotted lines); and Procedure # 2, intermediate situation, $I_D(V_G)$ at $V_{DS} = -6$ V(solid lines). (FS, circles; and BS, squares).

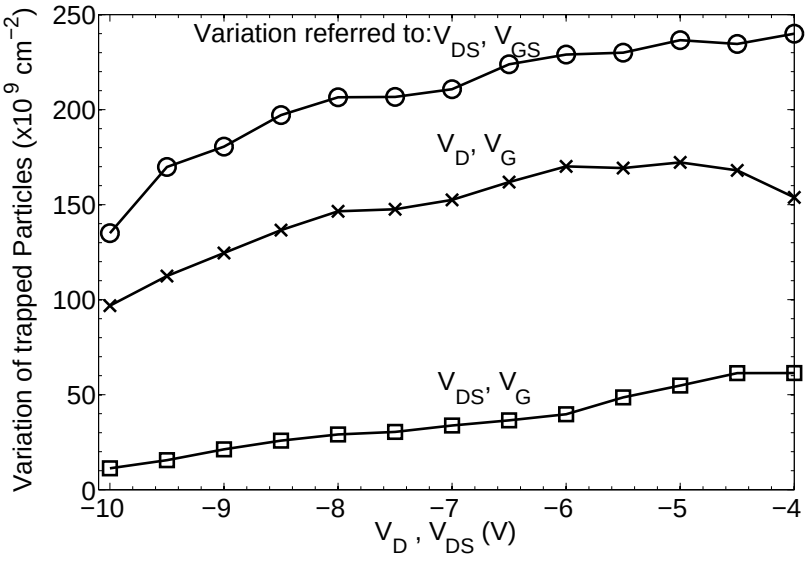

Figure 5.11: Variation of trapped particles obtained from the hysteresis cycles as a function of: V_{DS} and averaged over V_{GS} (circles); V_{DS} and averaged V_G (squares); and V_D and averaged over V_G (crosses).

directly from the experimental data $I_D = I_D(V_D, V_G)$. We work with the terminal voltages instead of the intrinsic ones. However, the mobility is extracted from the fitting of the experimental data with (5.3). The dotted lines in Fig. 5.10(b) show the drain current as a function of V_G at $V_D = -6$ V. By introducing the variation of the drain current $I_D(V_D, V_G)$ in (5.1), ΔP can be obtained. Its average value, evaluated over V_G at $V_D = -6$ V, is $\overline{\Delta P} = 1.7 \times 10^{11}$ cm^{-2}. Repeating this calculation at different V_{DS}, we obtain the crosses in Fig. 5.11. The average value over V_{DS} and V_{GS} is $\overline{\Delta P}(\#3) = 1.5 \times 10^{11}$ cm^{-2}, lower than in procedure #1. The relative difference between procedure #1 and #3 is 31 %. This relative variation is better than with procedure #2, but the result is not close enough to procedure #1.

In order to eliminate *in situ* the contact effects from the measurements, the four-terminal method is used. Authors in [14] determine the variation of trapped charge with this method obtaining a value of 10^{11} cm^{-2}. This value lies between our results in procedures #2 and #3, and the relative difference with procedure #1 is 60 %. Although all these results are of the same order of magnitude, it is interesting to discuss where these differences may come from. In the four-terminal method, the potential drop along the intrinsic channel is measured between the voltage-probing electrodes ($V_{C1} - V_{C2}$). They are separated such a distance from the drain and source terminals to eliminate the voltage the potential drop at the contact regions. The voltage drop in the intrinsic gate is estimated as the voltage V_{GS} between the gate contact and the channel region between these two voltage probes, where the channel conductivity is measured: $V_{GS} = V_G - (V_{C1} + V_{C2})/2$. These assumptions are necessary in order to determine the channel conductivity and the carrier mobility [14]. However, this represents a situation where the contact effects are eliminated from the drain to source voltage but not necessarily from the gate voltage, corresponding to the intermediate cases considered in our work. Actually, these authors confirmed some anomalies in the values of the mobility determined with this method.

- **Procedure #4**. We consider model (5.5) to fit the experimental data of Figs. 5.9(a) and (b). The values of the set of parameters (μ_o, γ , V_T and M) extracted with this model are different to those extracted with the model (5.3). In particular, we can study the effect of the contacts on the mobility and how this variable affects

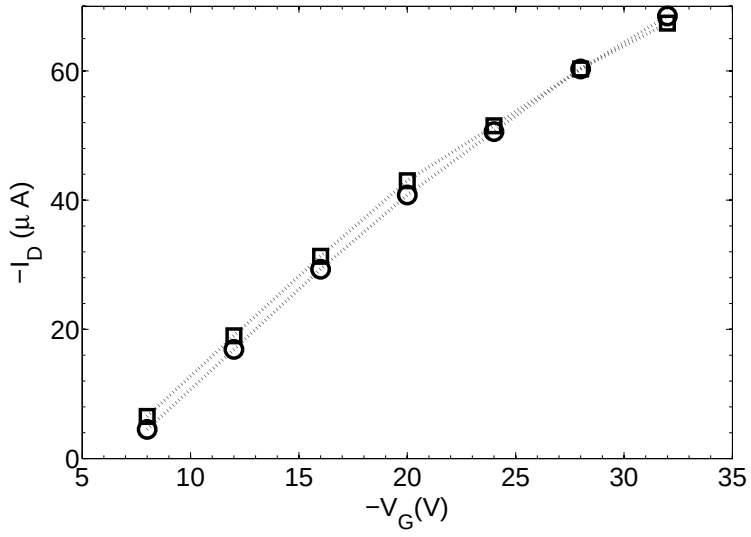

Figure 5.12: Transfer characteristics of the intrinsic transistor (circles FS and square BS); extracted after the fitting of the experimental data of Fig. 5.11 with model (5.5). $V_{DS} = -6$ V.

the determination of ΔP.

Once the parameter M that model the contact region, is extracted, the curve $I_D = I_D(V_C)$ can be determined and the relation $I_D = I_D(V_{DS}, V_G)$ can be obtained in both FS and BS (Sec. 5.3). Fig. 5.12 shows one of the results of this calculation, where I_D is represented as a function of V_G for $V_{DS} = -6$ V. The variation of the drain current $\Delta I_D(V_{DS}, V_G)$ of Fig. 5.12 can be inserted in (5.2) to determine ΔP as a function of V_G. The average value evaluated over V_G is $\overline{\Delta P} = 0.26 \times 10^{11}$ cm^{-2}. This procedure is repeated at different values of V_{DS} in the linear region. The average value over the linear region is $\overline{\Delta P}(\#4) = 0.27 \times 10^{11}$ cm^{-2}. This result is similar to the one in procedure #2. The mobility in this procedure is larger than the mobility in the procedure #2. However, the current voltage curves of the contact are also different. Therefore, the effect of using different values of the mobility is compensated with the effect of using different $I_D - V_C$ curves (or a different M parameter). We have to notice that procedures #2 and #4 represent cases where the contact effects are not eliminated from the gate-terminal voltage.

- **Procedure #5**. This procedure considers the curves $I_D - V_D$ measured at the transistor terminals. The variation of the trapped particles is determined by introducing

the variation of I_D in (5.1). In this case, the mobility used in (5.1) corresponds to the one extracted from model (5.5) ($\mu_o = 1.8$ cm^2/ Vs). Basically, the model (5.5) without considering the contact region reduces to the classical MOS model (7.1). At $V_D = -6$ V, the average value of ΔP over V_G is $\overline{\Delta P} = 0.36 \times 10^{11}$ cm^{-2}. Repeating this calculation at different V_D and averaging over V_D and V_G in the linear region, the result is $\overline{\Delta P}(\#5) = 0.32 \times 10^{11}$ cm^{-2}. This value can be compared with the one in procedure #3: ($\overline{\Delta P}(\#3)$) / ($\overline{\Delta P}(\#5)$) $\approx \mu$ (model (5.5)) /μ (model (5.3)). In these two cases, the value of the mobility is the only difference in the evaluation of $\overline{\Delta P}$

A summary of the study of the two kinds of $OTFT$ can be seen in Table 5.4. We can observe how the variation of ΔP deteriorates when a non proper value of the mobility is considered or the contact voltage is not eliminated from the terminal voltages. A proper estimation of the mobility is essential. In that sense, a model for the $OTFT$ including the contact region should be used. It should determine the value of the mobility and separate the contact voltage from the terminal voltages. The variation of the trapped charge during a hysteresis cycle must use the current curves of the intrinsic transistor. If the experimental data are used instead, an error of one order of magnitude can be obtained. The worst solution is, without any doubt, when the contact voltage is eliminated partially from the terminal voltages. The cases where the contact voltage, V_C, is eliminated from V_D but not from the V_G are clearly the worst of all, even considering a proper value of the mobility.

6

Conclusions

1. We have made use of a physical model to interpret contact effects in organic/polymeric thin film transistors, and we have incorporated it in a generic compact model that describes the output characteristics of $OTFTs$. The resulting model reproduces experimental data of output characteristics showing linear and highly non-linear responses at low drain voltages. Our model is compared with previous circuit models proposed to explain these behaviours. Our model provides a way to gain physical insight about the charge density in the low conductivity region near at the contact region and mirrors the changes of charge density in the rest of the device. Actually, the evolution with the gate voltage of the free to total charge density ratio in the low conductivity region at the contact is in agreement with the estimated charge density in the channel.

2. In parallel to this model, a parameter extraction procedure has been proposed in order to determine the model parameters, including the additional ones associated to the contact effects. The advantages of previous procedures (although less precise) are combined in our method. Although more physically advanced models are necessary in order to take into account all the effects that appear in the $OTFT$, previous simple models cannot be completely disregarded. We have demonstrated their usefulness in the characterization process.

3. The different steps of our procedure are monitored with experimental measurements from organic thin film transistors based on Zinc Phthalocyanine and data from other authors' experiments.

4. In addition, we have tested the characterization method in a transistor with known parameters obtaining no significant errors between the real parameters and the ones extracted with the method.

5. The characterization method has also been applied to transistors which output characteristics show both hysteresis and contact effects, making the characterization of these transistors more difficult. We have presented a technique, based on the previously developed compact model, to extract essential parameters, such as the carrier mobility, the threshold voltage and the variation of the trapped charge during a hysteresis cycle. The proposed technique overcomes the problems of having a greater number of parameters in the model and having an internal relation

between some of these parameters, such as the dependence of the threshold voltage with the trapped charge, especially at high gate voltages. The extraction of current voltage curves of both the contact region and the intrinsic channel from the experimental output characteristics has allowed for solving these problems. In particular, the study of the evolution of the charge density with the gate voltage, in the contact region and in the intrinsic channel, is essential to extract the parameters of the transistor. Transistors showing linear and non-linear contact effects have been studied. The results obtained with our technique have been compared with other results provided by different authors who employed more elaborate experimental techniques, and good agreements were obtained.

6. Different procedures to determine the variation of the trapped charge in an $OTFT$ during a hysteresis cycle have been presented. The procedures differ in the way the contact effects, present in the experimental data, are treated. The procedures separate the contribution of the intrinsic transistor and the contact region from the experimental data. The current voltage curves of the intrinsic transistor, of the external transistor, and of intermediate situations are used to determine the variation of the trapped charge. A comparison of these results is provided.

7. A study of the effects of the contact region on the value of the mobility extracted from different models has been made. A proper extraction of the mobility with a model that incorporates contact effects is essential to obtain good results, even if the terminal voltages are considered instead the intrinsic ones. In this regard, a compact model that describes the output characteristics of the transistor and includes the effect of the contact regions is considered as the best scenario. The worst scenario is when the contact voltage is eliminated partially from the terminal voltages.

8. The interpretation of output characteristics with hysteresis with different models shows how the values of the variation of the trapped charge are clearly altered by the inclusion or not of the contact effects on the terminal voltages and the mobility. The values obtained are always different and lower than the ones obtained with a compact model developed previously. From these results, we highlight the importance of using a compact model that properly considers the contact effects

of the transistor and accurately extracts information of the trapped charge in the semiconductor during a hysteresis cycle.

7

Resumen en español/Spanish summary

7.1. Resumen

El funcionamiento de los dispositivos semiconductores orgánicos modernos está limitado por efectos no ideales que no se caracterizan por modelos tradicionales de transporte. En este trabajo, se estudian dos grandes problemas que afectan al comportamiento de los transistores orgánicos y poliméricos de lámina delgada: los efectos de los contactos y los mecanismos de atrapamiento y emisión de carga que se producen en el interior del dispositivo. El hecho de que estos dos mecanismos estén presentes simultáneamente hace más complejo el estudio de estos transistores.

Se presenta en esta tesis un nuevo modelo compacto para transistores orgánicos de lámina delgada (OTFT). Permite describir características de salida de los transistores, incorporando los efectos de los contactos. El modelo se basa en expresiones físicamente realistas que describen el flujo de carga en la vecindad de los contactos que se han incorporado en un modelo de deriva desarrollado previamente. El modelo resultante sigue siendo compacto, al igual que el original, por lo que resulta de gran interés en simulaciones de circuitos con estos transistores. Un modelado adecuado necesita de parámetros que sean fácilmente extraíbles a partir de medidas experimentales y que contengan una relación con la física del dispositivo. Se propone también un método para extraer los parámetros del transistor, incluyendo los nuevos parámetros asociados a los contactos.

Se ha comprobado el modelo con medidas experimentales tomadas en transistores de lámina delgada donde el material orgánico es ftalocianina de zinc. Los contactos de drenador y fuente son de oro. Se analizan las respuestas de estos y otros transistores en la zona lineal y en la de saturación. En la región de bajas tensiones de drenador se pueden observar en general respuestas tanto lineales como no lineales. Ambas situaciones son analizadas en este trabajo. El método de extracción de parámetros sugerido en esta tesis proporciona una forma de estudiar la evolución de la densidad de carga en la región de baja conductividad próxima al contacto.

El método de extracción de parámetros se comprueba también con datos obtenidos de un transistor cuyos parámetros son conocidos. Este transistor conocido es realmente un artificio teórico que consta de un transistor ideal al que se le ha añadido en serie un elemento de dos terminales que simula unos contactos.

Otro problema que deteriora el funcionamiento de los transistores de lámina delgada es el mecanismo de atrapamiento y emisión de carga por parte de trampas situadas en la

estructura. Ello produce inestabilidades que son el origen de la histéresis en las curvas de salida o de transferencia de los transistores. La combinación de los fenómenos asociados a los contactos y a la histéresis hacen que el análisis de las curvas corriente tensión de los transistores sea más complicado. A pesar de ello se presenta un método de extracción de parámetros del transistor bajo la acción de estos dos mecanismos. El método se basa en el procedimiento desarrollado anteriormente en el caso de que no exista histéresis en las muestras. La nueva técnica de caracterización proporciona valores para la movilidad, la tensión umbral y la variación de la concentración de carga atrapada durante los ciclos de tensión. El hecho de que la tensión umbral varíe a medida que transcurre la medida incorpora dificultades a la hora de aplicar este método de extracción. En cualquier caso se proponen soluciones para solventar este inconveniente. Otro de los inconvenientes a los que también se les ha puesto solución es la existencia de varios conjuntos de parámetros que hacen coincidir el modelo teórico con los datos experimentales. Se han analizado las soluciones y buscado explicación física para ellas. Solo aquellas soluciones con un buen comportamiento físico se consideran aceptables. Para fijar qué soluciones son físicamente aceptables se analizan curvas corriente-tensión en el contacto y en el transistor intrínseco. Se estima el valor de la densidad de carga libre en la zona del contacto y en el canal a partir de estas curvas, se representan en función de la tensión de puerta y se comparan. La comparación de ambas permite encontrar la solución física buscada. Nuestros resultados se comparan con otros resultados que utilizan técnicas de medida más complejas, como es el caso de las medidas de cuatro puntas.

Por último, se comparan distintos procedimiento de extracción de curvas corriente tensión asociadas al canal intrínseco del transistor a partir de curvas de salida en el transistor. Cada procedimiento proporciona valores diferentes de la variación de la densidad de carga atrapada en el transistor durante los ciclos de histéresis. Algunos procedimientos tienen en común que, aunque utilizan distintos modelos de transistor, todos reproducen fielmente las curvas de corriente tensión. Se analizan también otros procedimientos basados en un mismo modelo pero que extraen los efectos de los contactos de forma diferente. Con ello se pretende mostrar la importancia que tiene el utilizar un método apropiado de extracción de los efectos de los contactos de las curvas características de un transistor. Los efectos de los contactos no deben afectar en ninguna manera ni a la movilidad ni a las tensiones medidas en los terminales externos del transistor. El modelo compacto desarrollado en esta tesis se presenta como la mejor alternativa para resolver todos estos

problemas.

7.2. Estructura de la Tesis

Durante las últimas décadas ha existido un enorme interés en el desarrollo de dispositivos electrónicos basados en películas de polímeros y materiales orgánicos, diferenciados estos por la longitud de sus cadenas, largas y cortas, respectivamente. A pesar de esta distinción, los denominaremos materiales orgánicos o polímeros indistintamente. Desde que se fabricó el primer material orgánico, los esfuerzos están centrados en buscar soluciones económicas [1]. Las ventajas de estos materiales, entre otras, son el bajo costo de fabricación y su posibilidad de combinarse junto a sustratos flexibles. [2]. Se pueden fabricar también a bajas temperaturas [3]. Estas ventajas hacen que los transistores orgánicos de lámina delgada sean atractivos en aplicaciones como etiquetas electrónicas o como controladores activos de pantallas gigantes. Sin embargo, también hay desventajas que deben ser mencionadas y a las que se debe poner solución. Hay muchos trabajos dedicados a encontrar materiales empleados en transistores con una movilidad de carga lo más grande posible [4]. Otros esfuerzos se centran en el estudio de los efectos de los contactos del transistor, pues parte de la tensión que se aplica entre drenador y fuente, V_D, cae en la zona de los contactos, pero principalemente en el contacto de fuente [5]. Además del límite impuesto por los mecanismos de transporte en el orgánico a la conducción de carga, hay que añadir el límite impuesto por los propios contactos del $OTFT$.

Las regiones de los contactos pueden alterar las características de salida del transistor, haciendo que el modelo tradicional del MOS cristalino (Metal-óxido-semiconductor) sea incapaz de interpretar el funcionamiento del transistor. En ese sentido, hay muchos trabajos dedicados a desarrollar modelos con el objetivo de reproducir las características de salida del transistor, y desarrollar métodos de extracción de parámetros [2][5][6][7][8]. El desarrollo de modelos precisos y eficientes computacionalmente es crítico para reducir el tiempo de ciclo entre diseño, fabricación y caracterización. Además, para guiar el proceso de diseño y para mostrar explícitamente las relaciones entre las propiedades del material y el diseño de un dispositivo y su rendimiento, es necesario disponer de un modelo compacto con base física sólida para los TFTs que emergen con las nuevas tecnologías [9]. En el Capítulo 2, trabajamos con esta idea. Allí se presentan los principales desafíos de la tesis. La gráfica 7.1 muestra un resumen de los mismos:

a) Proponer un modelo adecuado para las características de salida $I_D - V_D$ de un transistor,

b) Proponer un modelo adecuado para la característica de corriente-tensión en la región cerca del contacto, $I_D - V_C$, e incorporarlo en el modelo de las características de salida del transistor, y

c) Proponer un método de extracción de las curvas $I_D - V_C$ en el contacto y del resto de los parámetros del modelo resultante.

El objetivo es mejorar la modelización teórica de transistores orgánicos de lamina delgada con la inclusión de los efectos de contacto. El procedimiento de extracción se aplica inicialmente a datos experimentales tomados por nuestros colaboradores de la Universidad de Brunel (UK), en $OTFTs$ de ftalocianina de cinc.

En el Capítulos 3, el método se comprueba con unas características de salida de un transistor en el que se conocen sus parámetros. Un miembro de nuestro equipo crea un conjunto de características de salida de un transistor cuyos parámetros sólo esta persona sabe. Otro miembro del equipo tiene que utilizar el método desarrollado en el capítulo previo para encontrar los valores de los parámetros, y por lo tanto, dar validez al procedimiento.

En los Capítulos 4 y 5, se añade un nuevo problema a la caracterización de transistores orgánicos de lamina delgada: el tratamiento de las curvas de corriente-tensión que muestran fenómenos de histéresis y los efectos de contacto simultáneamente. Los orígenes del fenómeno de histéresis son los mecanismos atrapamiento y emisión que tienen lugar en el $OTFT$. Estos mecanismos pueden causar inestabilidades que a su vez provocan cambios en la movilidad de los portadores y en la tensión umbral de los transistores orgánicos [10]. El estudio de la histéresis es importante ya que puede proporcionar información acerca de la variación de carga atrapada en el material orgánico. Posteriormente, esta información se puede relacionar con parámetros tecnológicos, con el objetivo de encontrar un diseño de dispositivo mejor.

La combinación de los mecanismos de histéresis junto a los contactos hace más difícil la caracterización del transistor. Existen estudios previos que caracterizan la histéresis producida en las curvas de transferencia y de salida de los transistores. Algunos casos no consideran los efectos de los contactos [13]. En otros casos, los efectos de los contactos se

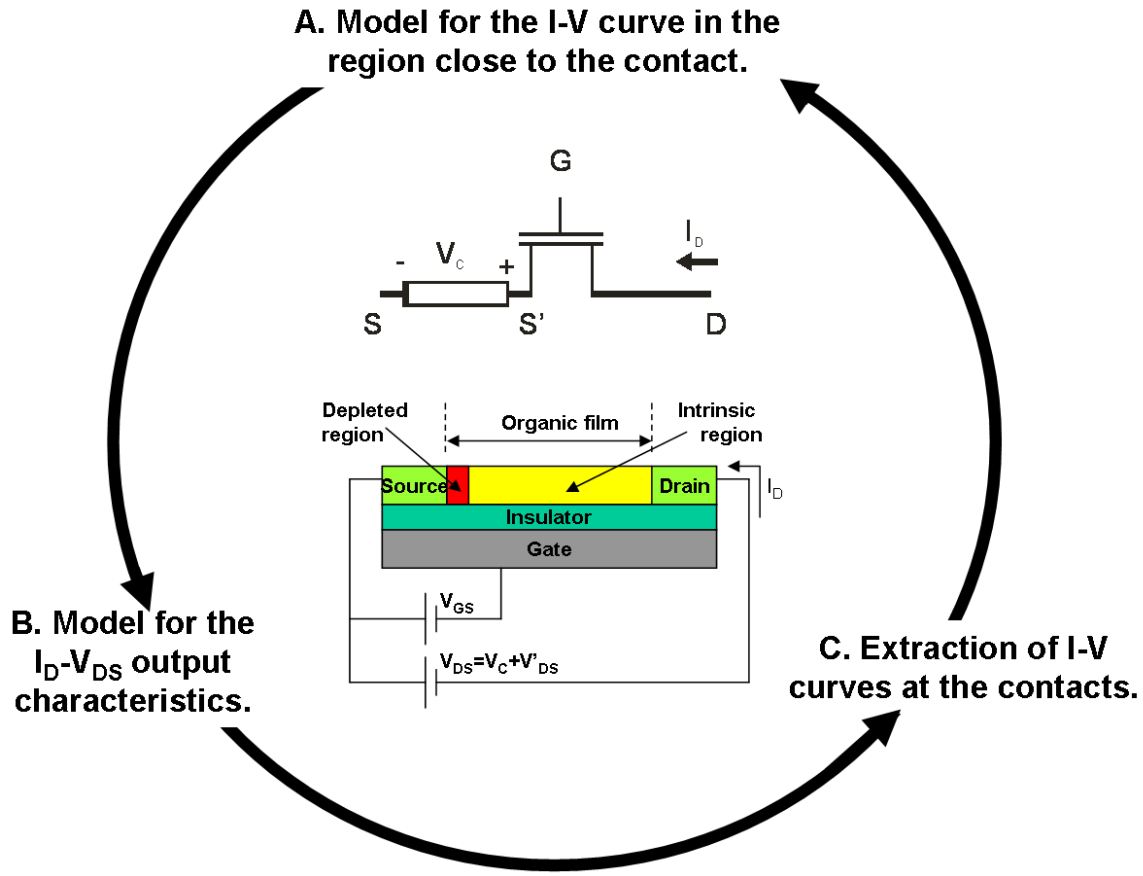

Figure 7.1: Esquema donde se enumeran los problemas que podemos encontrar al analizar curvas corriente-tensión en transistores afectados por los contactos: propuesta de un modelo para la región de los contactos, integración de este modelo en modelos compactos existentes para transistores y elaboración de una técnica que permita extraer los parámetros del modelo a partir de la comparación del mismo con medidas experimentales.

eliminan de los datos experimentales mediante el uso procedimientos experimentales algo más complejos, como el método de cuatro terminales, en lugar del método tradicional que emplea dos terminales [14].

En el capítulo 4, se propone un método para extraer información sobre la variación de la carga atrapada que se produce durante los ciclos de histéresis. Las curvas de corriente-tensión se miden con el procedimiento de dos terminales. El método resuelve el problema de procesamiento añadido de los efectos de los contactos que aparecen en las curvas I_D-V_D con histéresis. El método se aplica a curvas de corriente-tensión tomadas por otros autores donde se observan estos dos efectos [13][14]. Los resultados que se extraen para la

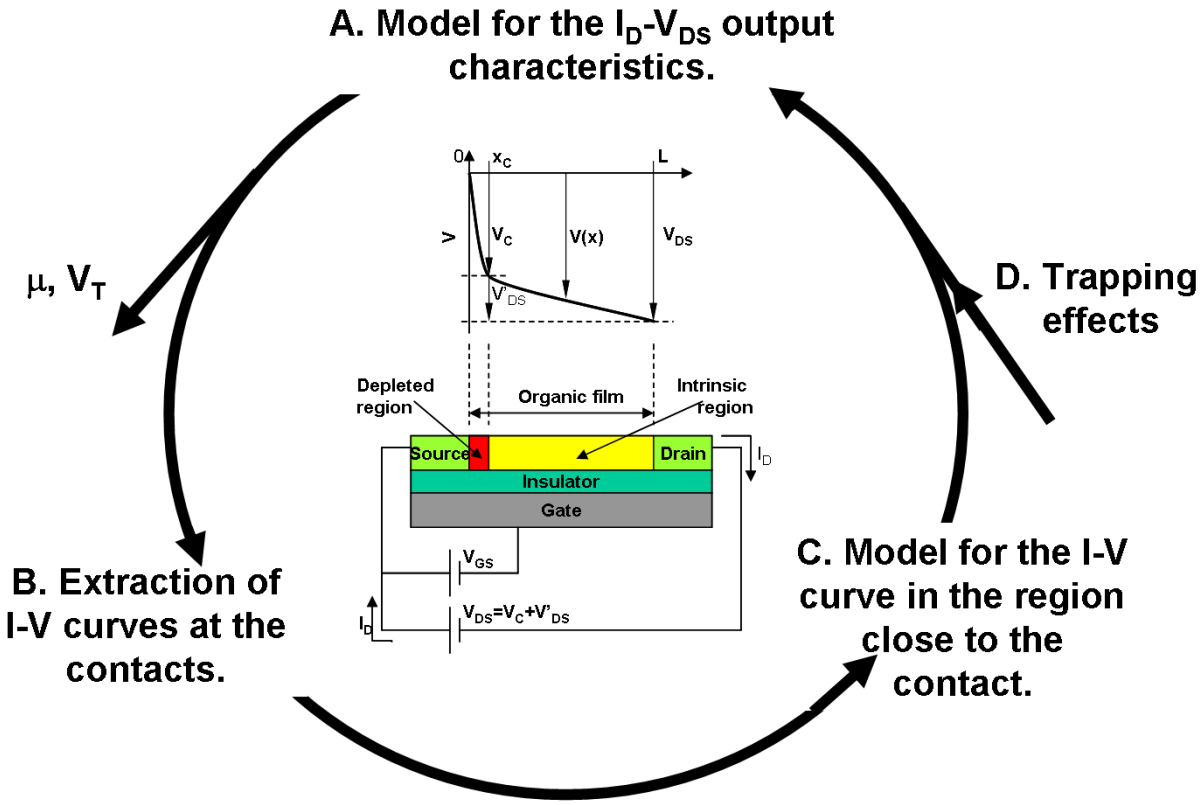

Figure 7.2: Esquema donde se enumeran los problemas que podemos encontrar al analizar curvas corriente-tensión en transistores afectados por los contactos e histéresis: los efectos del atrapamiento de carga se deben añadir a los ya detallados en el esquema de la figura 7.1.

variación de carga atrapada con este método se comparan con otros valores encontrados en la literatura. En concreto, comparamos nuestros resultados con los obtenidos por el método de cuatro terminales, que también considera los efectos de contacto.

En el Capítulo 5, se proponen diferentes maneras para extraer la variación de la carga atrapada durante el ciclo de histéresis. Se proponen diferentes métodos que varían en el grado de dificultad pero también en el grado de precisión de los resultados obtenidos. Un resumen gráfico de los capítulos 4 y 5 se puede ver en la figura. 7.2. A continuación, se enumeran los principales objetivos y la metodología general seguida en el trabajo, aunque los métodos específicos están detallados en cada capítulo. Se introducen también en este amplio resumen de la tesis algunos conceptos básicos utilizados en esta tesis. Finalmente se resumen las conclusiones.

7.3. Objetivos

1. Desarrollar un modelo compacto que describa las características de salida de los transistores orgánicos o poliméricos de lámina delgada y que incluya el efecto de los contactos. Después de la incorporación de los efectos de contacto, el modelo debe tener parámetros que se puedan caracterizar o intuir con relativa facilidad, evitando parámetros de ajuste innecesarios.

2. Proponer un método de caracterización que extraiga los parámetros del modelo (la movilidad, la tensión umbral y los nuevos parámetros de contacto) mediante la comparación de los datos experimentales con los resultados teóricos.

3. Aplicar el método a datos experimentales tomados por nuestro equipo o por otros autores.

4. Proponer una prueba para verificar la validez del modelo.

5. Adaptar el método de caracterización a datos experimentales que muestren los efectos tanto de los contactos como de histéresis, superando el problema de trabajar con una tensión umbral variable.

6. Caracterizar la presencia de trampas en el transistor mediante la determinación de la variación de la carga atrapada que se produce durante el ciclo de histéresis.

7. Analizar diferentes maneras para determinar la variación de la carga atrapada y comparar los resultados.

8. Encontrar una conexión física entre los mecanismos que tienen lugar en la región de contacto y en el canal intrínseco del transistor.

7.4. Metodología

El método para cumplir con todos estos objetivos se basa en los siguientes pasos principales:

1. El estudio del estado del arte de las técnicas de modelado compacto de transistores orgánicos de lámina delgada.

2. La propuesta de modelos matemáticos simples o modificaciones de otros ya existentes que describen las características de salida de un transistor.

3. El desarrollo de un procedimiento para extraer los parámetros del modelo propuesto basado en el análisis de datos experimentales. Los datos experimentales pueden ser tomados por algunos de nuestros colaboradores de fuera de la Universidad de Granada o extraídos de experimentos de otros autores. En este último caso la revisión bibliográfica vuelve a ser fundamental.

4. La implementación en software de dichos modelos y procedimientos.

   Los métodos específicos seguidos para tratar los diferentes temas de esta tesis se detallan en cada capítulo.

7.5. Conceptos generales usados en la tesis

Los materiales orgánicos

Los materiales orgánicos presentes en los dispositivos electrónicos se pueden clasificar en conductores y aislantes permanentes, semiconductores y otros materiales con propiedades añadidas como la piezoelectricidad y la histéresis.

Los polímeros conductores se emplean en conexiones y contactos en dispositivos orgánicos, debido a su idoneidad para ser impresos. Hay tres clases principales de polímeros conductores utilizados para la electrónica impresa: politiofenos (polipirroles y relacionados), polianilinas, y polímeros aislantes con inserciones de nanoestructuras conductoras.

El papel principal de un aislante dentro de los dispositivos orgánicos lo juega como aislante de puerta de los transistores de efecto campo orgánicos (OFETs). Algunos de estos polímeros pueden ser poli(metacrilato de metilo), poli(vinil fenol) y otros poliestirenos, alcohol de polivinilo, poliamidas, polímeros de redes de silicona y parileno. El papel del aislante de puerta también es primordial en temas de estabilidad del dispositivo como se mencionará un poco más adelante.

Los semiconductores orgánicos ($OSCs$) en forma de sólidos moleculares y/o polímeros semiconductores los podemos encontrar en transistores, diodos, sensores, transductores y elementos de memoria. Las aplicaciones de estos dispositivos se pueden encontrar en

circuitos de complejidad moderada, tales como controladores de pantallas de ledes, etiquetas de identificación por radiofrecuencia (RFID), o elementos sensibles a presión.

El orbital molecular desocupado de menor energía (LUMO) de la mayoría de los compuestos orgánicos más se encuentra fuera del rango preferido para el transporte de electrones. Esta es la razón por la que hay menos estructuras que se han identificado como semiconductores tipo n (transistores de canal n) en comparación con el número de semiconductores tipo p (transistores de canal p). La cantidad de huecos en un semiconductor viene determinada por la posición relativa del orbital molecular ocupado de mayor energía (HOMO) con respecto a la función trabajo del contacto, incluyendo las influencias ambientales que modifican esta relación

No por ello se ha dejado de buscar nuevos tipos de materiales tipo n debido fundamentalmente a las ventajas que ofrecen los circuitos con transistores complementarios n y p. Las conocidas ventajas de los circuitos con transistores complementarios son el bajo consumo y la sencillez de diseño de los circuitos, en comparación con los que emplean un solo tipo de transistor n o p. En los últimos años ha habido una atención creciente hacia los materiales de canal n, con mejoras notables en el aumento de la movilidad, el cociente de corrientes on/off y la tensión umbral [15][16][17][18][19][20][21]. A pesar de todo, el funcionamiento de los mejores materiales de canal n no es tan bueno como el de lo materiales p, como el caso del pentaceno, [22] que es el material de referencia en aplicaciones con transistores. Algunos de los materiales tipo p incluyen combinaciones de anillos (tales como el mencionado pentaceno o thienothiophene, benzodithiophene, dithienoanthracene, y tetraceno), cadenas cortas oligoméricas de anillos (diversas combinaciones de tiofenos, fenilenos, tiazoles, y pirroles), copolímeros de etileno y grupos etinileno, y selenofenos. Algunas de estas estructuras se muestran en la figura. 7.3.

Transistores orgánicos de efecto campo

Un transistor orgánico de efecto campo ($OTFT$) es un dispositivo electrónico cuyo funcionamiento gira en torno a una estructura metal-aislante-semiconductor. Está formado por una puerta metálica, un dieléctrico, y capas de semiconductores. Dos contactos de metal, fuente y drenador, están conectados eléctricamente a la lámina semiconductora, tal como se muestra esquemáticamente en la figura. 7.4. La posición de estos electrodos en la parte superior de la estructura o incrustados entre el semiconductor y el aislante

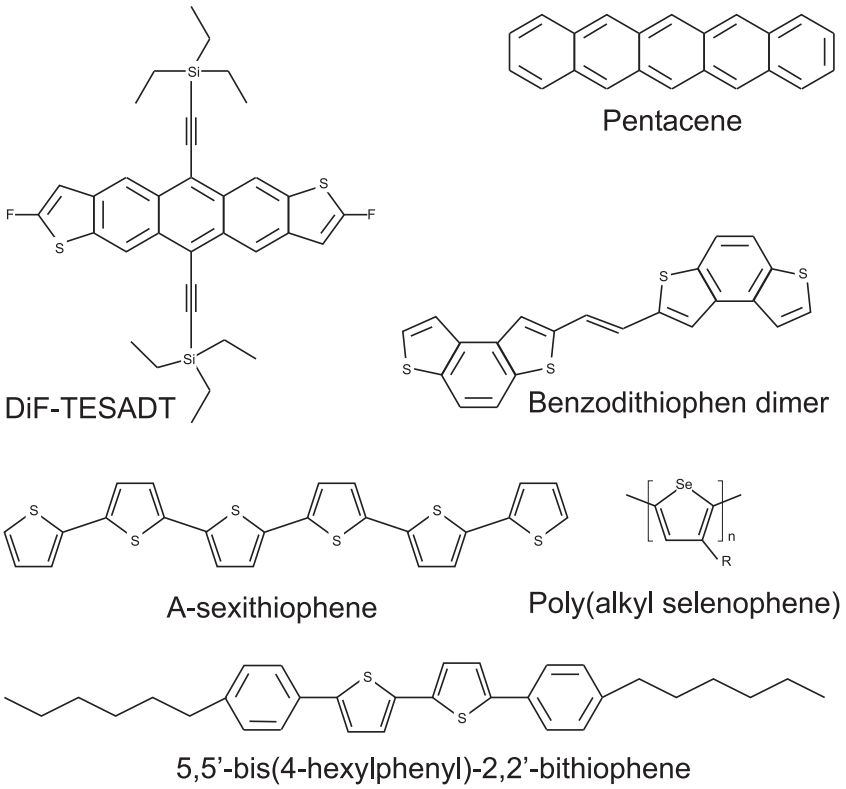

Figure 7.3: Algunos semiconductores tipo p.

definen dos configuraciones típicas de transistores: el transistor de contactos superiores o el transistor de contactos inferiores, respectivamente. Esta estructura fue desarrollada inicialmente para los transistores de silicio amorfo [23][24]. El electrodo de puerta también se utiliza como substrato, proporcionando un soporte a toda la estructura. El óxido aislante o los polímeros aislantes recubre la puerta metálica con o sin tratamiento de superficie. Si no se aplica una tensión a la puerta V_{GS}, la conductividad intrínseca del semiconductor orgánico es baja; si se aplica una tensión V_{DS} entre drenador y puerta, fluirá muy poca corriente a través de la película semiconductora. Se dice que el dispositivo está en el estado OFF. Cuando una tensión V_{GS} se aplica a la puerta, el campo eléctrico que existe a través de la estructura MOS atrae cargas hacia la interfaz dieléctrico-semiconductor. Estas cargas acumuladas son en su mayoría móviles y dan lugar a un canal conductor entre la fuente y el drenador. Estas cargas móviles pueden moverse en respuesta a la tensión V_{DS} aplicada. El transistor está funcionando en el modo ON o acumulación.

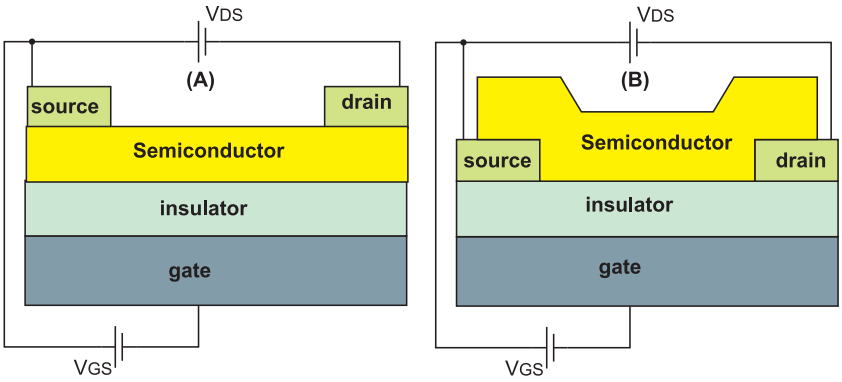

Figure 7.4: Estructuras típicas de (*OFETs*): (a) Configuración de contactos superiores; y (b) configuración de contactos inferiores.

El canal conductor aparece por encima de un valor umbral, V_T. El valor de esta tensión umbral depende de diferentes mecanismos internos de la estructura. La mayoría de los semiconductores orgánicos no están dopados intencionadamente por lo que las cargas existentes son inyectadas y extraídas a través de los electrodos. En la mayoría de los casos, hay un desajuste entre el nivel de Fermi de los electrodos y el *HOMO* (*LUMO*) de los semiconductores *tipo p* (*tipo n*), que da lugar a la existencia de barreras de inyección de carga. Es necesaria la aplicación de una tensión V_{GS} no nula a la puerta para modificar los niveles orbitales de los semiconductores hacia arriba o hacia debajo de manera que los orbitales moleculares entran en resonancia con el nivel de Fermi del electrodo y reduce las barreras de inyección de carga. Por otro lado, siempre hay estados asociados a trampas, impurezas y defectos en la película semiconductora, así como moléculas de H_2O y O_2 adsorbidas del ambiente. Es necesario aplicar una tensión V_{GS} no nula a la puerta para llenar estos estados trampa antes de que las cargas móviles pueden ser transportadas a lo largo del canal de conducción. El umbral de tensión V_T se define para tener en cuenta todos esos efectos.

Las curvas corriente-tensión experimentales de un *OFET* son muy similares a las de los MOSFETs. Esta es la razón por la que los *OFETs* han sido descritos con las ecuaciones clásicas que describen el transistor MOS:

$$\begin{aligned} I_D &= \frac{w\mu_o C_i}{L}[(V_{GS}-V_T)V_{DS}-\frac{V_{DS}^2}{2}], V_{DS} < V_{GS}-V_T \\ I_D &= \frac{w\mu_o C_i}{2L}[(V_{GS}-V_T)^2], V_{DS} \geq V_{GS}-V_T \end{aligned} \tag{7.1}$$

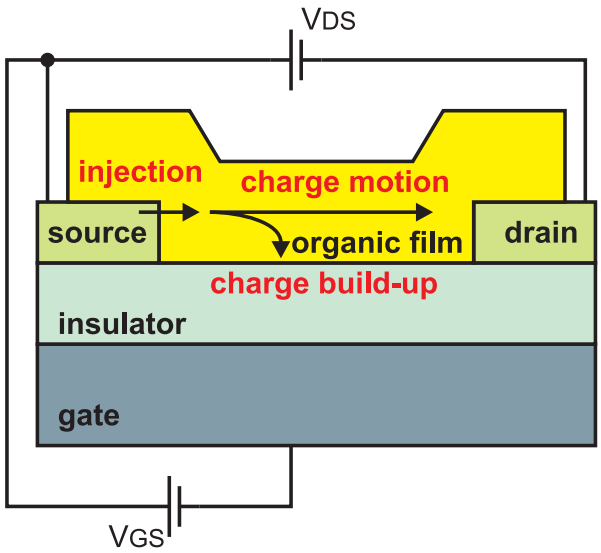

Figure 7.5: Mecanismos que hacen que el comportamiento de los OTFTs se aleje del modelo del transistor MOS cristalino ideal [29].

donde C_i es la capacidad del aislante de puerta por unidad de área, V_T es la tensión umbral, mu_o es la movilidad de los portadores y w y L son la anchura y la longitud del canal, respectivamente.

Hay algunos aspectos que requieren especial consideración y hacen que los $OTFTs$ se separen del modelo ideal del MOS: la inyección de carga de los contactos [25][26], el transporte de carga en el semiconductor orgánico [3][8][27] y las inestabilidades creadas por la carga acumulada en la estructura [28][25][8]. Se resumen en la figura 7.5. La inyección de carga desde el electrodo de fuente limita la cantidad de portadores que pueden entrar en el material orgánico por unidad de tiempo, mientras que la movilidad efectiva de los portadores (controlada por los mecanismos de hopping o salto entre moléculas) determina la deriva de los portadores hacia el electrodo de drenador [29]. La separación de carga eléctrica en un material polímero en partes móviles y atrapadas se ha propuesto con anterioridad en [29], y la carga atrapada se utiliza ampliamente para dar explicación de la histéresis en medidas I_D–V_{GS} [30] y del comportamiento no estacionario de la tensión de umbral V_T [8].

Movilidad de los portadores de carga

La transferencia de carga está directamente relacionada con la movilidad de carga. La movilidad de los portadores de carga μ define la relación entre la velocidad adquirida por los portadores de carga bajo el efecto de un campo eléctrico. La movilidad es generalmente una función de la tensión de puerta. Aunque el mecanismo de transporte de carga en transistores orgánicos está todavía bajo investigación, se han desarrollado varios modelos para interpretar la dependencia de voltaje de la puerta de la movilidad [31][32][33][34][24]. En general, hay trampas distribuidas en los semiconductores orgánicos. Por este motivo, a medida que el voltaje de puerta es mayor, más trampas son llenadas por las cargas inyectadas, dejando menos trampas que ralenticen el movimiento de las cargas. Por lo tanto, las cargas se mueven más rápido cuando el voltaje de la puerta aumenta, lo cual es consistente con el hecho de que la movilidad general aumenta con la tensión de puerta en la mayoría de $OFETs$.

Efectos de los contactos

En los casos en los que la movilidad no parece aumentar con la tensión de puerta, la resistencia de los contactos puede tener un efecto relativamente más fuerte en la corriente a tensiones de puerta superiores, disminuyendo la movilidad aparente. Las regiones de contacto del transistor orgánico requieren un estudio diferente. La figura. 7.6 muestra un esquema de un transistor, donde se destacan las regiones de baja conductividad próximas al drenador y a la fuente. Hay evidencia experimental que demuestra la existencia de estas regiones. La primera es evidente, debido a la propia naturaleza de los diferentes materiales que constituyen los contactos. Podemos encontrar una segunda razón en micro-fotografías de la interfaz. En ellas se muestra cómo la densidad de las moléculas en el material orgánico no son del mismo tamaño cerca del contacto metalúrgico o lejos del mismo [8]. Una tercera razón se encuentra en medidas de perfil de potencial a lo largo del canal del transistor. Estas medidas muestran una caída de tensión en el contato de fuente mayor que la que se produce cerca del drenador [35]. En esta situación, se puede prescindir de la caída de tensión entre el drenador y el canal intrínseco (Fig. 7.7).

Podemos encontrar muchos trabajos dedicados a mejorar las regiones de los contactos para favorecer la inyección o extracción de la carga entre el metal y el semiconductor orgánico [36][37][38][39]. Podemos citar obras donde se introduce una capa fina entre estos

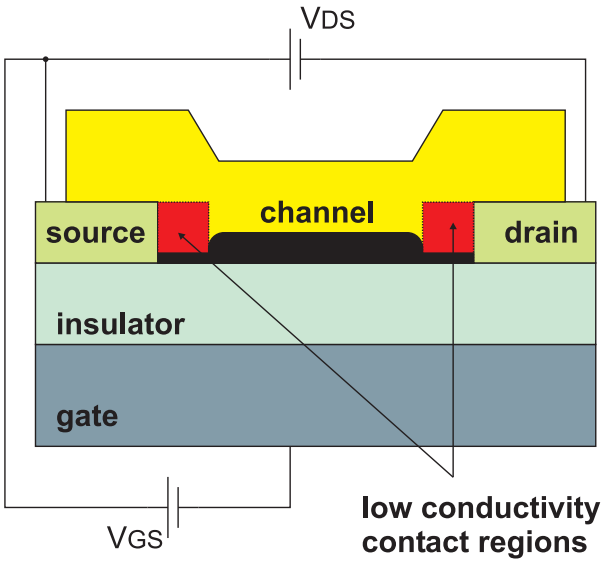

Figure 7.6: Transistor orgánico que muestra las regiones de baja conductividad cercanas a los contactos.

dos materiales con el fin de modular la altura de la barrera de energía en el contacto [38]. Nuestro interés en este trabajo es encontrar un modelo adecuado para la región de contacto que pueda ser incorporada en el modelo de transistor.

Fenómenos de histéresis en OTFTs

La histéresis en OTFTs se atribuye a defectos o trampas, ya sea en el dieléctrico de puerta o en el material semiconductor (o sus interfaces) [10][40][41]. El estudio de las curvas corriente de tensión con histéresis puede proporcionar información acerca de los defectos y las trampas presentes en el transistor orgánico. La caracterización de estas trampas se puede utilizar posteriormente para lograr un mejor diseño del dispositivo.

La histéresis se muestra como un ciclo en las características de transferencia ($I_D - V_G$) o en las características de salida ($I_D - V_D$) donde I_D depende de la dirección del barrido de V_G o V_D. Es frecuente observar este tipo de bi-estabilidades eléctricas reversibles en transistores orgánicos de efecto de campo. Dependiendo del origen microscópico, la localización de las trampas y defectos, la histéresis puede dar lugar a que el barrido de vuelta sea mayor o menor que el barrido de ida [40]. La histéresis se puede dividir en dos tipos: permanente (donde no hay cambios significativos de la tensión umbral con el tiempo) y

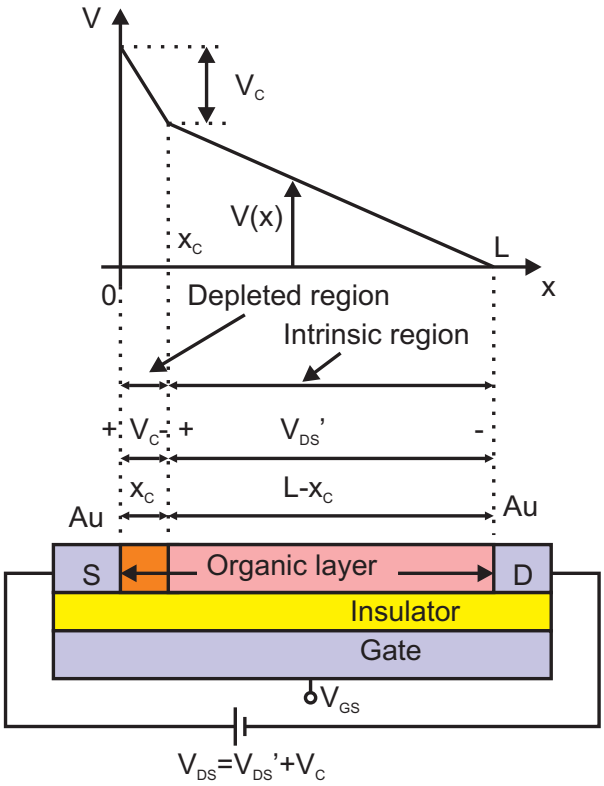

Figure 7.7: Esquema de un perfil de potencial que se puede observar a lo largo del canal de un OTFT. Se observa una región de baja conductividad cerca de los contactos, siendo menor en la zona de drenador de acuerdo con [35].

dinámica (donde si la hay y puede ser perjudicial a la hora de querer fabricar dispositivos estables y fiables). La permanente puede ser útil en dispositivos de memoria no volátiles (transistores de efecto campo ferroeléctricos). Se han dado muchas explicaciones para discutir el origen de la histéresis dinámica. Esta explicaciones se pueden agrupar en tres, como se muestra en la figura. 7.8:

(i) efectos inducidos en la interfaz canal/dieléctrico,

(ii) efectos inducidos por dipolos residuales (causada por la polarización lenta en el dieléctrico), y

(iii) los efectos de las cargas inyectadas desde el electrodo de puerta.

El mecanismo (i) se asocia a menudo con los electrones atrapados en los grupos hidroxilo (OH) en la interfaz canal/dieléctrico [43][44][45]. El mecanismo (ii) se relaciona con

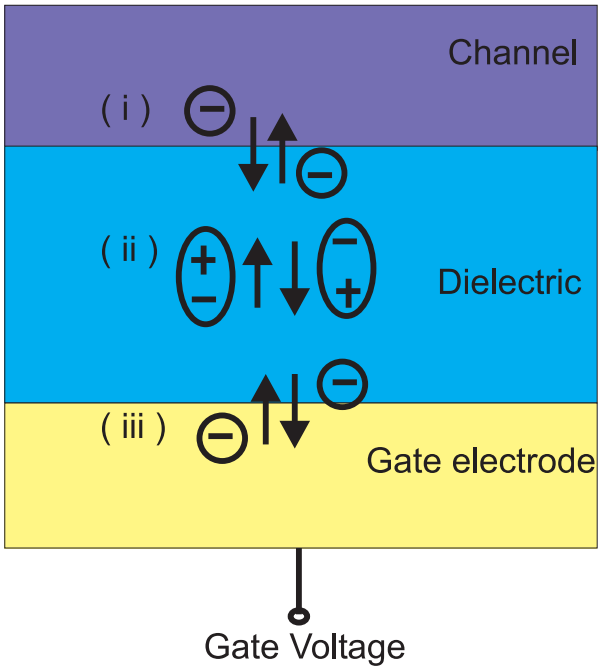

Figure 7.8: Ilustración de los mecanismos de histéresis: (i) canal /dieléctrico interfaz inducida, (ii) la lentitud de la polarización inducida, y (iii) puerta de carga inducidas por inyección histéresis.

grupos dipolares dentro del dieléctrico, tales como los grupos hidroxilo, que pueden ser lentamente reorientados por un campo eléctrico aplicado [42][44][46][47][45][48]. El mecanismo (iii) se atribuye a los electrones que pueden ser inyectados desde electrodo de puerta a un dieléctrico y quedar atrapados en el interior del mismo [49][50]

Desafortunadamente, todos los efectos que hacen que el transistor se aleje del comportamiento ideal no se muestran aislados, sino combinados entre sí. La figura. 7.9 muestra un esquema con las características de salida de un transistor incluyendo los efectos de histéresis y de los contacto, y como nuestro objetivo es separar los efectos de contacto de lo que ocurre en el canal intrínseco del transistor. La figura en la parte superior se muestra el modelo de un OTFT con una zona de contacto. La figura de abajo a la izquierda muestra las curvas de corriente-tensión de un OTFT con histéresis y los fenómenos de contacto. El uso de un modelo compacto para interpretar las características de salida de los OTFTs permite la separación de las curvas de tensión de corriente en el contacto y en el canal intrínseco. El estudio de estas curvas separadas permite la determinación de

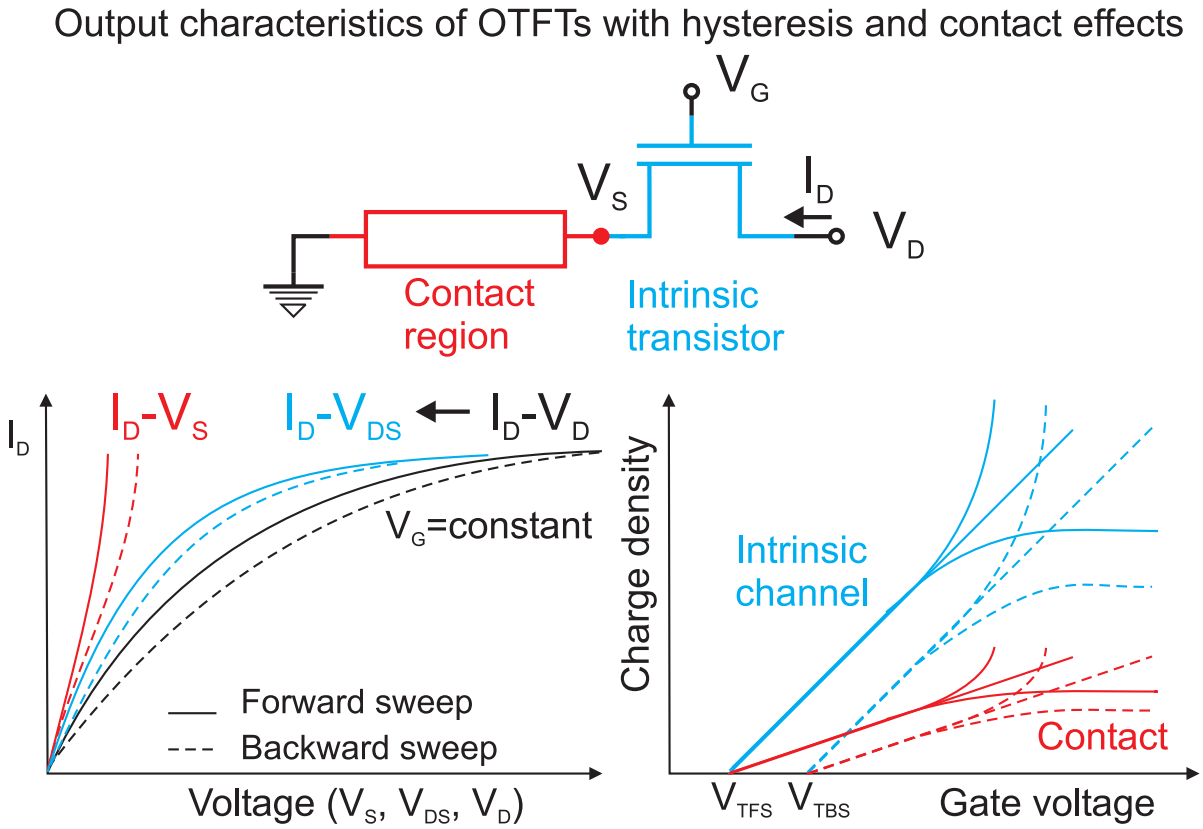

Figure 7.9: Resumen gráfico de la tesis. La figura superior se muestra el modelo de un OTFT con una zona de contacto. La figura de abajo a la izquierda muestra las curvas de tensión de corriente OTFTs con histéresis y los fenómenos de contacto. El uso de un modelo compacto para las características de salida de OTFTs permite la separación de las curvas de tensión de corriente en el contacto y en el canal intrínseco. El estudio de estas curvas separadas permite la determinación de la densidad de carga en el canal intrínseco y en el contacto (parte inferior derecha). Esto conduce, finalmente, a la determinación de la variación de la carga atrapada durante el ciclo de histéresis.

la densidad de carga en el canal intrínseco y en el contacto (parte inferior derecha). Esto conduce, finalmente, a la determinación de la variación de la carga atrapada durante el ciclo de histéresis. El objetivo principal de esta tesis es llevar a cabo un estudio en el que todos estos efectos están presentes simultáneamente.

7.6. Conclusiones

1. Hemos hecho uso de un modelo físico para interpretar los efectos de contacto en transistores orgánicos/poliméricos de lámina delgada, y lo hemos incorporado en un modelo compacto que describe las características de salida de estos transistores. El modelo resultante reproduce los datos experimentales de las características de salida que muestran respuestas tanto lineales como respuestas altamente no lineales en la región de bajos voltajes de drenador. Nuestro modelo se compara con otros modelos propuestos anteriormente. Nuestro modelo proporciona una visión física de la densidad de carga en la región de baja conductividad cerca del contacto y refleja los cambios de densidad de carga en el resto del dispositivo. De hecho, la evolución con la tensión de puerta de la densidad de carga libre en la zona del contacto está de acuerdo con la evolución de la densidad de carga libre estimada en el canal.

2. En paralelo a este modelo, se ha propuesto un procedimiento de extracción de parámetros con el fin de determinar los parámetros del modelo, incluyendo los nuevos parámetros ligados a los efectos de los contactos. Las ventajas que presentan procedimientos anteriores (aunque menos precisos) se introducen en nuestro método. Aunque se hacen necesarios modelos más avanzados físicamente, con el fin de tener en cuenta todos los efectos que aparecen en el transistor orgánicos, los modelos más simples no puede ser descartados completamente. Hemos demostrado su utilidad en el proceso de caracterización de los transistores.

3. Los diferentes pasos de nuestro procedimiento se comprueban con mediciones experimentales de transistores orgánicos de lámina delgada basados en Cinc Ftalocianina, así como a través de datos de otros autores.

4. Además, se ha probado el método de caracterización en un transistor con parámetros conocidos, donde no se han obtenido errores significativos entre los parámetros reales y los extraídos con el método.

5. El método de caracterización se ha aplicado también a otros transistores que muestran histéresis en las características de salida, además de tener presentes los efectos de los contactos. Ello ha hecho que la caracterización de estos transistores sea más

difícil. Hemos presentado una técnica, basada en el modelo compacto desarrollado previamente, para extraer los parámetros fundamentales del transistor, tales como la movilidad de los portadores, la tensión umbral y la variación de la carga atrapada durante un ciclo de histéresis. La técnica propuesta soluciona los problemas de tener un mayor número de parámetros en el modelo, así como el que exista una relación intrínseca entre algunos de estos parámetros, tales como la dependencia de la tensión de umbral con la carga atrapada, especialmente a altas tensiones de puerta.

La extracción de curvas de corriente tensión en la región de los contactos y en el canal intrínseco a partir de las características de salida experimentales ha permitido resolver estos problemas. En particular, el estudio de la evolución de la densidad de carga con la tensión de puerta, tanto en la región de contacto como en el canal intrínseco, es esencial para extraer los parámetros del transistor. Se han vuelto a analizar transistores que muestran respuestas lineales y no lineales en la zona de más bajas tensiones en las curvas características de salida. Los resultados obtenidos con nuestra técnica se han comparado con otros resultados proporcionados por diferentes autores que empleaban técnicas experimentales más elaboradas, encontrándose un buen acuerdo.

6. Se han presentado diferentes procedimientos para determinar la variación de la carga atrapada en un transistor orgánico durante un ciclo de histéresis. Los procedimientos difieren en la forma en la que se tratan los efectos de contacto presentes en los datos experimentales. Todos los procedimientos se basan en la separación de las contribuciones del transistor intrínseco y la región de contacto a partir de los datos experimentales. Con el objeto de determinar la densidad de carga atrapada, se han usado tres tipos de curvas de corriente-tensión: las correspondientes al transistor intrínseco, las del transistor externo, y las de situaciones intermedias donde los contactos se eliminan de forma parcial. Se han comparado los resultados de forma cuantitativa.

7. Se ha hecho un estudio de los efectos de la región de contacto sobre el valor de la movilidad extraída usando diferentes modelos. Una extracción correcta de la movilidad con un modelo que incorpora los efectos de contacto es esencial para obtener buenos resultados, incluso si se consideran las tensiones en los terminales

externos del transistor en lugar de las tensiones en el transistor intrínseco. En este sentido, un modelo compacto que describe las características de salida del transistor e incluye el efecto de las regiones de contacto se considera como el mejor escenario. El peor escenario es cuando la tensión de contacto se elimina parcialmente de las tensiones en los terminales.

8. La interpretación de las características de salida con histéresis con diferentes modelos muestra cómo los valores de la variación de la carga trampa están claramente alterados por la inclusión o no de los efectos de contacto sobre las tensiones en los terminales y la movilidad. Los valores obtenidos son siempre diferentes y más bajos que los obtenidos con nuestro modelo compacto. A partir de estos resultados, se destaca la importancia de utilizar el modelo compacto que tiene en cuenta los efectos de contacto del transistor y extrae de forma precisa la información de la carga atrapada en el semiconductor durante un ciclo de histéresis.

Bibliografía

[1] O. Marinov, M.J. Deen, and B. Iniguez. Charge transport in organic and polymer thin-film transistors: recent issues. *Circuits, Devices and Systems, IEE Proceedings*, 152(3):189 – 209, June 2005.

[2] Pablo Lara Bullejos. *Modelling of physical mechanisms in organic thin film transistors and related structure*. PhD thesis, Ph.D. dissertation, Universidad de Granada. Departamento de Electronica y Tecnologia de Computadores., Granada, Spain, 2009.

[3] Gilles Horowitz, Riadh Hajlaoui, Denis Fichou, and Ahmed El Kassmi. Gate voltage dependent mobility of oligothiophene field-effect transistors. *Journal of Applied Physics*, 85(6):3202–3206, 1999.

[4] Pablo Lara Bullejos, Juan A. Jiménez Tejada, M. J. Deen, O. Marinov, and W. R. Datars. Unified model for the injection and transport of charge in organic diodes. *Journal of Applied Physics*, 103(6):064504, 2008.

[5] C. K. Chiang, C. R. Fincher, Y. W. Park, A. J. Heeger, H. Shirakawa, E. J. Louis, S. C. Gau, and Alan G. MacDiarmid. Electrical conductivity in doped polyacetylene. *Phys. Rev. Lett.*, 39:1098–1101, Oct 1977.

[6] C. W. Tang and S. A. VanSlyke. Organic electroluminescent diodes. *Applied Physics Letters*, 51(12):913–915, 1987.

[7] Michael L. Chabinyc, William S. Wong, Alberto Salleo, Kateri E. Paul, and Robert A. Street. Organic polymeric thin-film transistors fabricated by selective dewetting. *Applied Physics Letters*, 81(22):4260–4262, 2002.

[8] I. Kymissis, C.D. Dimitrakopoulos, and S. Purushothaman. High-performance bottom electrode organic thin-film transistors. *Electron Devices, IEEE Transactions on*, 48(6):1060 –1064, Jun 2001.

[9] O. Marinov, M.J. Deen, U. Zschieschang, and H. Klauk. Organic thin-film transistors: Part I. Compact dc modeling. *Electron Devices, IEEE Transactions on*, 56(12):2952 –2961, dec. 2009.

[10] Jae Bon Koo, Chan Hoe Ku, Sang Chul Lim, Seong Hyun Kim, and Jung Hun Lee. Hysteresis and threshold voltage shift of pentacene thin-film transistors and inverters with Al_2O_3 gate dielectric. *Applied Physics Letters*, 90(13):133503, 2007.

[11] R. Schroeder, L. Majewski, and M. Grell. All-organic permanent memory transistor using an amorphous, spin-cast ferroelectric-like gate insulator. *Advanced Materials*, 16(7):633–636, 2004.

[12] Th. B. Singh, N. Marjanović, G. J. Matt, N. S. Sariciftci, R. Schwödiauer, and S. Bauer. Nonvolatile organic field-effect transistor memory element with a polymeric gate electret. *Applied Physics Letters*, 85(22):5409–5411, 2004.

[13] C. Ucurum, H. Goebel, F. A. Yildirim, W. Bauhofer, and W. Krautschneider. Hole trap related hysteresis in pentacene field-effect transistors. *Journal of Applied Physics*, 104(8):084501, 2008.

[14] C. Goldmann, S. Haas, C. Krellner, K. P. Pernstich, D. J. Gundlach, and B. Batlogg. Hole mobility in organic single crystals measured by a (flip-crystal) field-effect technique. *Journal of Applied Physics*, 96(4):2080–2086, 2004.

[15] Howard E. Katz, Jerainne Johnson, Andrew J. Lovinger, and Wenjie Li. Naphthalenetetracarboxylic diimide-based n-channel transistor semiconductors: Structural variation and thiol-enhanced gold contacts. *Journal of the American Chemical Society*, 122(32):7787–7792, 2000.

[16] Zhenan Bao, Andrew J. Lovinger, and Janelle Brown. New air-stable n-channel organic thin film transistors. *Journal of the American Chemical Society*, 120(1):207–208, 1998.

[17] A. Facchetti, M. Mushrush, H.E. Katz, and T.J. Marks. n-type building blocks for organic electronics: A homologous family of fluorocarbon-substituted thiophene oligomers with high carrier mobility. *Advanced Materials*, 15(1):33–38, 2003.

[18] Antonio Facchetti, Yvonne Deng, Anchuan Wang, Yoshihiro Koide, Henning Sirringhaus, Tobin J. Marks, and Richard H. Friend. Tuning the semiconducting properties of sexithiophene by a, w-substitution-a,w-diperfluorohexylsexithiophene: The first n-type sexithiophene for thin-film transistors. *Angewandte Chemie International Edition*, 39(24):4547–4551, 2000.

[19] Patrick R. L. Malenfant, Christos D. Dimitrakopoulos, Jeffrey D. Gelorme, Laura L. Kosbar, Teresita O. Graham, Alessandro Curioni, and Wanda Andreoni. N-type organic thin-film transistor with high field-effect mobility based on a n,n[sup [prime]]-dialkyl-3,4,9,10-perylene tetracarboxylic diimide derivative. *Applied Physics Letters*, 80(14):2517–2519, 2002.

[20] HE Katz, AJ Lovinger, J Johnson, C Kloc, T Siegrist, W Li, YY Lin, and A Dodabalapur. A soluble and air-stable organic semiconductor with high electron mobility. *NATURE*, 404(6777):478–481, MAR 30 2000.

[21] Z. Bao. Materials and fabrication needs for low-cost organic transistor circuits. *Advanced Materials*, 12(3):227–230, 2000.

[22] D.J. Gundlach, Li Li Jia, and T.N. Jackson. Pentacene TFT with improved linear region characteristics using chemically modified source and drain electrodes. *Electron Device Letters, IEEE*, 22(12):571 –573, dec. 2001.

[23] P.K. Weimer. The tft a new thin-film transistor. *Proceedings of the IRE*, 50(6):1462 –1469, June 1962.

[24] Howard E. Katz and Jia Huang. Thin-film organic electronic devices. *Annual Review of Materials Research*, 39(1):71–92, 2009.

[25] Gilles Horowitz and Philippe Delannoy. An analytical model for organic-based thin-film transistors. *Journal of Applied Physics*, 70(1):469–475, 1991.

[26] P. Murgatroyd. Theory of space-charge-limited current enhanced by Frenkel effect. *Journal of Physics D: Applied Physics*, 3(2):151, 1970.

[27] A. Lodha and R. Singh. Prospects of manufacturing organic semiconductor-based integrated circuits. *Semiconductor Manufacturing, IEEE Transactions on*, 14(3):281 –296, aug 2001.

[28] G. Ghibaudo, O. Roux, Ch. Nguyen-Duc, F. Balestra, and J. Brini. Improved analysis of low frequency noise in field-effect mos transistors. *physica status solidi (a)*, 124(2):571–581, 1991.

[29] O Marinov, MJ Deen, J Yu, G Vamvounis, S Holdcroft, and W Woods. Low-frequency noise in polymer thin-film transistors. *IEE Procedings-Circuits Devices and Systems*, 151(5):466–472, Oct 2004.

[30] Gilles Horowitz, Xuezhou Peng, Denis Fichou, and Francis Garnier. The oligothiophene-based field-effect transistor: How it works and how to improve it. *Journal of Applied Physics*, 67(1):528–532, 1990.

[31] Gilles Horowitz, Mohsen E. Hajlaoui, and Riadh Hajlaoui. Temperature and gate voltage dependence of hole mobility in polycrystalline oligothiophene thin film transistors. *Journal of Applied Physics*, 87(9):4456–4463, 2000.

[32] Gilles Horowitz. Organic thin film transistors: From theory to real devices. *Journal of Materials Research*, 19:1946–1962.

[33] Vissenberg M and Matters M. Theory of the field-effect mobility in amorphous organic transistors. *Phys. Rev. B*, 57:12964, 1998.

[34] C. D. Dimitrakopoulos, I. Kymissis, S. Purushothaman, D. A. Neumayer, P. R. Duncombe, and R. B. Laibowitz. Low-voltage, high-mobility pentacene transistors with solution-processed high dielectric constant insulators. *Advanced Materials*, 11(16):1372–1375, 1999.

[35] L. Bürgi, T. J. Richards, R. H. Friend, and H. Sirringhaus. Close look at charge carrier injection in polymer field-effect transistors. *Journal of Applied Physics*, 94(9):6129–6137, 2003.

[36] P. Lara Bullejos, J. A. Jiménez Tejada, S. Rodríguez-Bolivar, M. J. Deen, and O. Marinov. Model for the injection of charge through the contacts of organic transistors. *Journal of Applied Physics*, 105(8):084516, 2009.

[37] Dipti Gupta, Namho Jeon, and Seunghyup Yoo. Modeling the electrical characteristics of tips-pentacene thin-film transistors: Effect of contact barrier, field-dependent mobility, and traps. *Organic Electronics*, 9(6):1026 – 1031, 2008.

[38] I. H. Campbell, S. Rubin, T. A. Zawodzinski, J. D. Kress, R. L. Martin, D. L. Smith, N. N. Barashkov, and J. P. Ferraris. Controlling schottky energy barriers in organic electronic devices using self-assembled monolayers. *Phys. Rev. B*, 54:R14321–R14324, Nov 1996.

[39] R. A. Street and A. Salleo. Contact effects in polymer transistors. *Applied Physics Letters*, 81(15):2887–2889, 2002.

[40] Martin Egginger, Siegfried Bauer, Reinhard Schwoediauer, Helmut Neugebauer, and Niyazi Serdar Sariciftci. Current versus gate voltage hysteresis in organic field effect transistors. *Monatshefte Fur Chemie*, 140(7):735–750, Jul 2009.

[41] C. S. Fuller and J. C. Severiens. Mobility of impurity ions in germanium and silicon. *Phys. Rev.*, 96:21–24, Oct 1954.

[42] H. Klauk. *Organic Electronics*. Wiley, Weinheim, 2006.

[43] Gong Gu, Michael G. Kane, James E. Doty, and Arthur H. Firester. Electron traps and hysteresis in pentacene-based organic thin-film transistors. *Applied Physics Letters*, 87(24):243512, 2005.

[44] Gong Gu, Michael G. Kane, and Siun-Chuon Mau. Reversible memory effects and acceptor states in pentacene-based organic thin-film transistors. *Journal of Applied Physics*, 101(1):014504, 2007.

[45] D. K. Hwang, Kimoon Lee, Jae Hoon Kim, Seongil Im, Ji Hoon Park, and Eugene Kim. Comparative studies on the stability of polymer versus sio2 gate dielectrics for pentacene thin-film transistors. *Applied Physics Letters*, 89(9):093507, 2006.

[46] Howard E. Katz, X. Michael Hong, Ananth Dodabalapur, and Rahul Sarpeshkar. Organic field-effect transistors with polarizable gate insulators. *Journal of Applied Physics*, 91(3):1572–1576, 2002.

[47] Taeho Jung, Ananth Dodabalapur, Robert Wenz, and Siddharth Mohapatra. Moisture induced surface polarization in a poly(4-vinyl phenol) dielectric in an organic thin-film transistor. *Applied Physics Letters*, 87(18):182109, 2005.

[48] Sang Chul Lim, Seong Hyun Kim, Jae Bon Koo, Jung Hun Lee, Chan Hoe Ku, Yong Suk Yang, and Taehyoung Zyung. Hysteresis of pentacene thin-film transistors and inverters with cross-linked poly(4-vinylphenol) gate dielectrics. *Applied Physics Letters*, 90(17):173512, 2007.

[49] D. K. Hwang, J. H. Park, J. Lee, J. M. Choi, J. H. Kim, E. Kim, and J. S. Im. *Electrochem.* Soc. 8, G24, 2006.

[50] Cheon An Lee, Dong-Wook Park, Keum-Dong Jung, Byung ju Kim, Yoo Chul Kim, Jong Duk Lee, and Byung-Gook Park. Hysteresis mechanism in pentacene thin-film transistors with poly(4-vinyl phenol) gate insulator. *Applied Physics Letters*, 89(26):262120, 2006.

[51] Se Hyun Kim, Hoichang Yang, Sang Yoon Yang, Kipyo Hong, Danbi Choi, Chanwoo Yang, Dae Sung Chung, and Chan Eon Park. Effect of water in ambient air on hysteresis in pentacene field-effect transistors containing gate dielectrics coated with polymers with different functional groups. *Organic Electronics*, 9(5):673 – 677, 2008.

[52] Qingshuo Wei, Keisuke Tajima, and Kazuhito Hashimoto. Electrical instability of polymer thin-film transistors using contact film transfer methods. *Applied Physics Letters*, 96(24):243301, 2010.

[53] M. Coll, K. P. Goetz, B. R. Conrad, C. A. Hacker, D. J. Gundlach, C. A. Richter, and O. D. Jurchescu. Flip chip lamination to electrically contact organic single crystals on flexible substrates. *Applied Physics Letters*, 98(16):163302, 2011.

[54] Antonio Facchetti. pi-conjugated polymers for organic electronics and photovoltaic cell applications. *Chemistry of Materials*, 23(3):733–758, 2011.

[55] S. C. Jain, W. Geens, A. Mehra, V. Kumar, T. Aernouts, J. Poortmans, R. Mertens, and M. Willander. Injection- and space charge limited-currents in doped conducting organic materials. *Journal of Applied Physics*, 89(7):3804–3810, 2001.

[56] D. J. Gundlach, L. Zhou, J. A. Nichols, T. N. Jackson, P. V. Necliudov, and M. S. Shur. An experimental study of contact effects in organic thin film transistors. *Journal of Applied Physics*, 100(2):024509, 2006.

[57] B. H. Hamadani, C. A. Richter, D. J. Gundlach, R. J. Kline, I. McCulloch, and M. Heeney. Influence of source-drain electric field on mobility and charge transport in organic field-effect transistors. *Journal of Applied Physics*, 102(4):044503, 2007.

[58] S. Haas, A. F. Stassen, G. Schuck, K. P. Pernstich, D. J. Gundlach, B. Batlogg, U. Berens, and H.-J. Kirner. High charge-carrier mobility and low trap density in a rubrene derivative. *Phys. Rev. B*, 76:115203, Sep 2007.

[59] B.H. Hamadani and D. Natelson. Extracting contact effects in organic fets. *Proceedings of the IEEE*, 93(7):1306 –1311, july 2005.

[60] B. H. Hamadani and D. Natelson. Gated nonlinear transport in organic polymer field effect transistors. *Journal of Applied Physics*, 95(3):1227–1232, 2004.

[61] E. J. Meijer, G. H. Gelinck, E. van Veenendaal, B.-H. Huisman, D. M. de Leeuw, and T. M. Klapwijk. Scaling behavior and parasitic series resistance in disordered organic field-effect transistors. *Applied Physics Letters*, 82(25):4576–4578, 2003.

[62] P. V. Necliudov, M. S. Shur, D. J. Gundlach, and T. N. Jackson. Modeling of organic thin film transistors of different designs. *Journal of Applied Physics*, 88(11):6594–6597, 2000.

[63] P. Lara Bullejos, J. A. Jiménez Tejada, F. M. Gómez-Campos, M. J. Deen, and O. Marinov. Evaluation of the charge density in the contact region of organic thin film transistors. *Journal of Applied Physics*, 106(9):094503, 2009.

[64] Mahmut Durmus, Colette Lebrun, and Vefa Ahsen. Synthesis and characterization of novel liquid and liquid crystalline phthalocyanines. *Journal of Porphyrins and Phthalocyanines*, 08(10):1175–1186, 2004.

[65] Weiying Gao and Antoine Kahn. Controlled p-doping of zinc phthalocyanine by coevaporation with tetrafluorotetracyanoquinodimethane: A direct and inverse photoemission study. *Applied Physics Letters*, 79(24):4040–4042, 2001.

[66] Z. Xie, M. S. A. Abdou, X. Lu, M. J. Deen, and S. Holdcroft. Electrical characteristics and photolytic tuning of poly (3-lhexylthiophene) thin film metal- insulator-semiconductor field- effect transistors (misfets). *Canadian Journal of Physics*, 70(10-11):1171–1177, Oct-Nov 1992. 6Th Canadian Semiconductor Technology Conf, Ottawa, Canada, Aug, 1992.

[67] M. Jamal Deen, Mehdi H. Kazemeini, and S. Holdcroft. Contact effects and extraction of intrinsic parameters in poly(3-alkylthiophene) thin film field-effect transistors. *Journal of Applied Physics*, 103(12):124509, 2008.

[68] M. Shur and M. Hack. Physics of amorphous silicon based alloy field-effect transistors. *Journal of Applied Physics*, 55(10):3831–3842, 1984.

[69] M. C. J. M. Vissenberg and M. J. M. de Jong. Theory of electric-field-induced photoluminescence quenching in disordered molecular solids. *Phys. Rev. B*, 57:2667–2670, Feb 1998.

[70] E. Calvetti, A. Savio, Zs. M. Kovács-Vajna, and L. Colalongo. Analytical model for organic thin-film transistors operating in the subthreshold region. *Applied Physics Letters*, 87(22):223506, 2005.

[71] O. Marinov, M. J. Deen, and R. Datars. Compact modeling of charge carrier mobility in organic thin-film transistors. *Journal of Applied Physics*, 106(6):064501, 2009.

[72] M.J. Deen, O. Marinov, U. Zschieschang, and H. Klauk. Organic thin-film transistors: Part ii ;parameter extraction. *Electron Devices, IEEE Transactions on*, 56(12):2962 –2968, dec. 2009.

[73] A. Cerdeira, M. Estrada, R. Garcia, A. Ortiz Conde, and F.J. Garcia Sanchez. New procedure for the extraction of basic a-si:h tft model parameters in the linear and saturation regions. *Solid-State Electronics*, 45(7):1077 – 1080, 2001.

[74] K. Tsukagoshi, F. Fujimori, T. Minari, T. Miyadera, T. Hamano, and Y. Aoyagi. Suppression of short channel effect in organic thin film transistors. *Applied Physics Letters*, 91(11):113508, 2007.

[75] B. H. Hamadani and D. Natelson. Nonlinear charge injection in organic field-effect transistors. *Journal of Applied Physics*, 97(6):064508, 2005.

[76] D Chirvase, Z Chiguvare, M Knipper, J Parisi, V Dyakonov, and JC Hummelen. Temperature dependent characteristics of poly(3 hexylthiophene)-fullerene based heterojunction organic solar cells. *Journal of Applied Physics*, 93(6):3376–3383, Mar 15 2003.

[77] B. G. Streetman. *Solid State Electronic Devices*. Prentice-Hall, Englewood Cliffs, NJ, 1980.

[78] Mohamed S. A. Abdou, Xiaotang Lu, Zi W. Xie, Frank Orfino, M. Jamal Deen, and Steven Holdcroft. Nature of impurities in .pi.-conjugated polymers prepared by ferric chloride and their effect on the electrical properties of metal-insulator-semiconductor structures. *Chemistry of Materials*, 7(4):631–641, Apr 1995.

[79] Mohamed S. A. Abdou, Frank P. Orfino1, Zi W. Xie, M. Jamal Deen, and Steven Holdcroft. Reversible charge transfer complexes between molecular oxygen and poly(3-alkylthiophene)s. *Advanced Materials*, 6(11):838–841, Nov 1994.

[80] O. Marinov, M. J. Deen, B. Iniguez, and B. Ong. Charge localization in polymeric metal-oxide-semiconductor capacitors. *Journal of Vacuum Science Technology A: Vacuum, Surfaces, and Films*, 24(3):649 –653, may 2006.

[81] Gong Gu and Michael G. Kane. Moisture induced electron traps and hysteresis in pentacene-based organic thin-film transistors. *Applied Physics Letters*, 92(5):053305, 2008.

[82] D. K. Hwang, Min Suk Oh, Jung Min Hwang, Jae Hoon Kim, and Seongil Im. Hysteresis mechanisms of pentacene thin-film transistors with polymer/oxide bilayer gate dielectrics. *Applied Physics Letters*, 92(1):013304, 2008.

[83] J.A. Jiménez Tejada, K.M. Awawdeh, J.A. López Villanueva, J.E. Carceller, M.J. Deen, N.B. Chaure, Tamara Basova, and A.K. Ray. Contact effects in compact models of organic thin film transistors: Application to zinc phthalocyanine-based transistors. *Organic Electronics*, 12(5):832 – 842, 2011.

[84] C. Petit, D. Zander, K. Lmimouni, M. Ternisien, D. Tondelier, S. Lenfant, and D. Vuillaume. Gate pulse electrical method to characterize hysteresis phenomena in organic field effect transistor. *Organic Electronics*, 9(6):979 – 984, 2008.

[85] Jeong Ho Cho, Jung Ah Lim, Joong Tark Han, Ho Won Jang, Jong-Lam Lee, and Kilwon Cho. Control of the electrical and adhesion properties of metal/organic interfaces with self-assembled monolayers. *Applied Physics Letters*, 86(17):171906, 2005.

[86] K.M. Awawdeh, J.A.J. Tejada, J.A.L. Villanueva, J.E. Carceller, M.J. Deen, N.B. Chaure, T. Basova, and A.K. Ray. Compact modeling of the contact effects in organic thin film transistors. In *Electron Devices (CDE), 2011 Spanish Conference on*, pages 1 –4, feb. 2011.

[87] Martin Egginger. *Electrical Characterisation of Poly(vinyl alcohol) based Organic Field Effect Transistors*. PhD thesis, Ph.D. dissertation, Johannes Kepler University of Linz, Johannes Kepler University Linz, AltenbergerstraBe, Linz, Austria, 2009.

[88] M.J. Deen, O. Marinov, S. Holdcroft, and W. Woods. Low-frequency noise in polymer transistors. *Electron Devices, IEEE Transactions on*, 48(8):1688 –1695, aug 2001.

[89] M.J. Deen, M.H. Kazemeini, Y.M. Haddara, Jianfei Yu, G. Vamvounis, S. Holdcroft, and W. Woods. Electrical characterization of polymer-based fets fabricated by spin-coating poly(3-alkylthiophene)s. *Electron Devices, IEEE Transactions on*, 51(11):1892 – 1901, nov. 2004.

[90] P. López Varo, J.A. Jiménez Tejada, J.A. López Villanueva, J.E. Carceller, and M.J. Deen. Modeling the transition from ohmic to space charge limited current in organic semiconductors. *Organic Electronics*, 13(9):1700 – 1709, 2012.

[91] K. M. Awawdeh, J. A. Jiménez Tejada, P. López Varo, J. A. López Villanueva, F. M. Gómez Campos, and M. J. Deen. Characterization of organic thin film transistors with hysteresis and contact effects. *Organic Electronics*, x(x):x, 2013.

[92] Peter V Necliudov, Michael S Shur, David J Gundlach, and Thomas N Jackson. Contact resistance extraction in pentacene thin film transistors. *Solid-State Electronics*, 47(2):259 – 262, 2003.

Appendix I

Publicaciones.

Publicaciones a fecha de entrega en la Escuela de Posgrado de la Universidad de Granada:

Journal publications

a) Contact effects in compact models of organic thin film transistors: application to zinc phthalocyanine-based transistors. J. A. Jiménez Tejada, K. M. Awawdeh, J. A. López Villanueva, J. E. Carceller, M. J. Deen, N. B. Chaure, T. Basova, and A. K. Ray. *Organic Electronics* **2011**.

b) Characterization of organic thin film transistors with hysteresis and contact effects. K. M. Awawdeh, J. A. Jiménez Tejada, P. López Varo, J. A. López Villanueva, F. M. Gómez Campos, and M. J. Deen. *Organic Electronics* **2013**, *submitted*.

c) Determination of the variation of the trapped charge in organic thin film transistors during hysteresis. K. M. Awawdeh, J. A. Jiménez Tejada, P. López Varo, J. A. López Villanueva, M. J. Deen. **2013**, *In preparation*.

Conference publications

d) **Invited paper.** Towards a compact model for the injection of charge into organic/polymeric semiconductors. J. A. Jiménez Tejada, L. Puga Pedregosa, K. M. Awawdeh, M. J. Deen. *ISFE'10-3rd International Symposium on Flexible electronics, Meeting Abstracts*, **2010**.

e) Compact modeling of the contact effects in organic thin film transistors. K. M. Awawdeh, J. A. Jiménez Tejada, J. A. López Villanueva, J. E. Carceller, M. J. Deen, N. B. Chaure, T. Basova, and A. K.Ray. *IEEE Proceedings of the 8th Spanish Conference on Electron Devices, CDE'2011,* , **2011**.

f) **Invited paper.** Contact effects and hysteresis in organic thin film transistors J. A. Jiménez Tejada, K. M. Awawdeh, P. López Varo, A. K.Ray, M. J. Deen. *ECS-219th Electrochemical Society, Meeting Abstracts*, **2011**.

g) Study of electrical phenomena in organic devices: solar cells, diodes, thin film transistors P. López Varo, K. M. Awawdeh, J. A. Jiménez Tejada. *4th EMUNI Research Souk the Euro-Mediterranean Student Research Multi-Conference, Meeting Abstracts*, **2012**.

h) Method of extraction of mobility model parameters in organic diodes P. López Varo, J. A. Jiménez Tejada, J. A. López Villanueva, K. M. Awawdeh, M. J. Deen. *ICOE 2012-8th International Conference on Organic Electronics, Meeting Abstracts*, **2012**.

i) Influence of the contact effects on the variation of the trapped charge in the intrinsic channel of organic thin film transistors. K. M. Awawdeh, J. A. Jiménez Tejada, P. López Varo, J. A. López Villanueva, M. J. Deen. *IEEE Proceedings of the 9th Spanish Conference on Electron Devices, CDE'2013,* , **2013**.

j) **Invited paper.** Modeling of charge injection in organic/polymeric diodes J. A. Jiménez Tejada, P. López Varo, K. M. Awawdeh, M. J. Deen. *ECS-223th Electrochemical Society, Meeting Abstracts*, **2013**.

k) Monitoring the introduction of impurities in organic/polymeric diodes by the analysis of current voltage curves P. López Varo, J. A. Jiménez Tejada, K. M. Awawdeh, M. J. Deen. *ICOE 2013-9th International Conference on Organic Electronics, Meeting Abstracts*, **2013**.